IDENTIFICATION OF ATMOSPHERIC MERCURY SOURCES AND TRANSPORT PATHWAYS ON LOCAL AND REGIONAL SCALES

by

Lynne E. Gratz

A dissertation submitted in partial fulfillment
of the requirements for the degree of
Doctor of Philosophy
(Atmospheric and Space Sciences)
in the University of Michigan
2010

Doctoral Committee:

       Professor Gerald J. Keeler, Chair
       Professor Joel D. Blum
       Professor Perry J. Samson
       Assistant Professor Allison L. Steiner
       Associate Research Scientist Frank J. Marsik

To my parents,
who always support me when I need it the most

ACKNOWLEDGEMENTS

TABLE OF CONTENTS

LIST OF FIGURES

Figure

LIST OF TABLES

ABSTRACT

Mercury (Hg) is a hazardous air pollutant and bioaccumulative neurotoxin whose intricate atmospheric chemistry complicates our ability to define Hg source-receptor relationships on all scales. Our detailed measurements of Hg in its different forms together with atmospheric tracers have improved our understanding of Hg chemistry and transport. Daily-event precipitation samples collected from 1995 to 2006 in Underhill, VT were examined to identify Hg wet deposition trends and source influences. Analysis revealed that annual Hg deposition at this fairly remote location did not vary significantly over the 12-year period. While a decreasing trend in volume-weighted mean Hg concentration was observed, Hg wet deposition did not decline as transport of emissions from the Midwest and along the Atlantic Coast consistently contributed to the largest observed Hg wet deposition events. Receptor modeling of Hg and trace elements in precipitation indicated that ~60% of Hg wet deposition at Underhill could be attributed to emissions from coal-fired utility boilers (CFUBs), and their contribution to Hg wet deposition did not change significantly over time. Hybrid-receptor modeling further defined these CFUBs to be located predominantly in the Midwestern U.S.

Atmospheric Hg chemistry and transport from the Chicago urban/industrial area was the focus of speciated Hg measurements performed in the southern Lake Michigan basin during summer 2007. Transport from Chicago, IL to Holland, MI occurred during 27% of the study period, resulting in a five-fold increase in divalent reactive gaseous Hg

(RGM) at the downwind Holland site. Dispersion modeling of case study periods demonstrated that under southwesterly flow approximately half of the RGM in Holland could be attributed to primary RGM emissions from Chicago after transport and dispersion, with the remainder due to Hg^0 oxidation in the atmosphere en route. Precipitation and ambient vapor phase samples were also collected in Chicago, Holland, and Dexter, MI and analyzed for Hg isotopes. The Hg isotopic fractionation observed in atmospheric samples was in contrast to a recently published report which predicted that aqueous photoreduction may be a dominant source of atmospheric Hg. Our results suggest that other redox reactions and source related processes likely contribute to isotopic fractionation of atmospheric Hg.

CHAPTER 1

Introduction

1.1 Mercury as a Hazardous Air Pollutant

Mercury (Hg) is a hazardous air pollutant and bioaccumulative neurotoxin. It is a naturally occurring element in the earth's crust released to the atmosphere through natural and anthropogenic activities. The form of Hg in the atmosphere is predominantly inorganic and non-bioaccumulative (Schroeder and Munthe, 1998); however, once Hg is deposited in the terrestrial or aquatic ecosystem it can be converted to the more toxic organic form, methylmercury, which bioaccumulates in marine and freshwater environments and can ultimately threaten human and environmental health (U.S. EPA 1997; Schroeder and Munthe, 1998).

Elevated levels of Hg have been observed in several wildlife species, including the common loon (Evers et al., 2007) whose exposure to Hg has resulted in reduced reproductive success (Burgess, 2005). A primary concern for humans is the ability for Hg to bioaccumulate within the aquatic food chain, as ingestion of contaminated fish can lead to neurological damage including impaired cognitive thinking, memory loss, and reduced fine motor skills (U.S. EPA, 1997). Those at greatest risk for these effects are the developing fetus, infants, young children, women of childbearing age, and anyone

who consumes large amounts of commercial seafood or relies on self-caught fish as a major source of sustenance (U.S. EPA 1997). Atmospheric deposition is the dominant pathway for Hg to enter aquatic ecosystems (U.S. EPA, 1997; Landis and Keeler, 2002; Hammerschmidt and Fitzgerald, 2006). Therefore quantification of atmospheric Hg emission, transport, chemistry, and deposition is vital to understanding the impact of mercury pollution on the society and the environment.

1.2 Mercury in the Atmosphere: Speciation, Sources, and Chemistry

Mercury exists in three main forms in the atmosphere: gaseous elemental Hg (Hg^0), fine particle bound Hg (Hg_p), and divalent reactive gaseous Hg (RGM). Hg_p and RGM are commonly referred to collectively as Hg(II) or Hg^{2+}. Hg^0 comprises more than 90% of Hg in ambient air (Slemr et al., 1985, Lin and Pehkonen, 1999). It has low solubility in water and is relatively stable in the environment, allowing it to be transported long distances in the atmosphere (Schroeder and Munthe, 1998; Lin and Pehkonen, 1999). Deposited Hg can also be re-emitted to the atmosphere as Hg^0 due to its high volatility, further contributing to the global atmospheric Hg pool (Schroeder and Munthe, 1998).

RGM, on the other hand, is much more reactive than Hg^0 (Lin and Pehkonen, 1999). Consequently RGM has a much shorter atmospheric lifetime than Hg^0 and deposits readily through wet and dry deposition, not only close to emission sources but also following Hg^0 oxidation in the atmosphere (Schroeder and Munthe, 1998; Lin and Pehkonen, 1999). Hg_p is released directly from emission sources (Keeler et al., 1995) but may also form when gas-phase Hg binds to particles (Pirrone et al., 2000; Forlano et al., 2000). Similar to RGM, Hg_p is also readily removed through wet and dry deposition (Lin

and Pehkonen, 1999). As a result of the varying behavior of these species, Hg can be considered a local, regional, and global pollutant. Distinguishing the relative contributions from of local, regional, and global sources on Hg deposition in a given region is critical to effectively regulating mercury emissions to the atmosphere.

Mercury is released to the atmosphere from a variety of natural and anthropogenic sources. Today, natural and anthropogenic emissions are believed to contribute approximately equally to the global mercury pool (Lindberg et al., 2007); however these estimates are highly uncertain, and the relative contribution from natural and anthropogenic sources will vary geographically and temporally. Natural emissions occur through geologic processes, including volcanoes and geothermal activity, as well as through biomass burning, marine emissions, and evasion from terrestrial and aquatic surfaces (Nriagu, 1989; Gustin et al., 2008). Given that Hg can be rapidly recycled back to the atmosphere following deposition (Lindberg et al., 2007), it is estimated that a substantial portion of the emissions from terrestrial or aquatic surfaces represent the re-emission of previously deposited natural or anthropogenic Hg (Schroeder and Munthe, 1998; Gustin et al., 2008; Lindberg et al., 2007).

Anthropogenic emissions include point sources such as combustion (utility and industrial boilers, hazardous waste combustors, and crematories) and manufacturing (chlor-alkali, cement, batteries, byproduct coke, and refineries), and area sources such as agricultural burning, landfills, and mobile sources (U.S. EPA, 1997). In the United States, anthropogenic point sources emit ~105-110 tons per year (tpy) of Hg (U.S. EPA, 2005; Pacyna et al., 2006; Butler et al., 2008) while area sources emit only ~3 tpy of Hg (U.S. EPA, 1997). Manufacturing sources contribute ~15 tpy of Hg to the atmosphere,

with the remainder of point source emissions due to combustion sources (U.S. EPA, 1997). Fossil fuel combustion is the largest anthropogenic point source of atmospheric Hg in the U.S., with coal-fired utility boilers emitting ~50 tpy of Hg (U.S. EPA, 1997; Cohen et al., 2007; Butler et al., 2008).

While emissions from natural sources are predominantly Hg^0, anthropogenic emissions contain varying amounts of Hg^0, RGM, and Hg_p (Carpi, 1997; Landis et al., 2004; Seigneur et al., 2006; Cohen et al., 2007). Variability in the speciation of emissions by source type consequently influences the relative amounts of emitted Hg that can be rapidly removed following emission or instead be transported downwind. As an example, mercury emissions from waste incinerators are ~75-85% Hg(II) and ~10-20% Hg^0 (Carpi, 1997), while emissions from coal combustion are ~50-80% Hg(II), and ~20-50% Hg^0 (Carpi, 1997; Seigneur et al., 2006). The Hg(II) emitted from combustion sources is expected to be predominantly RGM, as Hg_p is more easily removed through filters and other control technologies in the stack (Carpi, 1997).

Additionally, there are a range of gas phase, aqueous phase, and heterogeneous reactions that Hg can undergo in the atmosphere following emission. Hg^0 can be oxidized to Hg(II) in the gas and aqueous phases by hydroxyl radicals, ozone, and reactive halogen compounds (Munthe, 1992; Lin and Pehkonen, 1997; Hynes et al., 2009). The oxidized Hg(II) can subsequently be removed from the atmosphere through wet and dry deposition (Lin et al., 2006). Hg^0 may also be removed through dry deposition (Schroeder and Munthe, 1998; Lin et al., 2006). Reduction of Hg^{2+} can also occur in the aqueous phase by sulfite, halogen species, and hydroperoxyl radicals (Lin and Pehkonen, 1999; Hynes et al., 2009; Munthe et al., 1991), as well as through

photochemical reactions and heterogeneous reactions in cloud droplets (Lin and Pehkonen, 1997; Seigneur et al., 1994). The relative importance of these reactions will vary seasonally and geographically based on the availability of oxidizing and reducing species. For example, in the Great Lakes region ozone is typically a readily available oxidant due to the prevalence of industrial emissions (Dye et al., 1995) and therefore reactions with ozone may dominate Hg^0 oxidation (Munthe and McElroy, 1992). Halogen reactions, on the other hand, are typically important in Arctic environments (Lindberg et al., 2002) and the marine boundary layer (Hedgecock and Pirrone, 2001; Lin et al., 2006); however, industrial halogen sources (Carpi, 1997) could also contribute to Hg^0 oxidation. The variable behavior of emitted Hg species and the inter-conversions that Hg undergoes in the atmosphere following emission add great complexity to understanding the spatial scale of source impacts and makes regulating Hg emissions particularly challenging.

1.3 Mercury Regulations

Mercury was recognized as a hazardous air pollutant (HAP) under the Clean Air Act Amendments of 1990 section 112(n)(1)(B), which required the U.S. EPA to study the environmental impacts of mercury pollution (U.S. EPA, 1997) and implement standards for sources that emit Hg to the atmosphere. An important outcome of the 1990 Amendments was the formation of the Great Waters Program, which mandated measurements of hazardous air pollutants, including Hg, in the Great Lakes, Lake Champlain, the Chesapeake Bay and other selected coastal waterways (U.S. EPA, 1994). Under this program, the U.S. EPA was required to establish monitoring networks, quantify pollutant deposition, and determine the impact of pollutants on the Great Waters

(U.S. EPA, 1994). This mandate was the impetus behind several monitoring studies in the region to quantify Hg sources, transport, and deposition (Burke et al., 1995; Rea et al., 1996; Landis et al., 2002; Landis and Keeler, 2002; Vette et al., 2002; Keeler et al., 2005).

Under section 129 of the Clean Air Act Amendments, the U.S. EPA specifically targeted emission reduction from solid waste combustors, previously one of the largest anthropogenic sources of atmospheric Hg (U.S. EPA, 1997). Restrictions placed on stack emissions from municipal and medical waste incinerators lead to ~95% reductions in total Hg emissions from these sources (Cohen et al., 2007). Declines in emissions occurred due to controls placed on stacks as well as bans on the use of Hg in manufactured products, such as batteries and paint, which reduced the amount of Hg in waste (U.S. EPA). These reductions occurred across the U.S., with some of the largest declines observed in the Northeast States where Hg emissions declined from 15.9 tpy to 4.7 tpy between 1998 and 2002 (Butler et al., 2008). However, emissions from coal-fired utility boilers and other major anthropogenic sources in the United States have remained fairly constant (Cohen et al., 2007; Butler et al., 2008).

In 2005 the Clean Air Mercury Rule (CAMR) was proposed, suggesting a cap-and-trade approach to regulating Hg emissions from coal-fired power plants. CAMR was developed based on the framework of the Clean Air Interstate Rule (CAIR), which was also issued in 2005 to regulate emissions of SO_2 and NO_x under similar regulatory techniques. The intention of CAMR was to ultimately reduce Hg emissions by 70%. The rule was overturned in 2008 in favor of using maximum available control technologies (MACT) to reduce Hg emissions, as proposed in the 1990 Clean Air Act

Amendments (U.S. EPA). To date EPA has yet to promulgate its final ruling as to how MACT will be implemented.

1.4 Quantifying Atmospheric Mercury in the Great Waters Regions

Numerous monitoring efforts following the creation of the Great Waters program offered insight into Hg sources and processes in the region using a range of available analytical tools. These studies first quantified the amounts of ambient Hg (Keeler et al., 1994; Keeler et al., 1995; Burke et al., 1995; Pirrone and Keeler, 1996) and Hg wet deposition (Burke et al., 1995; Hoyer et al., 1995; Rea et al., 1996; Landis et al., 2002) at urban and rural locations throughout the Midwest and Northeast states. The addition of continuous speciated Hg measurements (Lynam and Keeler 2005; Poissant et al., 2005; Lynam and Keeler, 2006; Liu et al, 2007; Liu et al., 2010) provided finer time resolution data and demonstrated the temporal variability in speciated Hg concentrations at urban and rural locations.

Several studies also explored the urban/industrial Hg source areas in the Great Waters regions, including Chicago/Gary (Landis and Keeler, 2002; Landis et al., 2002; Vette et al., 2002), Detroit, MI (Liu et al., 2007; Lynam and Keeler, 2005; Lynam and Keeler, 2006), and the Ohio River Valley (Keeler et al., 2006; White et al., 2009). Urban/industrial areas were shown to contribute significantly to atmospheric Hg levels in the region. For example, results from atmospheric deposition modeling during the Lake Michigan Mass Balance Study (LMMBS) suggested that the Chicago/Gary urban area alone contributed to ~20% of the annual atmospheric Hg deposition to Lake Michigan (Landis and Keeler, 2002). Furthermore, multivariate receptor models such as positive matrix factorization (PMF) were applied to aerosol (Polissar et al., 2001; Poirot et al.,

2001; Liu et al., 2003) and wet deposition measurements (Keeler et al., 2006) in order to identify the specific sources impacting the atmosphere at receptor locations. Results of these studies suggested that local and regional anthropogenic sources are major contributors to atmospheric Hg in the region. Specifically, ~70% of Hg wet deposition in the Ohio River Valley was attributed to emissions from coal-fired utility boilers (Keeler et al., 2006). It can be concluded from these past studies that atmospheric deposition is a dominant pathway for Hg to enter the terrestrial and aquatic ecosystem, and that local and regional anthropogenic sources contribute substantially to atmospheric Hg in the Great Waters regions.

Mercury stable isotope analysis is an additional new tool that may also be useful in further understanding sources of Hg to the atmosphere and Hg biogeochemical cycling, but until recently this technique had not been applied to atmospheric samples in the Great Waters regions. Mercury exists in seven stable isotopes, but the natural abundance of these isotopes may be altered as Hg undergoes physical, chemical, or biological processes. The variation from natural abundance that occurs during these processes is referred to as fractionation (Figure 1.1). Mass-dependent fractionation (MDF) results from differences in zero-point vibrational energies and bond strength between isotopes due to their differing masses (Bergquist and Blum, 2007) such that during chemical reactions and other processes the heavier and lighter isotopes will behave differently (Figure 1.1c).

Mass-independent fractionation (MIF) is fractionation that does not follow theoretically predicted mass-dependence, and measurements of MIF are reported as the deviation from predicted mass dependence (Figure 1.1d). MIF of Hg may occur during

equilibrium and kinetic reactions. During equilibrium reactions, MIF of Hg occurs due to variations in the nuclear charge radius of different isotopes that is caused by variability in the packing of protons and neutrons in the nucleus (nuclear volume theory) (Schauble, 2007). MIF may occur during kinetic reactions due to the influence of nuclear spin in the odd-mass isotopes on radical pair reaction rates (magnetic isotope effect) (Turro, 1983; Buchachenko, 2001; Buchachenko et al., 2007).

The magnitude and sign of MDF and MIF in a given environmental reservoir may therefore suggest the specific processes that Hg has undergone during biogeochemical cycling. Recent studies indicate that isotopic analyses can offer insight on the sources of Hg to the environment (Biswas et al., 2008) and the specific processes that Hg undergoes in the ecosystem (Bergquist and Blum, 2007; Carignan et al., 2009; Sherman et al., 2010), and may therefore be a valuable new approach to understanding Hg sources and cycling in the atmosphere.

1.5 Current Uncertainties in Our Understanding of Atmospheric Mercury

Given that consistent atmospheric Hg monitoring has only been ongoing for the past ~15-20 years and proper monitoring can be costly and time intensive, there is a shortage of long-term monitoring databases of ambient and wet deposition Hg measurements. While the ability to effectively monitor atmospheric Hg is continually improving, and the existence of long-term monitoring networks continues to grow (Butler et al., 2008; Keeler and Dvonch, 2005), there is still a need for additional evaluation of long-term ambient and wet deposition datasets in the literature in order to effectively assess the impact of emission regulations over time and sufficiently inform policy decisions.

Furthermore, while it is recognized that fossil fuel combustion is the dominant source of Hg in the U.S., the spatial extent over which emissions can travel and be subsequently removed is not fully understood. There is strong observational evidence for near-field (within 1 km of the stack) deposition of Hg(II) emissions (White et al., 2009). In a modeling study it was also suggested that Hg(II) emissions can travel beyond 50 km from the emission source (Siegneur et al., 2006) potentially influencing more remote locations. Given that the transport and behavior of Hg in the atmosphere following emission will vary with meteorological conditions, it is apparent that Hg emissions can have varying scales of spatial impact. The behavior of Hg once it is emitted to the atmosphere creates challenges for developing effective regulatory strategies for anthropogenic Hg emissions.

The relative importance of reactive Hg transport versus chemical production and loss in the atmosphere is also important to quantify in order to measure the spatial influence of Hg emissions. Various gas, aqueous, and heterogeneous reactions that Hg may undergo in the atmosphere have been studied (Munthe, 1992; Seigneur et al., 1994; Lin and Pehkonen, 1997; Lin and Pehkonen, 1999; Hynes et al., 2009), but their relative importance and effect on Hg transport and cycling is still not fully understood. Knowledge of Hg chemistry and speciation in the atmosphere is critical to the understanding of Hg transport and deposition on spatial scales.

1.6 Dissertation Structure

The subsequent chapters of this dissertation present analyses of atmospheric Hg observations in the Lake Champlain and Lake Michigan basins. These chapters are formatted for peer-reviewed publication. Chapter 2 was published in Atmospheric

Environment (Gratz et al., 2009). Chapter 5 was submitted to Environmental Science and Technology in February 2010 and is currently under review (Gratz et al., In Review).

Chapters 2 and 3 explore 12 years of Hg wet deposition measurements at Underhill, VT, a remote location in the Lake Champlain basin. Chapter 2 presents a long-term perspective on Hg wet deposition and meteorological influences at the Underhill site, while Chapter 3 explores the sources of Hg in precipitation at Underhill using multivariate and hybrid-receptor modeling techniques. The predominant hypothesis addressed in these two chapters is that Hg deposition at the remote Vermont location has not declined over time because of consistent transport of elevated amounts of Hg from coal combustion emissions in the industrialized Midwest and East Coast.

In Chapters 4 and 5, the focus shifts to the more urban and industrial Lake Michigan basin. These chapters present analysis of ambient and wet deposited Hg in the region and explore the processes that mercury may undergo in the atmosphere following emission. In Chapter 4, the impact of the Chicago/Gary industrial region on southwest Michigan is examined through analysis of speciated Hg observations and selected case studies which investigate the relative importance of direct RGM transport and chemical production in the atmosphere. It is suggested that Chicago/Gary sources are the dominant contributors to RGM in southwest Michigan during the summer months due to a combination of direct transport of emissions and chemical RGM production in the atmosphere. Chapter 5 summarizes the initial application of Hg isotope analysis to ambient and wet deposited Hg as a new approach to understanding Hg transport and cycling in the atmosphere. Preliminary findings are presented and the potential mechanisms contributing to Hg isotopic variation in the Great Lakes atmosphere are

suggested. The key findings and contributions of these studies are summarized in

Chapter 6 with recommendations for future work.
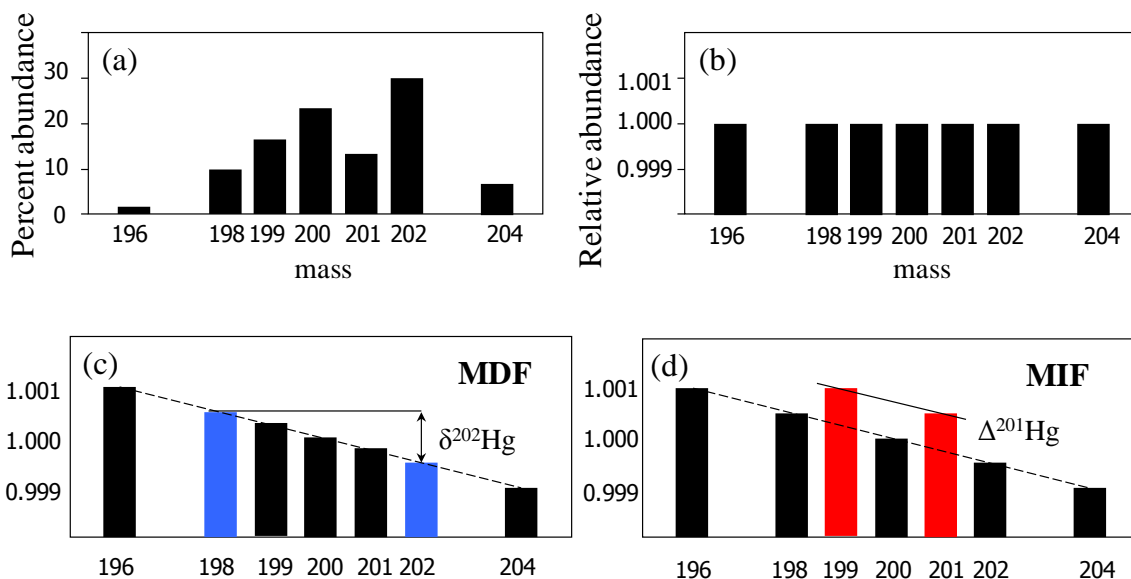
Figure 1.1: The definition of mass-dependent and mass-independent fractionation of Hg isotopes. (a) The natural abundance of Hg isotopes, (b) Hg isotopes normalized to a standard, (c) Mass-dependent fractionation (MDF) represented by δ^{202}Hg in permil (‰), and (d) Mass Independent Fractionation represented by Δ^{201}Hg in permil (‰) (Blum, 2008).

References

Bergquist, B.A., Blum, J.D., 2007. Mass-dependent and mass-independent fractionation of Hg isotopes by photoreduction in aquatic systems. Science 318, 417-420.

Biswas, A., Blum, J.D., Bergquist, B.A., Keeler, G.J., Zhouqing, X., 2008. Natural mercury isotope variation in coal deposits and organic soils. Environmental Science & Technology 42, 8303-8309.

Blum, J.D., 2008. Personal communication.

Buchachenko, A.L., 2001. The magnetic isotope effect: Nuclear spin control of chemical reactions. Journal of Physical Chemistry 105(44), 9995-10011.

Buchachenko, A.L., Ivanov, V.L., Roznyatovskii, V.A., Artamina, G.A., Vorob'ev, A.Kh., Ustynyuk, Yu.A., 2007. Magnetic isotope effect for mercury nuclei in photolysis of bis(p-trifluoromethylbenzyl)mercury. Doklady Physical Chemistry 413, 39-41.

Burgess, N.M., Evers, D.C., Kaplan, J.D., 2005. Mercury and other contaminants in common loons breeding in Atlantic Canada. Ecotoxicology 14, 241-252.

Burke, J., Hoyer, M., Keeler, G.J. and Scherbatskoy, T., 1995. Wet deposition of mercury and ambient mercury concentrations at a site in the Lake Champlain Basin. Water, Air and Soil Pollution 80, 353-362.

Butler, T.J., Cohen, M.D., Vermeylen, F.M., Likens, G.E., Schmeltz, D., Artz, R.S., 2008. Regional precipitation mercury trends in the eastern USA, 1998-2005: Declines in the Northeast and Midwest, no trend in the Southeast. Atmospheric Environment 42, 1582-1592.

Carignan, J., Estrade, N., Sonke, J.E., Donard, O.F.X., 2009. Odd isotope deficits in atmospheric Hg measured in lichens. Environmental Science & Technology 43, 5660-5664.

Carpi, A., 1997. Mercury from combustion sources: A review of the chemical species emitted and their transport in the atmosphere. Water, Air, and Soil Pollution 98, 241-254.

Cohen, M.D., Artz, R.S., Draxler, R.R., 2007. Report to Congress: Mercury Contamination in the Great Lakes. NOAA Air Resources Laboratory, Silver Spring, MD.

Dye, T.S., Roberts, P.T., Korc, M.E., 1995. Observations of transport processes for ozone and ozone precursors during the 1991 Lake Michigan Ozone Study. Journal of Applied Meteorology 34, 1877-1889.

Evers, D.C., Han, Y-J., Driscoll, C.T., Kamman, N.C., Goodale, M.W., Lambert, K.F., Holsen, T.M., Chen, C.Y., Clair, T.A., Butler, T., 2007. Biological Mercury Hotspots in the Northeastern United States and Southeastern Canada. BioScience 57, 29-43.

Forlano, L., Hedgecock, I.M., Pirrone, N., 2000. Elemental gas phase atmospheric mercury as it interacts with the ambient aerosol and its subsequent speciation and deposition. The Science of the Total Environment 259, 211-222.

Gustin, M.S., Lindberg, S.E., Weisberg, P.J., 2008. An update on the natural sources and sinks of atmospheric mercury. Applied Geochemistry 23, 482-493.

Gratz, L.E., Keeler, G.J., Miller, E.K., 2009. Long-term relationships between mercury wet deposition and meteorology. Atmospheric Environment 43, 6218-6229.

Gratz, L.E., Keeler, G.J., Blum, J.D., Sherman, L.S. Isotopic composition and fractionation of mercury in Great Lakes precipitation and ambient air. Environmental Science & Technology, In Review.

Hammerschmidt, C.R., Fitzgerald, W.F., 2006. Methylmercury in Freshwater Fish Linked to Atmospheric Mercury Deposition. Environmental Science and Technology 40, 7764-7770.

Hedgecock, I.M., Pirrone, N., 2001. Mercury and photochemistry in the marine boundary layer-modeling studies suggest the in situ production of reactive gas phase mercury. Atmospheric Environment 35, 3055-3062.

Hoyer, M., Burke, J., Keeler, G., 1995. Atmospheric sources, transport and deposition of mercury in Michigan: Two years of event precipitation. Water, Air, and Soil Pollution 80, 199-208.

Hynes, A.J., Donohue, D.L., Goodsite, M.E., Hedgecock, I.M., 2009. Our current understanding of major chemical and physical processes affecting mercury dynamics in the atmosphere and at the air-water/terrestrial interfaces. In *Mercury Fate and Transport in the Global Atmosphere*; Pirrone, N., Mason, R., Eds; Springer Science + Business Media: New York pp 427-457.

Keeler, G.J., Hoyer, M. E., Lamborg, C.H., 1994. Measurements of atmospheric mercury in the Great Lakes Basin. Mercury pollution: Integration and Synthesis, CRC Press Inc., Florida, pp 231-241.

Keeler, G., Glinsorn, G., Pirrone, N., 1995. Particulate mercury in the atmosphere: Its significance, transport, transformation and sources. Water, Air, and Soil Pollution 80, 159-168.

Keeler, G.J. and Dvonch, J.T., 2005. Atmospheric Mercury: A Decade of Observations in the Great Lakes. In: *Dynamics of Mercury Pollution on Regional and Global Scales: Atmospheric Processes and Human Exposures around the World.* N. Pirrone and K. Mahaffey Eds. Kluwer Ltd.

Keeler, G.J.; Gratz, L.E.; Al-Wali, K., 2005. Long-term atmospheric mercury wet deposition at Underhill, Vermont. Ecotoxicology 14, 71-83.

Keeler, G.J., Landis, M.S., Norris, G.A., Christianson, E.M., Dvonch, J.T., 2006. Sources of mercury wet deposition in Eastern Ohio, USA. Environmental Science and Technology 40, 5874-5881.

Landis, M.S., Keeler, G.J., 2002. Atmospheric mercury deposition to Lake Michigan during the Lake Michigan Mass Balance Study. Environmental Science and Technology 36, 4518-4524.

Landis, M.S., Vette, A.S., Keeler, G.J., 2002. Atmospheric mercury in the Lake Michigan Basin: Influence of the Chicago/Gary urban area. Environmental Science and Technology 36, 4508-4517.

Landis, M.S., Keeler, G.J., Al-Wali, K.I., Stevens, R.K., 2004. Divalent inorganic reactive gaseous mercury emissions from a mercury cell chlor-alkali plant and its impact on near-field atmospheric dry deposition. Atmospheric Environment 38, 613-622.

Lin, C.; Pehkonen, S.O., 1997. Aqueous free-radical chemistry of mercury in the presence of iron oxides and ambient aerosol. Atmospheric Environment 31, 4125-4137.

Lin, C., Pehkonen, S.O., 1999. The chemistry of atmospheric mercury. Atmospheric Environment 33, 2067-2079.

Lin, C.; Pongprueska, P.; Lindberg, S.E.; Pehkonen, S.O.; Byun, D.; Jang, C., 2006. Scientific uncertainties in atmospheric mercury models I: Model science evaluation. Atmospheric Environment 40, 2911-2928.

Lindberg, S.E., Brooks, S., Lin, C.-J., Scott, K.J., Landis, M.S., Stevens, R.K., Goodsite, M., Richter, A., 2002. Dynamic oxidation of gaseous mercury in the arctic troposphere at polar sunrise. Environmental Science & Technology 36, 1245-1256.

Lindberg, S., Bullock, R., Ebinghaus, R., Engstrom, D., Feng, X., Fitzgerald, W., Pirrone, N., Prestbo, E., Seigneur, C., 2007. A synthesis of progress and uncertainties in attributing the sources of mercury in Deposition. Ambio 36 (1), 19-32.

Liu, B., Keeler, G.J., Dvonch, J.T., Barres, J.A., Lynam, M.M., Marsik, F.J., Taylor-Morgan, J., 2007. Temporal variability of mercury speciation in urban air. Atmospheric Environment, 41, 1911-1923.

Liu, B., Keeler, G.J., Dvonch, J.T., Barres, J.A., Lynam, M.M., Marsik, F.J., Taylor-Morgan, J., 2010. Urban-rural differences in atmospheric mercury speciation. Atmospheric Environment 44(16), 2013-2023.

Liu, W., Hopke, P.K., Han, Y., Yi, S., Holsen, T.M., Cybart, S., Kozlowski, K., Milligan, M., 2003. Application of receptor modeling to atmospheric constituents at Potsdam and Stockton, NY. Atmospheric Environment 37, 4997-5007.

Lynam, M.M., Keeler, G.J., 2005. Automated speciated mercury measurements in Michigan. Environmental Science and Technology 39, 9253-9262.

Lynam, M.M., Keeler, G.J., 2006. Source-receptor relationships for atmospheric mercury in urban Detroit, MI. Atmospheric Environment 40, 3144-3155.

Munthe, J.; Xiao, Z.F.; Lindqvist, O., 1991. The aqueous reduction of divalent mercury by sulfite. Water, Air, and Soil Pollution 56, 621-630.

Munthe, J., 1992. The aqueous oxidation of elemental mercury by ozone. Atmospheric Environment 26A, 1461-1468.

Munthe, J., McElroy, W.J., 1992. Some aqueous reactions of potential importance in the atmospheric chemistry of mercury. Atmospheric Environment 26A, 553-557.

Nriagu, J.O., 1989. A global assessment of natural sources of atmospheric trace metals. Nature 338, 47-49.

Pacyna, E.G., Pacyna, J.M., Steenhuisen, F., Wilson, S., 2006. Global anthropogenic mercury emission inventory for 2000. Atmospheric Environment 40, 4048-4063.

Pirrone, N., Keeler, G.J., 1996. The Rouge River watershed pollution by trace elements: Atmospheric depositions and emission sources. Water Science and Technology 33, 267-275.

Pirrone, N., Hedgecock, I.M., Forlano, L., 2000. Role of the ambient aerosol in the atmospheric processing of semivolatile contaminants: A parameterized numerical model (Gas-Particle Partitioning (GASPAR)). Journal of Geophysical Research – Atmospheres 105, 9773-9790.

Poirot, R.L., Wishinski, P.R., Hopke, P.K., Polissar, A.V., 2001. Comparative Application of Multiple Receptor Methods to Identify Aerosol Sources in Northern Vermont. Environmental Science and Technology 35, 4622-4636.

Poissant, L., Pilote, M., Beauvais, C., Constant, P., Zhang, H.H., 2005. A year of continuous measurements of three atmospheric mercury species (GEM, RGM, and Hg_p) in southern Quebec, Canada. Atmospheric Environment 39, 1275-1287.

Polissar, A.V., Hopke, P.K., Poirot, R.L., 2001. Atmospheric Aerosol over Vermont: Chemical Composition and Sources. Environmental Science and Technology 35, 4604-4621.

Rea, A.W., Keeler, G.J., Scherbatskoy, T., 1996. The deposition of mercury in throughfall and litterfall in the Lake Champlain watershed: A short-term study. Atmospheric Environment 30, 3257-3263.

Schauble, E.A., 2007. Role of nuclear volume in driving equilibrium stable isotope fractionation of mercury, thallium, and other very heavy metals. Geochimica et Cosmochimica Acta 71, 2170-2189.

Schroeder, W.H., Munthe, J., 1998. Atmospheric mercury - An overview. Atmospheric Environment 32, 809-822.

Seigneur, S; Wrobel, J.; Constantinou, E., 1994. A chemical kinetic mechanism for atmospheric inorganic mercury. Environmental Science and Technology 28, 1589-1597.

Seigneur, C., Lohman, K., Vijayaraghavan, K., Jansen, J., Levin, L., 2006. Modeling atmospheric mercury deposition in the vicinity of power plants. Journal of Air and Waste Management 56, 743-751.

Sherman, L.S., Blum, J.D., Johnson, K.P., Keeler, G.J., Barres, J.A., Douglas, T.A., 2010. Mass-independent fractionation of mercury isotopes in Arctic snow driven by sunlight. Nature Geoscience 3, 173-177.

Slemr, F., Schuster, G., Seiler, W., 1985. Distribution, speciation, and budget of atmospheric mercury. Journal of Atmospheric Chemistry 3, 407-434.

Turro, N.J., 1983. Influence of nuclear spin on chemical reactions: Magnetic isotope and magnetic field effects (A review). Proceedings of the National Academy of Sciences 80, 609-621.

U.S. Environmental Protection Agency (U.S. EPA), 1994. An Introduction to the Issues and the Ecosystems. EPA-453/B-94/030, Office of Air Quality Planning and Standards: Durham, NC.

U.S. Environmental Protection Agency (U.S. EPA), 1997. *Mercury Study Report to Congress;* EPA-452/R-97-003; Office of Air Quality Planning and Standards, Office of Research and Development: Washington DC.

U.S. Environmental Protection Agency (U.S.EPA) 2005 National Emissions Inventory (NEI) Data and Documentation (www.epa.gov/ttnchie1/net/2005inventory.html).

U.S. Environmental Protection Agency (U.S. EPA). Controlling Power Plant Emissions. (http://www.epa.gov/mercury/control_emissions/index.htm).

Vette, A.S., Landis, M.S., Keeler, G.J., 2002. Deposition and emission of gaseous mercury to and from Lake Michigan during the Lake Michigan Mass Balance Study (July, 1994 – October, 1995). Environmental Science and Technology 36, 4525-4532.

White, E.M.; Keeler, G.J.; Landis, M.S., 2009. Spatial variability of mercury wet deposition in Eastern Ohio: Summertime meteorological case study analysis of local source influences. Environmental Science and Technology 43, 4946-4953.

CHAPTER 2

Long-Term Relationships Between Mercury Wet Deposition and Meteorology

Abstract

Daily-event precipitation samples collected in Underhill, VT from 1995-2006 were analyzed for total mercury and results suggest that there were no statistically significant changes in annual mercury wet deposition over time, despite significant emissions reductions in the Northeast United States. Meteorological analysis indicates that mercury deposition has not decreased as transport of emissions from major source regions in the Midwest and East Coast have consistently contributed to the largest observed mercury wet deposition amounts over the period. In contrast, annual volume-weighted mean (VWM) mercury concentration declined slightly over the 12-years, and a significant decrease was observed from CY 2001-2006. An increase in the total annual precipitation amount corresponded with the decline in annual VWM mercury concentration. Analysis suggests that the increase in precipitation observed was strongly related to changes in the amount and type of precipitation that fell seasonally, and this departure was attributed to a response in meteorological conditions to climate variability and the El Niño-Southern Oscillation (ENSO) cycle. Increased amounts of rainfall and mixed precipitation (mixture of rainfall and snowfall), particularly in the spring and fall seasons, enhanced annual precipitation amounts and resulted in declining VWM mercury concentrations

during these periods. Thus, declines in concentration at the more remote Underhill site appear to be more directly linked to local scale meteorological and climatological variability than to a reduction in emissions of mercury to the atmosphere.

2.1. Introduction

Mercury is a hazardous air pollutant and bioaccumulative neurotoxin. It is a naturally occurring element in the earth's crust released to the atmosphere by natural and anthropogenic sources. Anthropogenic emissions, including combustion, manufacturing, agricultural burning, and mobile sources (U.S. EPA, 1997), are the most significant source of mercury to the environment (Schroeder and Munthe, 1998). In the United States, fossil fuel combustion is the most significant anthropogenic source of atmospheric mercury (U.S. EPA, 1997).

Mercury exists in three main forms in the atmosphere: gaseous elemental mercury (Hg^0), fine particle bound mercury (Hg_p), and divalent reactive gaseous mercury (RGM). Hg^0, the primary form of mercury in the atmosphere, is not very water soluble (Carpi, 1997; Schroeder and Munthe, 1998). Hg(p) and RGM (collectively Hg(II)), however, are very water soluble and much more reactive than Hg^0. Hg(II) is removed readily through wet and dry deposition (Lin and Pehkonen, 1999) whereas Hg^0 can travel long distances before being oxidized to Hg(II) and depositing (Schroeder and Munthe, 1998).

Oxidation of gaseous Hg^0 through photochemistry or reactions with ozone (O_3), hydroxyl radical (OH), and reactive halogens is likely the first step in mercury removal from the atmosphere (Lin et al., 2006). Dry deposition of Hg^0 may also be an important removal mechanism (Schroeder and Munthe, 1998; Lin et al., 2006). Reduction of Hg(II)

21

to Hg^0 leads to additional transport away from sources but is dependent on the particular $Hg(II)$ species involved, given that each has its own kinetic properties. The relative predominance of these reactions varies based on the availability of the oxidizing and reducing species, as well as meteorological conditions and source emissions (Lin et al, 2006). Therefore, the relative amounts of Hg^0 and $Hg(II)$ in the atmosphere vary seasonally and geographically, impacting the amount of mercury available to be removed through wet deposition.

Given the continued growth in worldwide industrialization and energy use, quantification of mercury emissions, transport, and deposition is vital to understanding the impact of mercury pollution on the environment and society. Currently, most states in the United States have fish consumption advisories due to mercury contamination in lakes and rivers. Consequently, the Great Waters Program was created under the Clean Air Act Amendments of 1990 to mandate measurements of mercury wet deposition in the Great Lakes, Lake Champlain, the Chesapeake Bay and other selected coastal waterways (U.S. EPA, 1994). This program prompted the initial monitoring efforts in Underhill, VT.

In 1998, the Northeast Governors and Eastern Canadian Premiers formed a task force to eliminate regional anthropogenic sources of mercury. Mercury emissions in the northeastern United States consequently declined from 15.9 ton/yr to 4.7 ton/yr from 1998-2002 (NESCAUM, 2005). These reductions occurred primarily due to the nationwide U.S. EPA rule that required 95% reductions in municipal and medical waste combustion emissions, previously two of the largest anthropogenic sources of mercury in the Northeast. Municipal waste combustion currently comprises 22% of all mercury

emissions in the Northeast. Other major emitters in the Northeast include electric utility boilers, residential heating, and sewage sludge incinerators; however, emissions from these sources have not declined as significantly (NESCAUM, 2005).

Mercury emissions across the United States also decreased throughout the 1990s by approximately 100 tons, primarily due to reductions in waste incineration emissions (Cohen et al., 2007), and more substantial declines occurred in the Northeast than the Midwest (Butler et al., 2008). Emissions from utility coal boilers, industrial boilers, and other major anthropogenic sources in the United States remained relatively constant from the early 1990s to 2002 (Cohen et al., 2007; Butler et al., 2008).   Today, elevated levels of mercury in fish and wildlife remain a persistent problem in the Northeast states, with much of the contamination attributed to atmospheric deposition (Hammerschmidt and Fitzgerald, 2006; Evers et al., 2007). Therefore, despite regulatory achievements, there is still much to be understood about mercury emissions, transport, and deposition in the United States.

Mercury wet deposition measurements at Underhill represent one of the longest running mercury records to date. An earlier analysis from 1993-2003 showed no statistically significant linear trend in mercury deposition, and identified important seasonal and meteorological relationships with mercury wet deposition. In addition, the highest deposition events were largely associated with air mass transport from the Ohio River Valley region (Keeler et al., 2005).

The present manuscript examines long-term patterns in precipitation, mercury concentration and wet deposition at Underhill from 1995-2006. Relationships between mercury in precipitation and local meteorology, including temperature, precipitation

amount, and precipitation type, are used to interpret the observations. In light of recent studies showing the impact of climate variability and large scale meteorological phenomena on precipitation in the Northeast (Barlow et al., 2000; Patten et al., 2003; Huntington and Hodgkins, 2004; Griffiths and Bradley, 2007), seasonal and local scale climate variability are also examined at Underhill in conjunction with mercury deposition measurements. Through these analyses, the unique Underhill precipitation record is used to examine the influence of meteorological parameters on mercury deposition over time.

2.2. Methodology

2.2.1 Site Description

The Underhill site is located on the west slope of Mount Mansfield at the Proctor Maple Research Center (PMRC) (elevation 399m), approximately 25 km east of Lake Champlain (Figure 2.1). Daily-event wet-only precipitation samples were collected for mercury and trace elements in collaboration with the Vermont Monitoring Cooperative (VMC) using a modified MIC-B (MIC, Thornhill, Ontario) automatic precipitation collector (Landis and Keeler, 1997). Sample collection commenced at Underhill in December 1992 and continued through September 2007.

2.2.2 Sampling and Analysis

When sample collection began in 1992, precipitation was collected into 10 L borosilicate glass bottles through a Teflon-coated funnel in the MIC-B wet-only collector. In September 1994, the sampling train was redesigned and replaced with separate sampling trains for mercury and trace elements, as described in Landis and Keeler (1997). The sampling trains minimized enrichment of trace elements in precipitation samples, and reduced effects caused by the absorptive behavior of trace metals to the

walls of the sampling bottles (Church et al., 1984). The mercury sampling train consisted of a borosilicate glass funnel (collection area 191 ± 9 cm^2), a Teflon adapter with a glass vapor lock to prevent loss of mercury from the samples, and a 1L Teflon bottle. The trace element sampling train consisted of a polypropylene funnel (collection area 167 ± 7 cm^2), a polypropylene adapter, and a 1L polypropylene bottle. Due to the change in sample collection technique in 1994, only data from the 12 complete years of consistent sample collection (1995-2006) will be discussed in this manuscript.

All field supplies were rigorously prepared at the University of Michigan Air Quality Laboratory (UMAQL), and after collection samples were shipped back to the UMAQL for processing and analysis. The sampling trains were prepared in an 11-day acid-cleaning procedure (Landis and Keeler, 1997) and were replaced after individual precipitation events. Precipitation samples were processed at the UMAQL using clean techniques and were analyzed for mercury using cold-vapor atomic fluorescence spectrometry (CVAFS) (Keeler et al., 2005).

Precipitation amounts derived from samples collected at Underhill were compared with the on-site National Weather Service standard 8-inch rain gauge, and results indicated that the MIC-B precipitation collection agreed with the NWS rain gauge to within 1% (Miller et al., in prep.), confirming that the MIC-B is effective in collecting precipitation. In this study event precipitation depths were calculated using MIC-B measured sample volumes and the average recorded funnel area. All precipitation samples greater than 0.10 cm were included in this data analysis. Only 81 of 1,236 (6.5%) samples collected were excluded, and no statistically significant trends were observed in the concentration or deposition for these low volume samples.

2.2.3 Statistical Analysis

Precipitation samples collected at Underhill were examined on annual and seasonal time scales for the 12-year period (1995-2006) and the recent six-year period (2001-2006). Seasons were determined using true dates of solstice and equinox for each year. The statistical significance of changes in annual and seasonal precipitation depth, VWM mercury concentration, and mercury wet deposition were determined using linear regression and ANOVA tests (SPSS V16.0). Wilcoxon and Kruskal-Wallis tests were also used to determine if mercury deposition was significantly different among individual meteorological clusters (SAS V9.1).

2.2.4 Meteorological Data

Meteorological data for the Underhill site, including ambient temperatures and tipping bucket rain gauge data, was provided by the PMRC Basic Meteorological Monitoring program. Data was recorded on hourly intervals prior to July 1998, and every 15 minutes from July 1998 onward. The hour of maximum precipitation for each event was determined from the tipping bucket rain gauge. Belfort rain gauge charts were used when tipping bucket data was unavailable. Precipitation type was categorized as rain, snow, or mixed precipitation (mixture of rainfall and snowfall) by an on-site operator.

Air mass transport to the Underhill site was modeled using the Hybrid Single-Particle Lagrangian Integrated Trajectory (HYSPLIT) Model Version 4.8 (Draxler and Hess, 1997). HYSPLIT back trajectories were calculated using the National Weather Service's National Center for Environmental Prediction (NCEP) Nested Grid Model (NGM) for 1995-1996 and the Eta Data Assimilation System (EDAS) for 1997-2006. Data was obtained from the National Oceanic and Atmospheric Administration's Air

Resources Laboratory (NOAA-ARL). The hour of maximum precipitation was used as the starting time for each trajectory. The starting height was set to one-half of the mixed-layer height, as determined from upper-air soundings, in order to best represent air mass transport within the boundary layer. Cluster analysis was performed using Ward's Minimum-Variance method (Ward, 1963; Moody and Samson, 1989; Landis et al., 2002). Clusters were determined using trajectory endpoints as well as the mean on-site temperature on the day of the event, the total precipitation amount, and the precipitation type associated with each event. While three-day back-trajectories are often used to represent regional transport regimes, two-day back trajectories were used here due to the frequency of missing data points associated with three-day back trajectories which would have reduced the number of precipitation samples used in the cluster analysis. A comparison of the calculated two- and three-day clusters resulted in equivalent transport regimes and thus, the choice of trajectory length did not have a significant impact on the findings discussed in the next section.

2.3 Results and Discussion

2.3.1 1995-2006

There were 1,155 daily-event precipitation samples collected at Underhill from 1995-2006. The annual VWM mercury concentration and total wet deposition for 1995-2006 are shown in Figure 2.2. Error bars were calculated using 8.1% uncertainty in the measured concentration (Landis and Keeler, 1997) and 5% uncertainty in the precipitation depth (Keeler et al., 2006). The VWM mercury concentration for 1995-2006 was 8.3±0.7 ng/L and the mean event mercury wet deposition was 0.10±0.01 μg/m^2. The range in sample concentration was 0.9 ng/L – 90.5 ng/L. On average 96 samples

were collected each year, and the average event precipitation depth was 1.24±0.06 cm. The highest annual mercury deposition occurred in 1998 and 2004. These were two of the wettest years of the period as well, partially explaining the elevated deposition. CY 1998 also had the greatest number of events collected (n=124) and the highest average annual temperature (8.1°C for the entire year; 10.0°C on days when precipitation occurred). In both years, approximately 80% of the total precipitation fell as rain, whereas for the other 10 years only 70% of the total precipitation was in the form of rain, on average. This suggests that meteorological parameters, including temperature, precipitation amount, and precipitation type were important in controlling the wet removal of mercury from the atmosphere.

From 1995-2006, annual precipitation amount at Underhill increased significantly by 3.9 cm/year (4.2%/yr; r^2=0.43; p=0.02). Annual VWM mercury concentrations declined slightly by 0.1 ng/L/yr (1.4%/yr) from 1995-2006 but the relationship was not significant (r^2=0.21; p=0.14). Total annual deposition measured at Underhill did not change significantly over the 12-year period (r^2=0.08, p=0.36).

Analysis of weekly precipitation samples collected by the Mercury Deposition Network (MDN) indicated a decline in VWM concentration at four of 12 sites in New England from 1998-2005 (Butler et al., 2008). A significant 1.7% per year decline in concentration was observed (14±4% over the eight-year period) (Butler et al., 2008). Although the decline in concentration at Underhill was not significant from 1995-2006, or from 1998-2005, a statistically significant decline of 0.6 ng/L/yr (6%/yr) was observed during the second half of the study (2001-2006).

A significant decline in mercury wet deposition was not observed at the MDN sites (Butler et al., 2008) or at Underhill. The coincident decrease in VWM concentration and increase in precipitation amount at Underhill suggests that a relatively constant amount of mercury was available for scavenging in an increasing amount of precipitation, resulting in declining annual concentrations. This observation begs the question of why mercury wet deposition was approximately constant during a period of reported emission reductions for waste incinerators (USEPA, 2005). Because mercury emissions from waste incineration are primarily $Hg(II)$ (Carpi, 1997; Dvonch et al., 1999), and $Hg(II)$ is readily deposited (Lin and Pehkonen, 1999; White et al. 2009), it is logical to predict that a substantial emissions reduction in New England region would have had a measurable impact on mercury deposition in many of the Northeast States. However, such a decline was not observed in northern Vermont based upon analysis of the daily-event deposition data from Underhill. Analysis of the prevailing flow regimes and upwind history of air masses associated with the largest mercury deposition events suggests that the consistent annual deposition may be due to the dominance of regional transport from mercury sources in high-density source regions where there are numerous source types that have not reported declines as significant as the waste incineration sector over the course of the study.

Studies of mercury deposition in the northeastern United States have identified major source regions as the Midwest and East Coast (Han et al., 2005; Choi et al., 2008), demonstrating the importance of transport on mercury deposition. To elucidate the impact of source regions on the Underhill site, cluster analysis was performed on HYSPLIT two-day back trajectories from 1995-2006. Sixteen clusters were computed,

explaining 76% of the variance in the data. Wilcoxon and Kruskal-Wallis tests indicated that the mercury deposition was significantly different among individual clusters (p<0.0001). The clusters with the highest mean and median wet deposition at the Underhill site represented transport from the Midwest and East Coast in conjunction with rainfall and average temperatures ranging from 4.9°C to 27.2°C (Figures 2.3 a-c; Table 2.1). The clusters with the lowest mean and median event wet deposition displayed transport from the northwest and southwest when average temperatures were between -22.4° C and 6.7° C and predominantly snowfall or mixed precipitation was recorded (Figures 2.3 d-f; Table 2.1). Although southwest transport was observed in both the highest and lowest deposition clusters, lower wet deposition was accompanied with advection of cold air and snowfall. Similar to earlier studies (Hoyer et al 1995), the cluster analysis indicates that the meteorological conditions leading up to and during precipitation events are critical factors for understanding deposition amounts. These results also demonstrate the importance of regional transport to Underhill from sources south and southwest of the site.

To statistically determine whether the largest mercury deposition amounts were consistently associated with transport from these major source regions over time, cluster analysis of back trajectories was performed on individual years. In each year from 1995-2006, the meteorological clusters with the highest mean deposition were associated with precipitation falling as rainfall, average on-site temperatures above 10°C, and transport from the Midwest or East Coast. The clusters with the lowest mean deposition were associated primarily with northwesterly flow, average on-site temperatures below 5°C and snowfall or mixed precipitation. Thus, the dominant transport regimes and air mass

history associated with the highest deposition events at Underhill did not change appreciatively from year to year, and consequently, the annual deposition amounts did not decrease.

Finally, cluster analysis was also performed on individual seasons to further examine the effect of meteorological conditions on deposition patterns. In all seasons, the clusters with the highest mean mercury deposition occurred with southerly or southwesterly flow and warm air advection to the region. In winter the highest deposition clusters had average temperatures at the site above 0°C, southwesterly transport, and either rainfall or mixed precipitation. The lowest deposition clusters displayed temperatures less than -4°C, northerly flow, and either snowfall or mixed precipitation. In the summertime, when all precipitation was in the form of rainfall, the highest deposition clusters had average temperatures between 12°C and 24°C with southerly or southwesterly flow, and the lowest deposition occurred with temperatures between 8°C and 20°C with either easterly or northwesterly transport. The mean mercury deposition for the summertime clusters was three times greater than the clusters with the highest mean deposition in winter. Therefore, the combined effects of temperature, transport regime (upwind history including pathway and air mass characteristics), and precipitation type were critical in determining wet deposition amounts at Underhill. These factors are also important when considering the physicochemical transformations that occur en route between source and receptor.

Relationships between temperature, precipitation type, and mercury wet deposition at this site were reported previously (Keeler et al. 2005). Temperature is a critical parameter in the atmospheric chemistry of mercury and plays a major role in

determining the speciation and amount of mercury that reaches the site (Han et al, 2004; Lynam and Keeler, 2006). Temperature appears weakly correlated to deposition on an event basis, but is more strongly correlated on monthly time scales (r^2=0.50; Figure 2.4), indicating that the temperature at the site on the day of each event may not be as important as the regional, upwind meteorology in determining total deposition amounts. Mercury wet deposition is also highly seasonal, with greater wet deposition observed during the warmer months (Figure 2.4), suggesting the importance of both mercury speciation and the removal efficiency of different precipitation types.

RGM is typically higher when temperatures are warm and during periods of increased photo-oxidation of Hg^0 (Liu et al. 2007; Lynam and Keeler, 2006). RGM is also readily removed by precipitation (Lin and Pehkonen, 1999; White et al. 2009). In contrast, during cold winter months particulate mercury is somewhat elevated at Underhill (Burke et al. 1995), and VWM mercury concentrations and wet deposition are noticeably lower. The relationship between precipitation type and mercury wet deposition is, in part, due to the fact that rain is more efficient than snow in scavenging mercury from the atmosphere (Hoyer et al., 1995; Landis et al., 2002; Keeler et al., 2006). Over 80% of the mercury wet deposition at Underhill was in the form of rain, with only 5% depositing as snow, and 12% as mixed precipitation. Figure 2.5 shows the VWM mercury concentration and number of samples collected for different ranges of precipitation amount for each precipitation type. For a given precipitation amount, rain appears more efficient at removing mercury from the atmosphere than mixed precipitation or snowfall, further suggesting that precipitation type is one of many

important factors determining the concentration of mercury in precipitation, and ultimately the amount of mercury that will deposit to the surface during a given event.

2.3.2 2001-2006

The 12-year record from Underhill was divided into two six-year segments (1995-2000 and 2001-2006) to further examine changes in mercury deposition and meteorology over time and determine the cause for the recently observed increase in annual precipitation amount. The first six years of data (1995-2000) did not show any significant variability in precipitation amount, VWM mercury concentration, or total mercury wet deposition. However, from 2001-2006 there was an approximately 0.6 ng/L/yr decline in VWM concentration (6%/yr; $r^2 = 0.79$; p=0.02) and an 11.3 cm/yr increase in total precipitation amount (12%/yr; $r^2 = 0.78$; p=0.02). The decline in VWM concentration coincided with the increase in precipitation amount starting in 2001, and both changes were significant. There was no significant change in the annual total deposition from 2001-2006. The highest concentrations were typically observed with low precipitation amounts (Figure 2.5), suggesting that at this remote site most of the mercury was removed during the onset of precipitation, and additional precipitation acted to dilute samples throughout the remainder of the event. This relationship was consistent among all precipitation types (Figure 2.5), suggesting that the observed decline in concentration from 2001-2006 was likely caused by the increase in annual precipitation amount.

To determine whether the increase in annual precipitation amount from 2001-2006 was isolated to the Underhill site or was in fact a regional phenomenon, annual precipitation totals from the PMRC and five regional airports (NCDC) were examined (Figure 2.6). These airports were chosen because of their proximity to Underhill and the

availability of data for the time period of interest. All sites showed an increase in annual precipitation amount from 2001-2006 of 10.8 cm/year on average (r^2=0.92). This rate of change was equivalent to the change observed at Underhill (11.3 cm/yr) considering the 5% uncertainty in the precipitation depth measurement. Precipitation measurements from the other sites indicate that the increase was prevalent throughout the Northeast (Figure 2.6). Further examination demonstrates that the greatest increase occurred in spring (April-May) and fall (October-November) months, indicating a possible change in the form and duration of precipitation during these seasons. This analysis was extended to airports across the Midwest and East Coast, and results indicate that the increase in precipitation from 2001-2006 was primarily isolated to the Northeast states. Although annual precipitation increased slightly at stations in New Jersey and eastern Pennsylvania (6.9 cm/yr; r^2=0.55) primarily in spring and fall, on average there was no change in annual precipitation for the Midwest or other East Coast locations examined here. Therefore, the decline in concentration at Underhill cannot be attributed to an increase in upwind wet removal of mercury in the high emission source regions.

A significant increase in the frequency of large volume precipitation samples collected at Underhill may further explain the increase in annual precipitation amount (Figure 2.7). The precipitation sampling train was capable of collecting up to 2 inches (5.08 cm) of precipitation into a 1L bottle. While the mean sample volume for the 12-year period was 237 mL (0.5 in; 1.27 cm), from 2001-2006, there was a nearly three-fold increase in the number of daily-event samples with at least 500 mL (1 inch; 2.54 cm) of precipitation. The number of samples collected each year from 1995-2006 did not change significantly, potentially indicating longer duration periods of precipitation that

lead to larger volumes being collected into individual daily-event samples. Because large volume events at Underhill typically lead to equivalent amounts of mercury diluted within a given sample, the decline in annual VWM mercury concentration was more likely influenced by an increase in the number of large precipitation events rather than a decline in atmospheric mercury available to be removed by precipitation.

Changes in precipitation type were also examined from 2001-2006 (Figure 2.8). While there were no statistically significant changes in the annual amounts of rainfall or snowfall from 1995-2006, the annual mixed precipitation amount increased significantly by 1.7 cm/yr ($r^2 = 0.75$; p=0.0003) from 1995-2006. From 2001-2006, rainfall increased by 9.0 cm/yr ($r^2=0.58$; p=0.082), mixed precipitation increased by 3.1 cm/yr ($r^2=0.89$; p=0.005), and both changes were statistically significant. Snowfall did not change significantly from 2001-2006. While additional years of data may be required to detect a statistically significant trend in annual snowfall, the increase in mixed precipitation and rainfall may indicate important changes in meteorology both seasonally and annually.

2.3.3 Observations of Local Climate Variability

Changes in the form and amount of precipitation received at a given site may signal changes in the local or regional climate (Huntington and Hodgkins, 2004; Griffiths and Bradley, 2007). To investigate the presence of local scale climate variability at the Underhill site, precipitation amounts were examined with respect to precipitation type and season. Not unexpectedly, there were no significant year to year changes in any precipitation type during summer or winter, but spring and fall showed interesting variability (Figure 2.9).

From 1995-2006, spring rainfall amount increased significantly by 1.8 cm/yr ($r^2 =$ 0.43; p=0.02) (Figure 2.9a). From 2001-2006, this change was more extreme with an increase of 5.4 cm/yr ($r^2 = 0.83$; p=0.012). There were no significant springtime patterns for mixed precipitation or snowfall amounts from 1995-2006 or from 2001-2006. However, it is interesting to note that there was no springtime snowfall observed in 2003, 2005, and 2006. A lack of recorded spring snowfall did not occur in any year prior to 2003. In the fall from 1995-2006, mixed precipitation amount increased significantly by 1.3 cm/yr ($r^2 = 0.82$; p=0.0001; Figure 2.9b). There was an even greater increase in mixed precipitation amount of 1.5 cm/yr ($r^2 = 0.69$; p=0.04) from 2001-2006. However, there were no significant changes in fall snowfall or rainfall amounts.

Significant changes in VWM concentration were observed from 1995-2006 and 2001-2006. From 1995-2006 the spring VWM concentration for rainfall declined significantly by 0.6 ng/L/yr (r^2=0.65; p=0.002) (Figure 2.9c). From 2001-2006, the spring VWM concentration declined for rainfall (0.9 ng/L/yr; r^2=0.75; p=0.08) and mixed precipitation (1.5 ng/L/yr; r^2=0.59; p=0.07) (Figure 2.9c). Fall VWM also decreased for rainfall (1.1 ng/L/yr; r^2=0.59; p=0.07) from 2001-2006 (Figure 2.9d).

Changes in total mercury deposition from 1995-2006 and 2001-2006 for any precipitation type or season were not significant (Figures 2.9e-f), with the exception of fall mercury deposition from mixed precipitation, which increased significantly from 1995-2006 by 0.05 μg/m^2/yr (r^2=0.44; p=0.02).

This analysis shows that changes in seasonal precipitation type and amount from year to year may have in part contributed to the observed increase in annual precipitation amount and the subsequent decline in VWM concentration. Further analysis

demonstrates that in addition to local scale climate variability, other large scale meteorological phenomena may also be influencing changes in annual precipitation as well as the duration and volume of individual daily-events.

2.3.4 Impacts of the ENSO Cycle on Precipitation

Changes in annual precipitation associated with the El Niño -Southern Oscillation (ENSO) cycle are an indication of climate variability on a larger scale (Barlow et al., 2000; Patten et al., 2003). The increased frequency of El Niño in recent years is a possible explanation for the increase in annual precipitation amount and large volume events from 2001-2006 at Underhill. Acknowledging that there is limited data from this study to perform a long-term analysis, the data available does allow us to hypothesize on the relationship between ENSO and the observed increase in precipitation amount at Underhill.

ENSO is a phenomenon associated with changes in sea surface pressure that alter the general circulation of the equatorial Pacific and significantly impact global weather patterns. El Niño events typically occur every 3-7 years. During this time, some regions of the world experience increased precipitation while others experience increased drought (Rohli and Vega, 2008). The meteorological impacts of ENSO vary across the United States (Meehl et al., 2007). Although the relationship to El Niño is not as strongly observed in the Northeast as in the southern and central United States, stronger events can alter the jet stream flow enough to have a noticeable impact on the Northeast (Rohli and Vega, 2008).

Research on ENSO is often focused on wintertime variability because this is when ENSO conditions are most extreme; however there is potential for ENSO to impact

summertime meteorology as well (Barlow et al., 2000). This may be due to a significant lag time between the peak of El Niño and the time at which the meteorological patterns in the Northeast United States are most strongly impacted. During El Niño years in the Northeast, there is often increased precipitation in June, with slightly drier conditions in July and very dry conditions in August (Barlow et al. 2000). As the frequency and intensity of El Niño vary over time, there is an apparent general shift in the El Niño teleconnections, or the large scale impacts of this climatological anomaly, toward the north and east in the United States (Meehl et al., 2007).

The ENSO cycle for 1995-2006 was quantified using the Southern Oscillation Index (SOI), where an SOI less than -1 represents El Niño and an SOI larger than +1 represents La Niña (NOAA Climate Prediction Center; Rohli and Vega, 2008). By this analysis, a powerful El Niño occurred in 1997-1998, which had a significant impact on global weather patterns. Following this event, there was an extended La Niña from mid 1998 through early 2001. Although El Niño episodes typically occur every 3-7 years, an El Niño occurred every other year from 2001-2007 (NOAA Climate Prediction Center) (Figure 2.10). These periods coincide with the variability in precipitation from 1995-2006 at Underhill, both in the annual precipitation amount (Figure 2.2) and the annual frequency of large volume daily-event samples (Figure 2.11). Figure 2.11 shows the number of large volume daily-events (sample volume >500mL) occurring each month from 1995-2006, with El Niño years (red) distinguished from La Niña (blue) and neutral years (black; no fill), and 1995-2000 (squares) distinguished from 2001-2006 (triangles). Note that during La Niña and neutral years, Underhill typically experienced 1-2 large volume daily-events. During El Niño years, Underhill often received 2-6 large volume

38

daily-events, especially from 2001-2006. These events mostly occurred from May-September. Additionally, t-tests showed that significantly more summer rainfall was recorded during El Niño years as compared to La Niña or neutral years (p=0.07). While more extensive analysis is necessary in order to identify a clear linkage between ENSO and the precipitation patterns observed at Underhill, the data does indicate that more extended periods of rain and/or higher rainfall amounts occurred in the summer months of El Niño years, which consequently contributed to the increase in annual precipitation and the decline in VWM concentration.

2.4 Conclusions

Analysis of 12 years of daily-event precipitation samples shows that although the VWM mercury concentration has declined at Underhill, VT, there has not been a significant change in mercury wet deposition. Meteorological transport analysis suggests that the largest contributors to mercury wet deposition at Underhill are sources in the Midwest and East Coast regions, and the influence of these source regions has not changed significantly over the years studied. This apparently consistent atmospheric input from the high emission source areas is likely responsible for the observed lack of decline in mercury wet deposition at Underhill. Changes in the type and amount of precipitation at the Underhill site are also playing a critical role in determining mercury concentrations in precipitation.

While the decline in mercury concentration at Underhill could be attributed to a combination of emission reductions and increased precipitation over time, this analysis indicates that changes in the local meteorological factors are a more dominant influence in this decline. Since mercury is a persistent, bioaccumlative toxic pollutant only a

decline in the total mercury deposition can demonstrate the efficacy of any reduction in atmospheric mercury emissions. Thus, investigating trends in precipitation concentration data must be performed with great care as to not falsely ascribe variability in concentration to changes in pollutant emissions. Future receptor modeling of daily-event trace element deposition data at Underhill will identify the major source types contributing to mercury measured in precipitation, and elucidate how these source influences have changed over time, the results of which will aid in further explaining the observed patterns in mercury wet deposition.

References

Barlow, M., Nigam, S., Berbery, E.H., 2000. ENSO, Pacific Decadal Variability, and U.S. Summertime Precipitation, Drought, and Stream Flow. Journal of Climate 14, 2105-2128.

Butler, T.J., Cohen, M.D., Vermeylen, F.M., Likens, G.E., Schmeltz, D., Artz, R.S., 2008. Regional precipitation mercury trends in the eastern USA, 1998-2005: Declines in the Northeast and Midwest, no trend in the Southeast. Atmospheric Environment 42, 1582-1592.

Burke, J.B., Hoyer, M.E., Keeler, G.J., Scherbatskoy, T., 1995. Wet Deposition of mercury and ambient mercury concentrations at a site in the Lake Champlain Basin. Water, Air, and Soil Pollution 80, 353-362.

Carpi, A., 1997. Mercury from combustion sources: A review of the chemical species emitted and their transport in the atmosphere. Water, Air, and Soil Pollution 98, 241-254.

Choi, H-D., Sharac, T.J., Holsen, T.M., 2008. Mercury deposition in the Adirondacks: A comparison between precipitation and throughfall. Atmospheric Environment 42, 1818-1827.

Church, T.M., Tramontano, J.M., Scudlark, J.R., Jickells, T.D., Tokos, J.J., Knap, A.H., Galloway, J.N., 1984. The wet deposition of trace-metals to the western Atlantic Ocean at the mid-Atlantic coast and on Bermuda. Atmospheric Environment 18, 2657-2664.

Cohen, M.D., Artz, R.S., Draxler, R.R., 2007. Report to Congress: Mercury Contamination in the Great Lakes. NOAA Air Resources Laboratory, Silver Spring, MD.

Draxler, R.R. and Hess G.D., 1997. Description of the HYSPLIT_4 Modeling System. NOAA TECHNICAL MEMORANDUM ERL ARL-224.

Dvonch, J.T., Graney, J.R., Keeler, G.J., and Stevens, R.K. Utilization of Elemental Tracers to Source Apportion Mercury in South Florida Precipitation. Environmental Science and Technology 33, 4522-4527. 1999.

Evers, D.C., Han, Y-J., Driscoll, C.T., Kamman, N.C., Goodale, M.W., Lambert, K.F., Holsen, T.M., Chen, C.Y., Clair, T.A., Butler, T., 2007. Biological Mercury Hotspots in the Northeastern United States and Southeastern Canada. BioScience 57, 29-43.

Environment Canada 2007 National Pollutant Release Inventory (NPRI) (www.ec.gc.ca/inrp-npri/).

Griffiths, M.L., Bradley, R.S., 2007. Variations of Twentieth-Century Temperature and Precipitation Extreme Indicators in the Northeast United States. Journal of Climate 20, 5401-5417.

Hammerschmidt, C.R., Fitzgerald, W.F., 2006. Methylmercury in Freshwater Fish Linked to Atmospheric Mercury Deposition. Environmental Science and Technology 40, 7764-7770.

Han, Y-J., Holsen, T.M., Lai, S-O., Hopke, P.K., Yi, S-M., Liu, W., Pagano, J., Falanga, L., Milligan, M., Andolina, C., 2004. Atmospheric gaseous mercury concentrations in New York State: relationships with meteorological data and other pollutants. Atmospheric Environment, 38, 6431-6446.

Han, Y-J., Holsen, T.M., Hopke, P.K., Yi, S-M., 2005. Comparison between Back-Trajectory Based Modeling and Lagrangian Backward Dispersion Modeling for Locating Sources of Reactive Gaseous Mercury. Environmental Science and Technology 39, 1715-1723.

Hoyer, M., Burke, J., Keeler, G.J., 1995. Atmospheric Sources, Transport and Deposition of Mercury in Michigan – 2 Years of Event Precipitation. Water, Air, & Soil Pollution 80, 199-208.

Hungtington, T.G., Hodgkins, G.A., 2004. Changes in the Proportion of Precipitation Occurring as Snow in New England (1949-2000). Journal of Climate 17, 2626-2635.

Keeler, G.J.; Gratz, L.E.; Al-Wali, K., 2005. Long-term Atmospheric Mercury Wet Deposition at Underhill, Vermont. Ecotoxicology 14, 71-83.

Keeler, G.J., Landis, M.S., Norris, G.A., Christianson, E.M., Dvonch, J.T., 2006. Sources of Mercury Wet Deposition in Eastern Ohio, USA. Environmental Science and Technology 40, 5874-5881.

Landis, M.S., Keeler, G.J., 1997. Critical Evaluation of a Modified Automatic Wet-Only Precipitation Collector for Mercury and Trace Element Determinations. Environmental Science and Technology 31, 2610-2615.

Landis, M.S., Vette, A.S., Keeler, G.J., 2002. Atmospheric Mercury in the Lake Michigan Basin: Influence of the Chicago/Gary Urban Area. Environmental Science and Technology 36, 4508-4517.

Lin, C., Pehkonen, S.O., 1999. The chemistry of atmospheric mercury. Atmospheric Environment 33, 2067-2079.

Lin, C., Pongprueksa, P., Lindberg, S., Pehkonen, S.O., Byun, D., Jang, C., 2006. Scientific uncertainties in atmospheric mercury models I: Model science evaluation. Atmospheric Environment 40, 2911-2928.

Liu, B., Keeler, G.J., Dvonch, J.T., Barres, J.A., Lynam, M.M., Marsik, F.J., Morgan, J.T., 2007. Temporal variability of mercury speciation in urban air. Atmospheric Environment 41, 1911-1923.

Lynam, M.M., Keeler, G.J., 2006. Source-receptor relationships for atmospheric mercury in urban Detroit, Michigan. Atmospheric Environment 40, 3144-3155.

Meehl, G.A., Tebaldi, C., Teng, H., Peterson, T.C., 2007. Current and future U.S. weather extremes and El Nino. Geophysical Research Letters 34, L20704.

Miller, E.K., Gay, D., Nilles, M., Keeler, G.J., Sweet, C., Artz, R., Lawson, S., Pendleton, M., Barres, J., 2009. VT99 precipitation collector comparison. Manuscript in preparation.

Moody, J.L., Samson, P.J., 1989. The influence of atmospheric transport on precipitation chemistry at two sites in the Midwestern United States. Atmospheric Environment, 23, 2117-2132.

National Climatic Data Center, Local Climatological Data Publication (http://www7.ncdc.noaa.gov/IPS/lcd/lcd.html).

National Oceanographic and Atmospheric Administration (NOAA) Climate Prediction Center (http://www.cpc.noaa.gov/products/analysis_monitoring/).

Northeast States for Coordinated Air Use Management (NESCAUM), 2005. Inventory of Anthropogenic Mercury Emissions in the Northeast. November 30, 2005 Report.

Patten, J.M., Smith, S.R., O'Brien, J.J., 2003. Impacts of ENSO on Snowfall Frequencies in the United States. Weather and Forecasting 18, 965-980.

Rohli, R.V., Vega, A.J., 2008. Climatology. Jones and Bartlett Publishers, pp. 70-78.

Schroeder, W.H., Munthe, J., 1998. Atmospheric mercury - An overview. Atmospheric Environment 32, 809-822.

U.S. Environmental Protection Agency (U.S. EPA), 1997. Mercury Study Report to Congress, Volume 2. EPA-452/R-97-003; Office of Air Quality Planning and Standards, Office of Research and Development: Washington DC.

U.S. Environmental Protection Agency (U.S. EPA), 1994. An Introduction to the Issues and the Ecosystems. EPA-453/B-94/030, Office of Air Quality Planning and Standards: Durham, NC.

U.S. Environmental Protection Agency (U.S.EPA) 2005 National Emissions Inventory (NEI) Data and Documentation (www.epa.gov/ttnchie1/net/2005inventory.html).

Ward, J.H., 1963. Hierarchical grouping to optimize objective function. Journal of the American Statistical Association 58, 236-244.

White, E.M., Keeler, G.J. and Landis, M.S. 2009. Spatial variability of mercury wet deposition in Eastern Ohio: Summertime meteorological case study analysis of local source influences. Environmental Science and Technology 43, 4946-495.
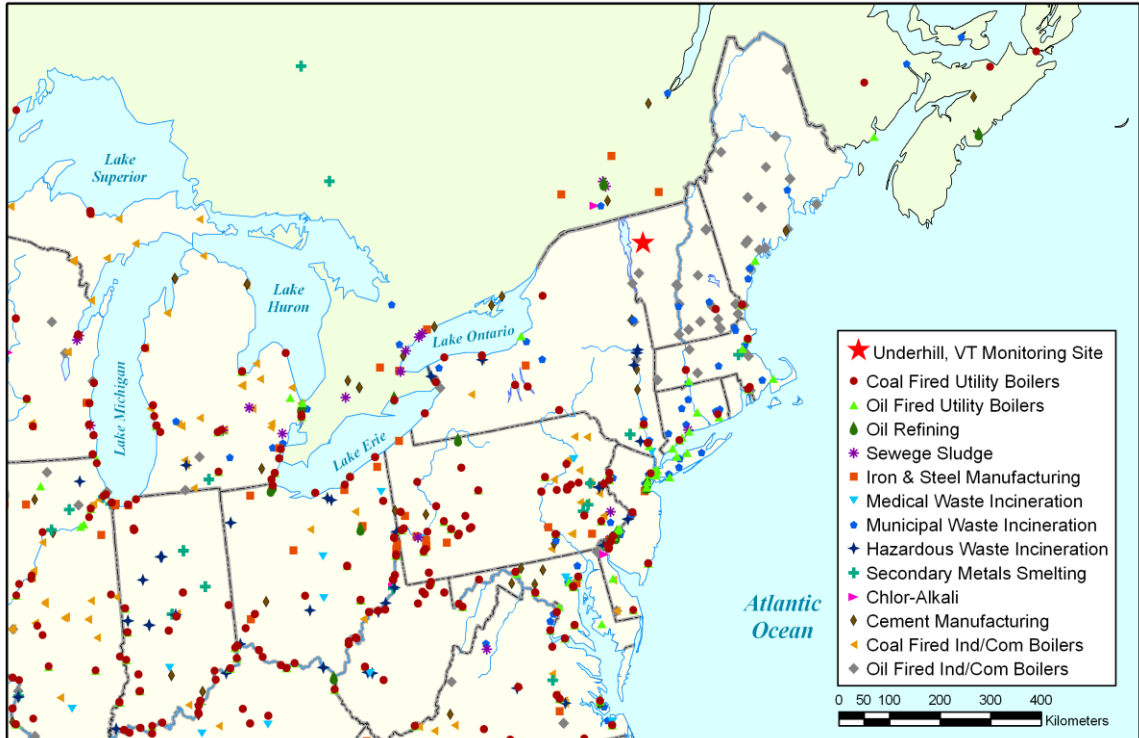
Figure 2.1: Location of the Underhill, VT monitoring site and major mercury point sources emitting ≥ 0.1 kg/yr (2005 U.S. EPA NEI; 2007 Environment Canada NPRI).
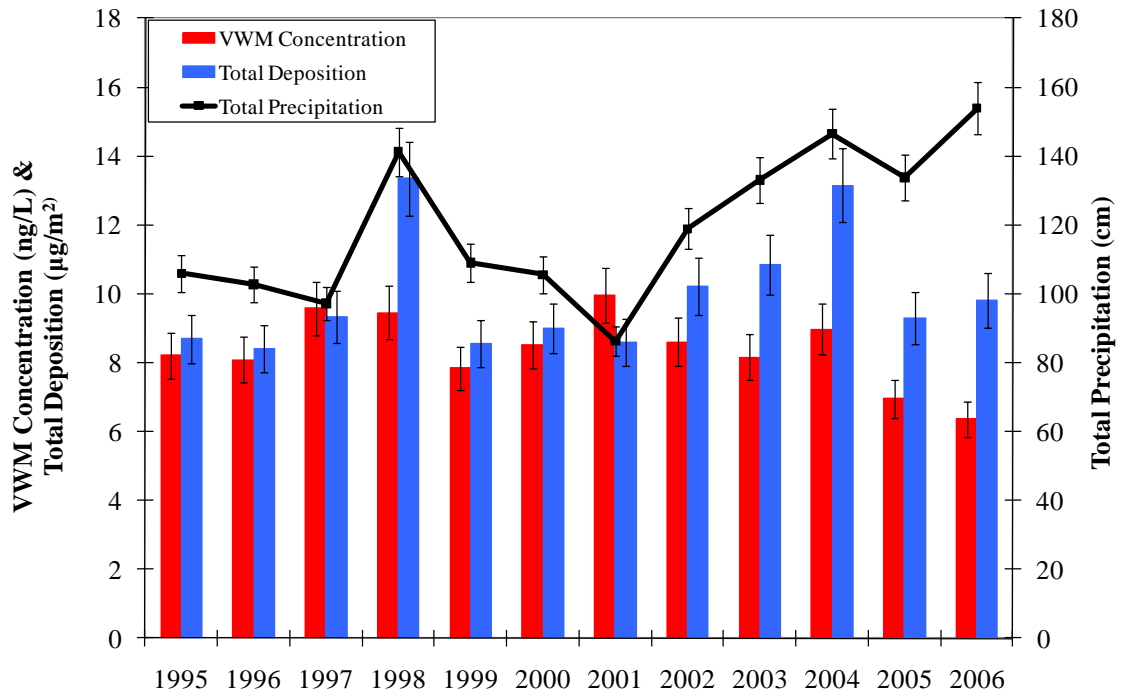
Figure 2.2: Annual mercury and precipitation measurements.
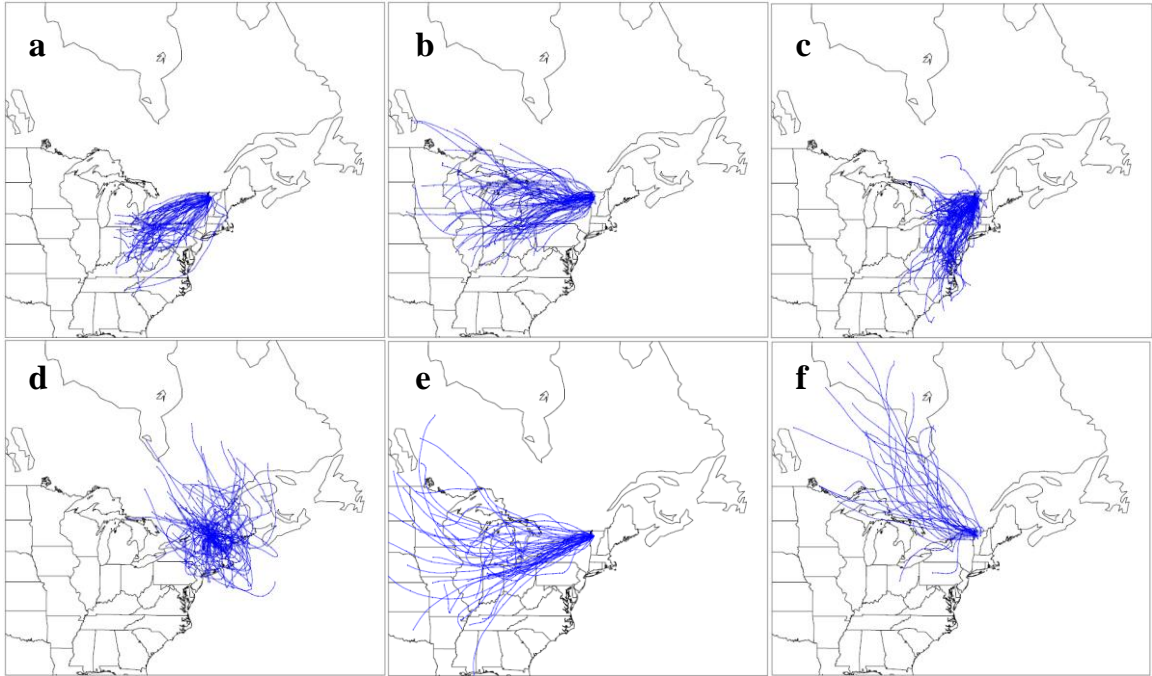
Figure 2.3: Back-trajectory clusters for highest (a-c) and lowest (d-f) mean and median mercury wet deposition events.
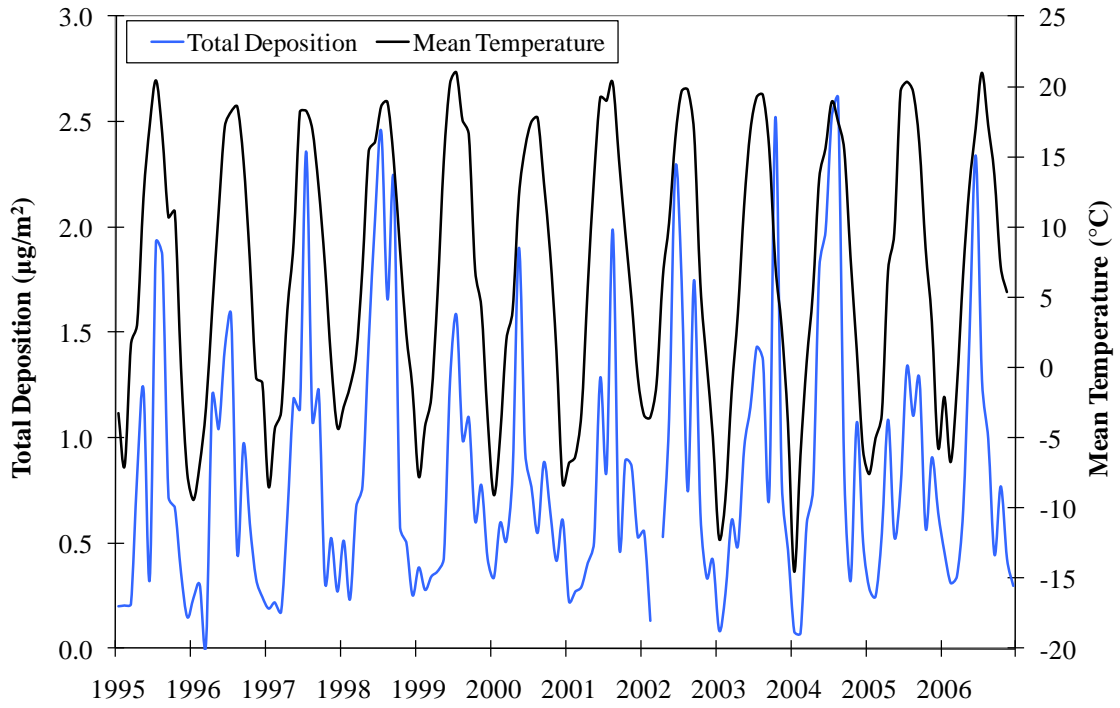
a.
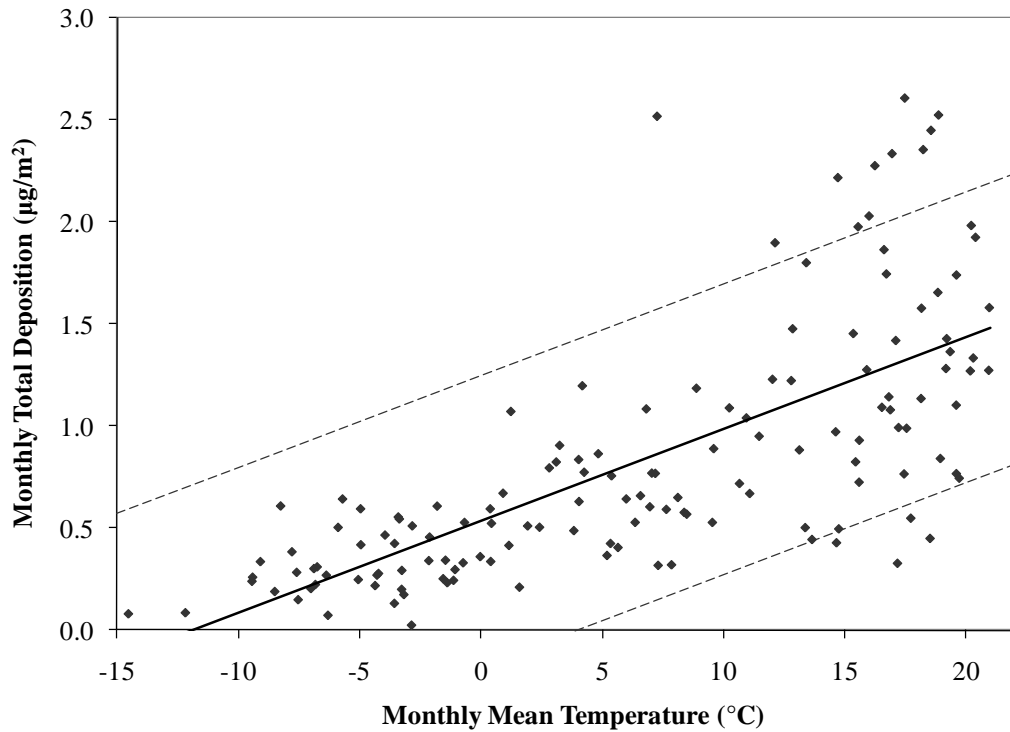
b.

Figure 2.4: (a) Seasonal relationship and (b) linear regression between monthly total deposition and monthly mean temperature with 90% confidence intervals shown.
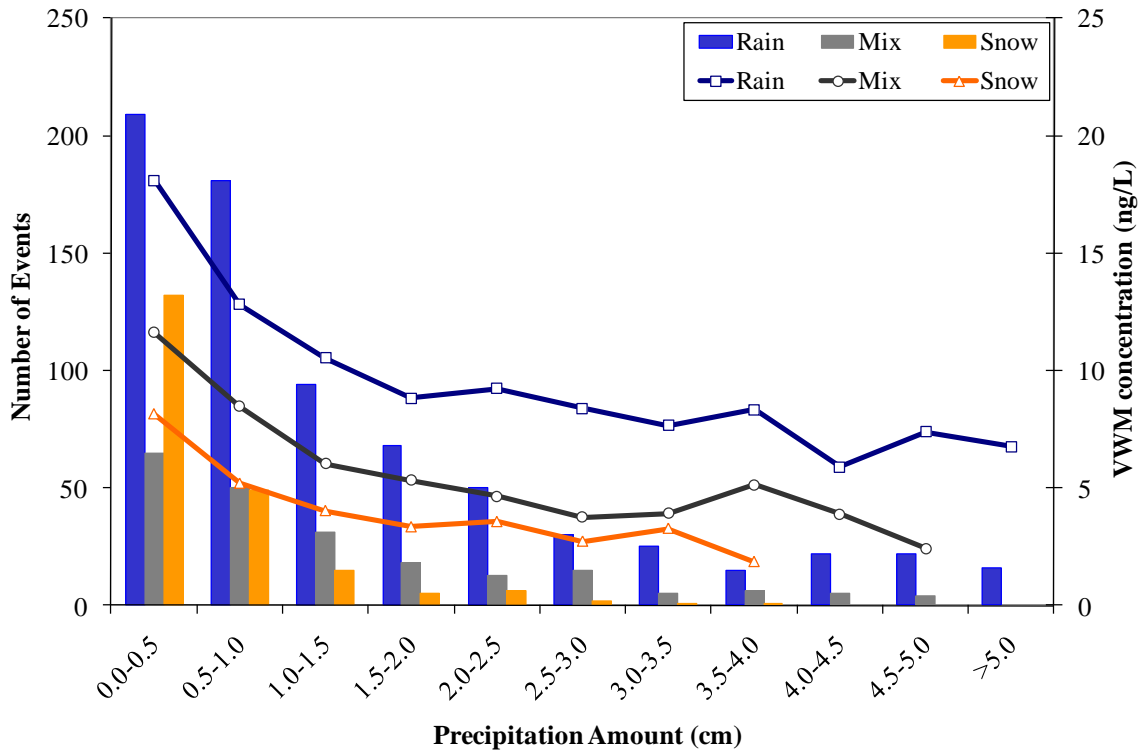
Figure 2.5: VWM mercury concentrations (lines) and number of daily-events (bars) for different precipitation amount ranges based on precipitation type for 1995-2006.
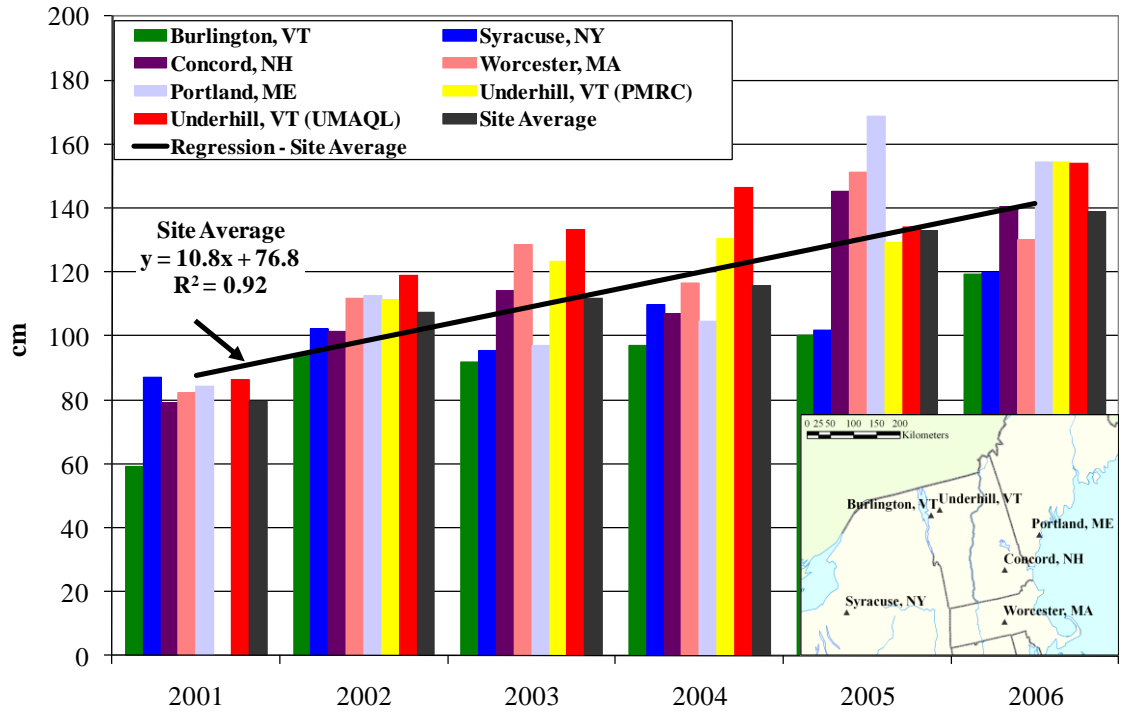
Figure 2.6: Annual total precipitation from regional airports and Underhill, VT. PMRC rain gauge data from 2001 was omitted due to missing data.

50
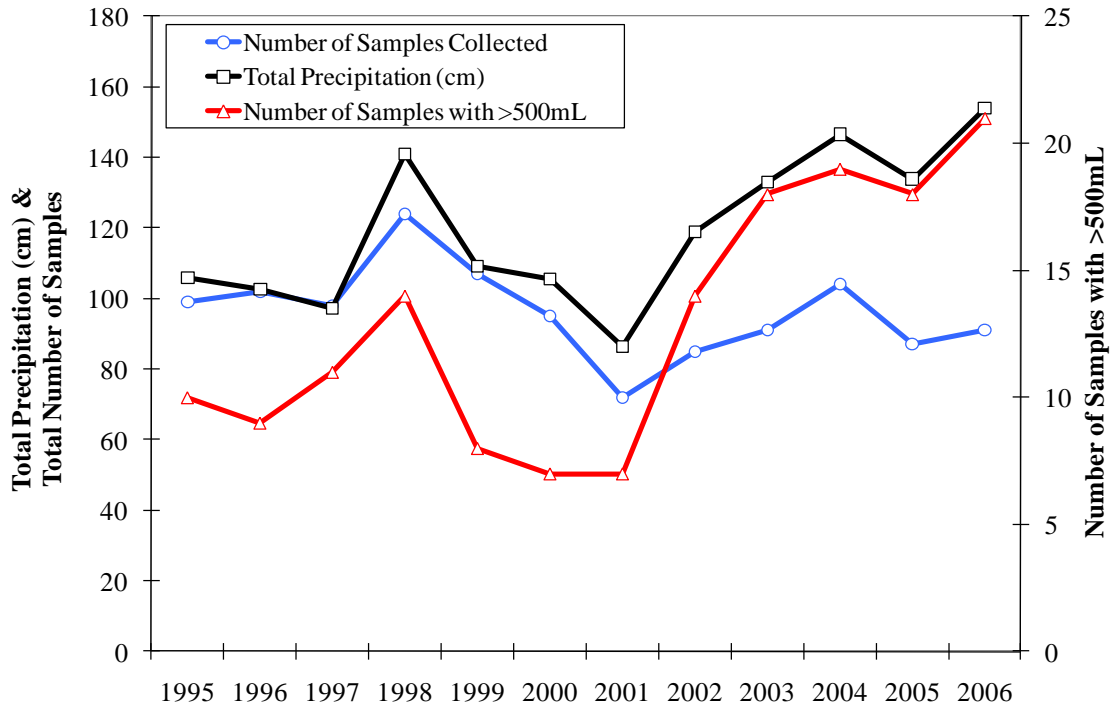
Figure 2.7: Annual precipitation depth and number of daily-event samples collected.
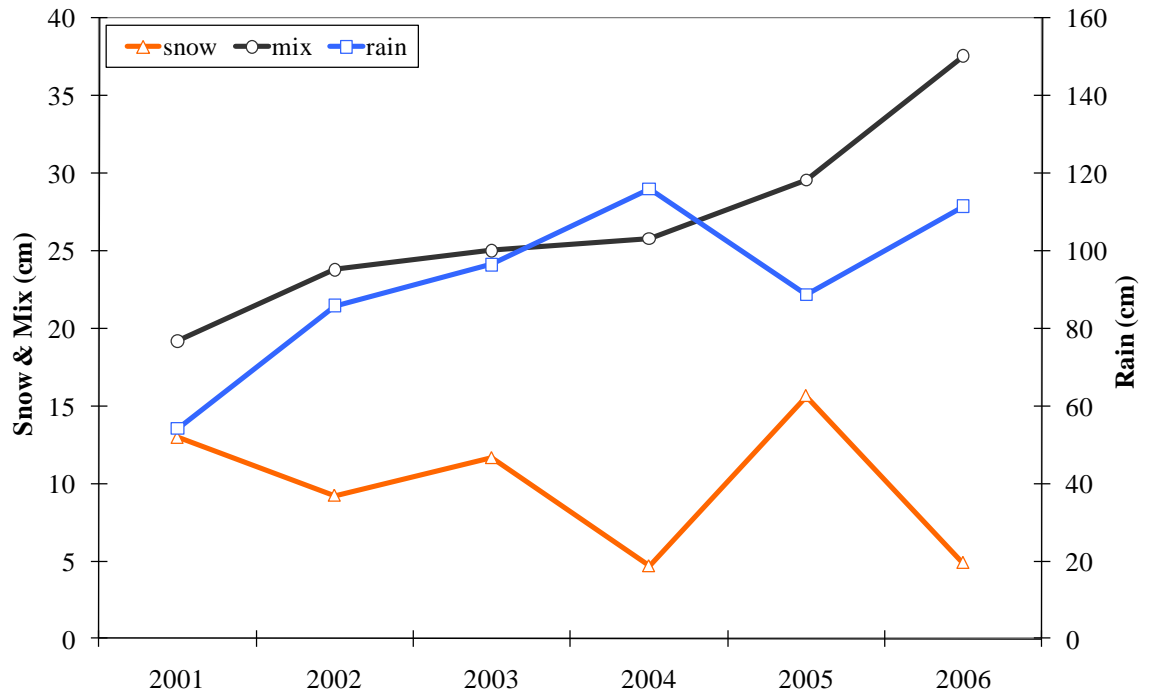
Figure 2.8: Annual precipitation depth by precipitation type for 2001-2006.
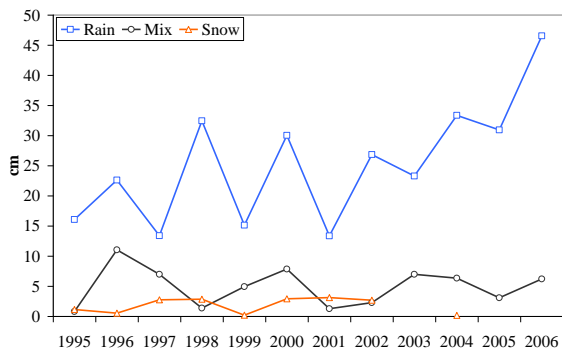
9a. Spring precipitation amount
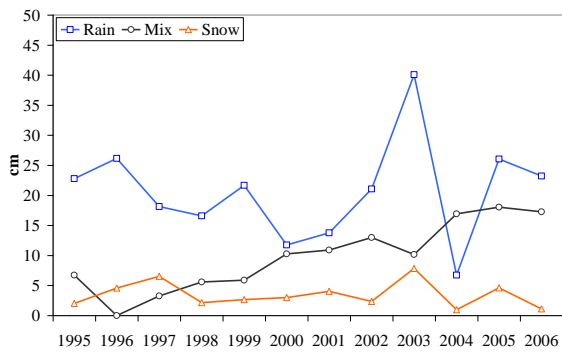
9b. Fall precipitation amount
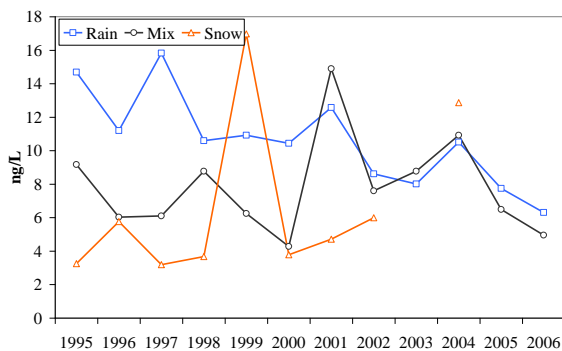
9c. Spring VWM concentration
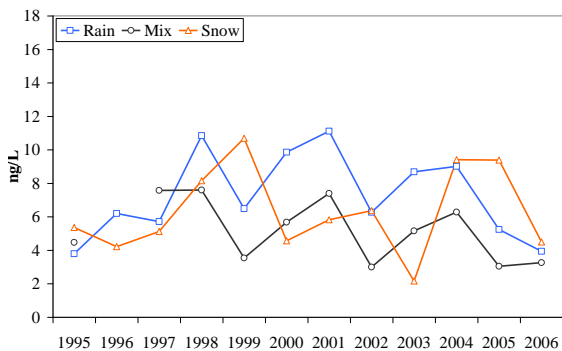
9d. Fall VWM concentration
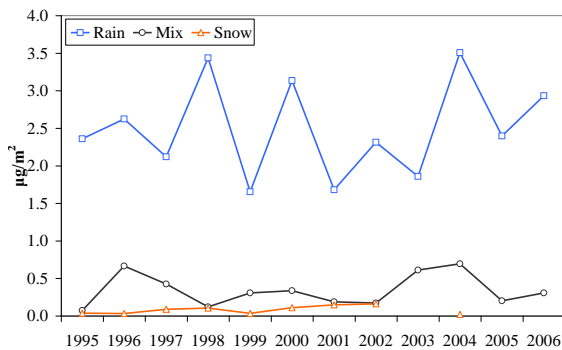
9e. Spring total deposition
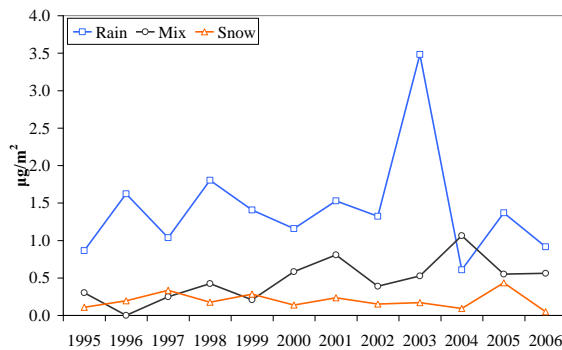
9f. Fall total deposition

Figure 2.9: Spring and Fall precipitation amount, VWM mercury concentration, and total mercury deposition for each precipitation type.
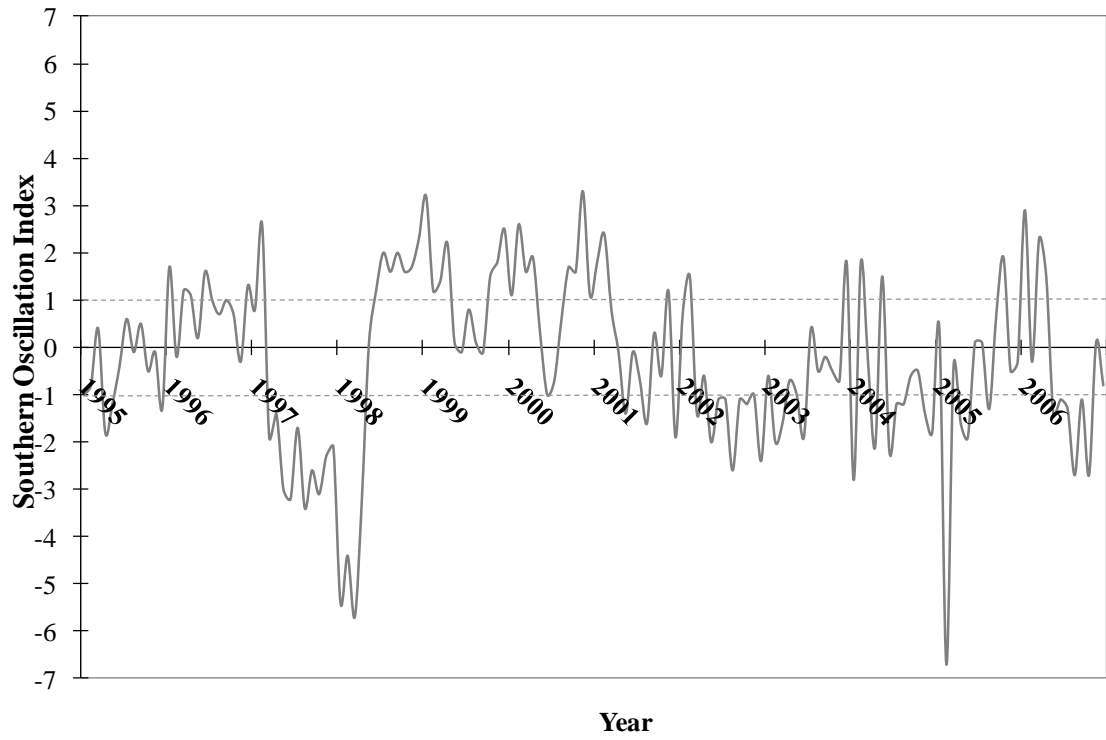
Figure 2.10: SOI for 1995-2006.
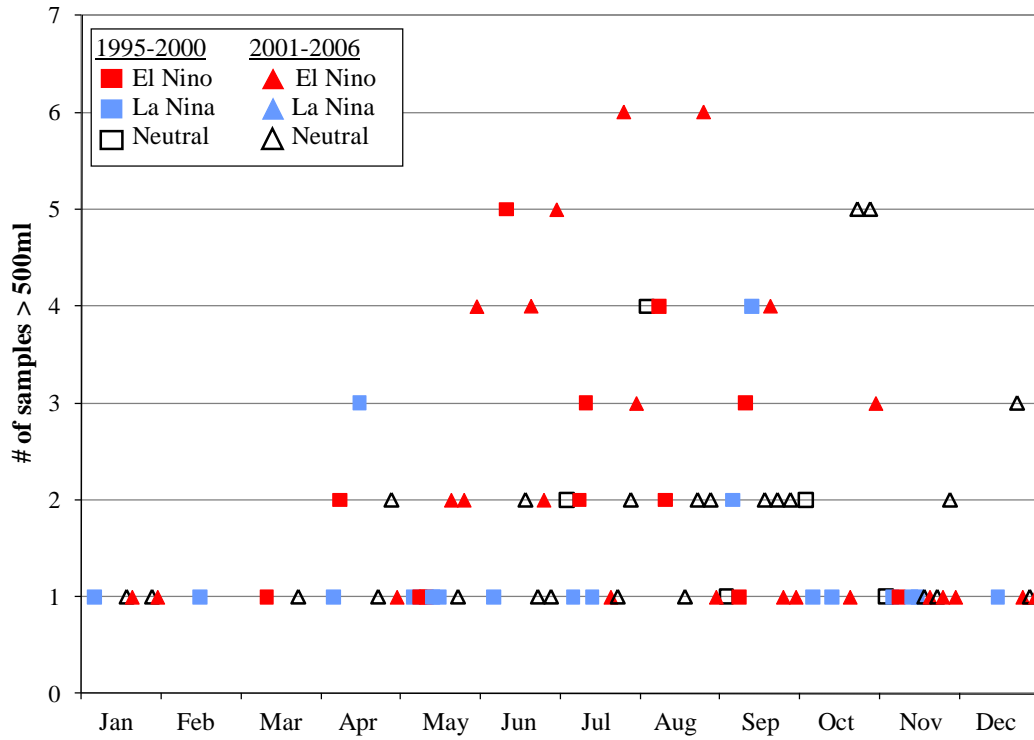
Figure 2.11: Frequency of large volume daily-event samples by month for 1995-2006.

Table 2.1: Summary of daily-event mercury measurements and on-site meteorological conditions associated with back-trajectory clusters.

Cluster	VWM Hg Concentration (ng/L)	Mean Hg Deposition ($\mu g/m^2$)	Median Hg Deposition ($\mu g/m^2$)	Mean Temperature (°C)	Median Temperature (°C)	Temperature Range (°C)	Mean Precipitation Amount (cm)	Median Precipitation Amount (cm)	N Rain	N Snow	N Mix
a	11.1	0.18	0.13	14.4	14.9	4.9 – 21.3	1.6	1.3	47	0	5
b	11.3	0.15	0.12	19.2	19.4	12.5 – 26.5	1.4	0.9	95	0	2
c	12.4	0.15	0.11	20.5	20.4	10.2 – 27.2	1.2	0.8	64	0	0
d	4.6	0.04	0.03	-5.2	-4.9	-15.1 – 1.6	0.9	0.5	3	56	25
e	10.0	0.04	0.03	-3.1	-3.1	-13.8 – 6.7	0.4	0.3	3	34	6
f	6.3	0.02	0.02	-6.9	-6.9	-22.4 – 5.9	0.4	0.2	3	23	4

CHAPTER 3

Sources of Mercury in Precipitation to Underhill, VT

Abstract

Daily event precipitation samples were collected from 1995 to 2006 in Underhill, VT and analyzed for mercury (Hg) and trace elements. Over the 12-year period, annual Hg deposition levels at the northern Vermont site did not decline significantly despite management efforts to reduce emissions in the United States. Mercury and trace element wet deposition data were examined using the multivariate receptor model EPA PMF 3.0 to identify the sources contributing to Hg deposition at the Underhill site. Results indicate that coal combustion, a mixture of incineration and non-ferrous metal smelting, and a phosphorus source contributed to the observed Hg wet deposition. The model consistently indicated that coal combustion contributed to ~60% of the total measured Hg wet deposition, and the contribution from this source did not change significantly over time. Mercury and trace element deposition were further analyzed using quantitative transport bias analysis (QTBA), a hybrid-receptor model, to identify the likely source locations contributing to Hg deposition at Underhill. Results from QTBA indicate that the majority of Hg deposition at Underhill is due to transport from the Midwestern United States, where the density of U.S. coal-fired utility boilers is largest.

57

3.1 Introduction

Mercury (Hg) is a persistent hazardous air pollutant and bioaccumulative neurotoxin released to the atmosphere from natural and anthropogenic sources. Once released into the environment, Hg can be converted to the organic form, methyl Hg, which bioaccumulates in the aquatic food chain and poses a danger to public health (Schroeder and Munthe, 1998). Atmospheric deposition is a dominant mechanism by which Hg enters the aquatic ecosystem and contaminates fish and wildlife (Hammerschmidt and Fitzgerald, 2006, Evers et al., 2007).

Mercury chemistry in the atmosphere is quite complex leading to challenges in understanding its behavior in the atmosphere and its transport away from sources (Lin and Pehkonen, 1999; Schroeder and Munthe, 1998). Mercury is emitted to the atmosphere in three main forms: gaseous elemental Hg (Hg^0), fine particle bound Hg (Hg_p), and divalent reactive gaseous Hg (RGM). Elemental mercury is relatively stable in the atmosphere and is able to travel long distances before being chemically converted to the divalent form (Hg(II)) that is much more soluble and deposits readily (Schroeder and Munthe, 1998; Lin and Pehknonen, 1999). This behavior allows Hg to deposit locally, regionally, and globally so that Hg deposition at downwind locations may be a mixture of various source types and atmospheric processes.

Following the Clean Air Act Amendments of 1990 regulatory efforts were undertaken to reduce Hg emissions and deposition, including restrictions on stack emissions from municipal and medical waste incinerators, previously one of the largest anthropogenic sources of atmospheric Hg (U.S. EPA, 1997). From 1990 to 1995 the emissions from municipal and medical waste incinerators declined by 50% and 75%,

respectively (U.S. EPA, 1997). By 1999 the targeted 95% reductions in municipal and medical waste incineration emissions had largely been met (Cohen et al., 2007), and by 2002 total annual anthropogenic Hg emissions in the United States had declined by approximately 100 tons (Cohen et al., 2007; Butler et al., 2008). Some of the largest emission reductions were observed in the Northeastern states where in 1998 municipal waste incineration accounted for ~55% of the Northeast Regional Mercury Emissions Inventory (NEIWPCC, 2007). Between 1998 and 2002, emissions from municipal and medical waste incinerators declined by ~70% in the Northeast states (NESCAUM, 2005).

Despite these regional and nationwide efforts to regulate Hg emissions, fossil fuel combustion remains the largest source of anthropogenic Hg to the atmosphere as emissions from anthropogenic combustion sources such as coal-fired utility boilers (CFUBs) have not declined as significantly over time (Cohen et al., 2007; Butler et al., 2008). Although reductions in CFUB emissions were anticipated under U.S. EPA's cap and trade approach proposed in the 2005 Clean Air Mercury Rule (Cohen et al., 2007), the rule was overturned in 2008 as states and other parties argued for enforcement of the 1990 Clean Air Act Amendments that required the use of maximum achievable control technology (MACT) for reducing Hg emissions. The U.S. EPA is currently working to determine a widely applicable approach for MACT implementation.

Underhill, VT is a remote downwind location at which atmospheric Hg deposition remains a critical issue due to elevated levels of Hg observed in the region's fish and wildlife (Evers et al., 2007) and unchanging annual Hg wet deposition amounts over time (Keeler et al., 2005; Gratz et al., 2009). Declines in atmospheric deposition were projected in response to the efforts in the Northeast states to reduce waste incinerator

emissions (NESCAUM, 2005; NESCAUM, 2007). Yet analysis of daily-event Hg wet deposition samples collected at Underhill from 1995 to 2006 showed that annual Hg wet deposition has not declined significantly over time (Gratz et al., 2009). However, waste incinerator emissions should not necessarily have a substantial influence on Hg deposition at the remote Underhill site due to the fact that there are no major municipal or medical waste incinerators within 100 km of the Underhill site (Figure 3.1). Approximately 75% and 95% of Hg in municipal and medical waste incinerator emissions are RGM (Carpi, 1997; Dvonch et al., 1999), which tends to deposit close to emission sources (Lin and Pehkonen, 1999; White et al., 2009) and should not be readily available for transport to the downwind Underhill site.

Furthermore, transport from the industrialized Midwestern U.S. and the urban corridor along the East Coast of the U.S. consistently contributed to the largest observed wet deposition amounts from 1995 to 2006 (Gratz et al., 2009). Past source apportionment studies in Midwest and East Coast locations have continually demonstrated the influence of industrial sources in addition to waste incineration (e.g. coal- and oil-fired utility boilers, iron and steel manufacturing) on the composition of aerosols (Olmez et al., 1998; Lucey et al., 2001; Liu et al., 2003; Morishita et al., 2006; Hammond et al. 2008), and precipitation (Keeler et al., 2006; White, 2009) in the regional atmosphere. Considering the consistent transport of Hg from the Midwest and East Coast to Underhill (Gratz et al., 2009), deposition at Underhill should also be influenced by these regional sources, of which CFUBs are the largest source of total Hg to the atmosphere (Cohen et al., 2007; Keeler et al., 2006). Unlike waste incinerator emissions which are dominated by RGM (Carpi, 1997), Hg emitted from CFUBs can be

~ 50-80% RGM, and ~ 20-50% Hg^0 (Carpi, 1997; Seigneur et al., 2006). While a large portion of these emissions can be removed through near-field deposition (White et al., 2009), the relative amount that is available to be transported downwind should be greater than in emissions from waste incineration.

Source apportionment models are widely used in air quality studies to identify the major sources impacting a given receptor site (Dvonch et al., 1999; Polissar et al., 2001; Poirot et al., 2001; Liu et al., 2003; Keeler et al., 2006). Application of these models to aerosol concentrations measured at Underhill indicated that the dominant sources of fine aerosol mass included fuel combustion (oil and coal), local wood smoke, and secondary sulfate production (Polissar et al., 2001; Gao et al., 2006). Polissar et al. (2001) also identified municipal waste incineration as a major factor influencing aerosol composition from 1988 to 1995, but it was not identified as a stand-alone source in 2001-2003 aerosol samples due to the emission reductions (Gao et al., 2006). Application of similar techniques to precipitation samples allows for examining the removal of pollutants from the atmosphere and their introduction into the ecosystem.

Daily-event precipitation samples collected at the Underhill, VT site comprise the only long-term wet deposition dataset for Hg and trace elements collected in the Northeast United States, making this a truly unique study of the source contributions to Hg deposition over time. The present manuscript contains the first extensive application of source apportionment and hybrid-receptor modeling techniques to wet deposition at the Underhill site.

3.2 Methodology

3.2.1 Sample Collection and Analysis

The Underhill measurement site is located ~ 25 km east of Lake Champlain on the west slope of Mount Mansfield at the Proctor Maple Research Center (PMRC) (elevation 399m) (Figure 3.1). Daily-event wet-only precipitation samples were collected for Hg and trace element analysis using a modified MIC-B (MIC, Thornhill, Ontario) automatic precipitation collector (Landis and Keeler, 1997). Separate sampling trains were used for Hg and trace elements, as described in Keeler et al. (2005) and Gratz et al. (2009). The Hg sampling train consisted of a borosilicate glass funnel (collection area 191 ± 9 cm^2), a Teflon adapter with a glass vapor lock in the interior, and a 1L Teflon bottle. The trace element sampling train consisted of a polypropylene funnel (collection area 167 ± 7 cm^2), a polypropylene adapter, and a 1L polypropylene bottle. Field supplies for the Hg and trace element sampling trains were prepared at the University of Michigan Air Quality Laboratory (UMAQL) using an 11-day acid-cleaning procedure (Landis and Keeler, 1997) to ensure that they were essentially Hg-free before use in the field. Sampling trains were replaced after individual daily precipitation events. Precipitation samples greater than 0.10 cm were used in the subsequent data analysis.

Samples were analyzed for Hg using cold-vapor atomic fluorescence spectrometry (CVAFS) (Keeler et al., 2005) and a suite of trace elements using a Finnigan MAT Element magnetic sector high resolution inductively coupled plasma mass spectrometer (ICP-MS) (Table 3.SI-1). The volume of each precipitation sample was determined gravimetrically, and the precipitation depth was determined using the average glass funnel area.

3.2.2 Multivariate Source Apportionment Modeling

Source apportionment analysis was performed on the Underhill precipitation data using EPA PMF 3.0. This multivariate receptor model uses positive matrix factorization (PMF) (Paatero, 1997) to decouple the measured sample deposition amounts into estimated source profiles and source contributions to each sample. It utilizes non-negativity constraints imposed by the physical reality of the source-receptor problem (Norris et al., 2008). PMF differs from most multivariate models in that it additionally uses the uncertainty associated with each sample to perform a weighted least-squares factor analysis on the measured sample composition (Norris et al., 2008).

Sample concentrations were converted to deposition using the measured precipitation depth prior to input to the model. Concentrations less than zero were replaced with one half of the method detection limit (MDL), which was calculated as described in Keeler et al. (2006). Uncertainties for PMF were calculated using the MDL, sample collection uncertainty (SC = 10%), analytical measurement uncertainty (AM = standard deviation of three replicate analysis for each sample), and precipitation depth measurement uncertainty (PD = 5%) as shown below (Equation 1; Keeler et al., 2006).

(1) $\quad U = (MDL) + \sqrt{(SC)^2 + (AM)^2 + (PD)^2}$

The variability in the PMF solution was estimated using a block bootstrap technique that calculates the stability of the model solution by randomly re-sampling blocks of the input dataset and computing the variability between model solutions (Norris et al., 2008). One hundred bootstrap runs were used and the elemental contributions to each factor were deemed significant when the fifth percentile of the bootstrap uncertainty was greater than zero (Keeler et al., 2006).

3.2.3 Meteorological Trajectory Analysis

Air mass transport to the Underhill site was modeled using the Hybrid Single-Particle Lagrangian Integrated Trajectory (HYSPLIT) Model Version 4.8 (Draxler and Hess, 1997). HYSPLIT three-day back trajectories were calculated using the National Weather Service's National Center for Environmental Prediction (NCEP) Nested Grid Model (NGM) for 1995-1996 and the Eta Data Assimilation System (EDAS) for 1997-2006. All data was obtained from the National Oceanic and Atmospheric Administration's Air Resources Laboratory (NOAA-ARL). The hour of maximum precipitation, determined by the onsite tipping bucket rain gauge, was used as the starting time for each event. Trajectory starting heights were set to one-half of the mixed layer depth, as determined by the HYSPLIT model, at the hour of maximum precipitation. Event-specific trajectory starting heights were chosen over a fixed starting height because the mixed layer, in which atmospheric mixing and pollutant dispersion occurs, can vary both diurnally and seasonally (Godish, 2004). Precipitation amounts along the trajectory path were also obtained from HYSPLIT gridded meteorological data for use in the Quantitative Transport Bias Analysis (QTBA) model.

3.2.4 Quantitative Transport Bias Analysis (QTBA)

QTBA is a trajectory-based hybrid-receptor model that combines air mass back-trajectories with measured amounts of analytes at the receptor site to determine the most probable source regions of those pollutants (Keeler and Samson, 1989). The air mass back-trajectories are weighted by the deposition amounts at the receptor site (Keeler and Samson, 1989). QTBA was previously applied to ambient Hg (Burke, 1998; Liu, 2007; Yoo, 2006) and aerosol trace elements (Keeler and Samson, 1989; Yoo, 2006) and was

proven to be a powerful tool in examining source-receptor relationships. Unlike most other trajectory-based receptor models, QTBA takes into account the increasing uncertainty in the computed trajectory moving away from the receptor site due to the significant uncertainty in the back trajectory location beyond 72-hours upwind of the starting location (Kahl and Samson, 1986). The model also accounts for wet and dry deposition along the trajectory path as it can lower the probability of transport and is important in studies of Hg deposition (Liu, 2007). The QTBA model is described in detail in Keeler and Samson (1989).

3.3 Results and Discussion

3.3.1 Mercury

There were 1,155 samples collected in Underhill, VT from 1995 to 2006. During this period, 96 samples were collected on average each year, and the mean event precipitation depth was 1.24 cm. The volume-weighted mean (VWM) Hg concentration was 8.31 ng/L and the mean Hg wet deposition per event was 0.10 $\mu g/m^2$. A detailed summary of this analysis can be found in Chapter 2 (Gratz et al., 2009).

3.3.2 Preliminary Analysis of Trace Element Data

Of the over 1,000 samples collected at Underhill from 1995 to 2006, 1,096 contained sufficient volume for analysis in both the Hg and trace elements sampling trains. The data was initially examined using Principle Components Analysis (PCA), a form of factor analysis often used to examine source receptor relationships in trace element data (Dvonch et al., 1999) and between chemical species and meteorological parameters (Liu, et al., 2007). PCA was applied to the Underhill samples using Varimax rotation with Kaiser Normalization (SPSS v16) for an exploratory look at the factors

associated with the precipitation samples and as a means for identifying potential sample outliers. It was determined by simultaneous examination of the data distribution that samples with a PCA factor score >5 or <-5 were extreme outliers that strongly influenced the data and source profiles. Extreme outliers (41 samples; 3.7% of dataset) were subsequently removed before examining the data in PMF, leaving 1,055 samples in the final combined Hg and trace metal dataset.

Interrogation of trace element concentration ratios in event precipitation samples prior to multivariate statistical analysis can provide insight into their major source influences (Olmez et al., 1998; Dvonch et al., 1998; Dvonch et al., 1999; Polissar et al., 2001). However, these ratios should be applied carefully with respect to wet deposition samples, as wet removal of atmospheric constituents may vary with aerosol size fraction, distance between source and receptor, meteorological conditions and atmospheric chemistry during transport. Several factors should be considered when examining previously reported elemental ratios, such as whether the ratios are based on stack measurements (Dvonch et al., 1999, Olmez et al., 1988; Polissar et al., 2001) or ambient aerosol measurements (Olmez et al., 1998), whether the measurements were gas- or particle-phase, and whether the particulate measurements were fine, coarse, or total particulate matter. Although the chemical compositions and elemental ratios of many pollutants are reasonably well preserved with transport (Keeler and Samson, 1989; Rahn and Lowenthal, 1994), elements such as Hg demonstrate more complex behavior in the atmosphere which may alter their relative abundances near sources and at downwind locations. Thus while elemental ratios are a valid approach for initial data exploration,

the aforementioned limitations should also be acknowledged when interpreting wet deposition datasets.

In light of the 70% reduction in Hg emission in the Northeast states between 1998 and 2002 (NESCAUM, 2005), it was of interest to explore elemental ratios representative of waste incinerator emissions in the Underhill precipitation. These ratios were examined from 1995 to 1998 and from 1999 to 2006 to distinguish the periods before and after major emission reductions. A Zn/Pb ratio of 1.8 was shown to represent fine particle emissions from municipal waste incinerators (Olmez et al., 1988; Polissar et al., 2001); however, similar to Polissar et al. (2001) the Zn/Pb ratios in event precipitation at Underhill were largely above this value with only 0.9% of samples displaying ratios of 1.8 ± 0.5 (uncertainty determined from the standard deviation of reported Zn and Pb concentrations in Olmez et al., 1988) and on average the Zn/Pb ratio in Underhill precipitation suggests minimal impact from municipal waste incinerators (1995-1998 Zn/Pb slope = 4.9, R^2 = 0.22, p < 0.001; 1999-2006 Zn/Pb slope = 4.0, R^2 = 0.14, p < 0.001; Figure 3.SI-1). In addition to municipal waste incineration (Greenberg et al., 1978) Zn and Pb are also emitted from various non-ferrous metal smelters (Polissar et al., 2001). For example, Zn smelters are located east of St. Louis, MO and north of Pittsburgh, PA (U.S. EPA 2002 NEI), and Zn refineries are also located near Montreal, QC and in central Ontario (Annual survey of U.S. and Canadian Smelters). Zn and Pb along with As, Cd, and Cr may also be released from cement production (Schuhmacher et al., 2004) while additional Pb sources in the region also include biomass burning, fossil fuel burning (e.g. coal, oil, wood, and peat), and motor vehicles (Olmez et al., 1998; Graney et al., 1995). Polissar et al. (2001) suggested that the variety of Zn and Pb

sources upwind of Underhill may cause difficulty in identifying a distinct incineration source in aerosol samples collected at this site.

The Hg/Pb ratios from stack measurements performed in South Florida were used to define the signatures for medical (Hg/Pb = 8.08) and municipal (Hg/Pb = 0.06 ± 0.02) waste incineration (Dvonch et al., 1999). Taking these ratios to be representative of waste incinerator emissions, the Hg/Pb ratio for medical waste was far greater than any Hg/Pb ratio in the Underhill precipitation (Figure 3.SI-1). From 1995 to 1998 and from 1999-2006, only 9.8% and 11.0% of samples contained Hg/Pb ratios of 0.06 ± 0.02, respectively, (1995-1998 Hg/Pb slope = 0.014, R^2 = 0.45, p < 0.001; 1999-2006 Hg/Pb slope = 0.006, R^2 = 0.19, p < 0.001; Figure 3.SI-1). This is consistent with the prediction that due to the speciation of Hg emissions from waste incinerators and the distance of waste incinerators more than 100 km from the Underhill site, a large contribution to Hg deposition from incinerators would not be expected.

Elemental ratios can also be used to explore the influence of oil- and coal-fired utility boilers on Underhill precipitation. Rare earth elements are naturally present in crustal material but their abundances may be altered during the combustion process due to their presence in catalytic material (Olmez and Gordon, 1985; Krachler et al., 2003). For example, the La/Ce ratio is ~1-2 in oil combustion emissions (Kitto, 1993; Dvonch et al., 1998), and 0.5 ± 0.04 for the average continental crustal composition (Olmez and Gordon, 1985). The La/Ce ratios for Underhill are closest to the predicted crustal composition (La/Ce slope = 0.51; R^2 = 0.95; p < 0.001; Figure 3.SI-2). These ratios suggest that La and Ce would have minimal contribution from oil combustion. La and Ce are also emitted from oil refining, catalytic crackers (Kitto et al., 1992; Olmez and

Gordon, 1985; Olmez et al., 1998), iron and steel production (Geagea et al., 2007) and the use of rare earth elements in production of alloys (Krachler et al., 2003), which could further alter the abundance of these elements in the atmosphere.

Ratios of rare earth elements with vanadium (V) can also be used to identify the oil combustion signature as oil combustion accounts for 91% of worldwide atmospheric V emissions (Mamane and Pirrone, 1998). The La/V ratios for the average continental crust and in oil-fired power plants emissions are approximately 0.13 ± 0.06 and 0.045 ± 0.015, respectively (Olmez and Gordon, 1985). The La/V ratios in the Underhill wet deposition samples varied widely from 0.004 to 1.0 (La/V slope = 0.082; $R^2 = 0.40$; $p < 0.001$; Figure 3.SI-2). This suggests the contribution of these elements from more than one source and indicates the need for more sophisticated multivariate analysis to accurately identify the specific sources of La and V. In addition to oil-fired power plants, V is also released from coal combustion and residual fuel burning (Tuncel et al., 1985; Mamane and Pirrone, 1998; Grahame and Hidy, 2004) and is used in ceramics; as a catalyst; and as a stabilizer in steels (Handbook of Chemistry and Physics). The daily event La/V ratios followed a seasonal pattern, with lower values (La/V < 0.2) typically observed in fall and winter. Elevated V emissions during colder months explains this observation as residual oil burning is commonly used for both commercial and residential heating purposes in the Northeast states (Zoller et al., 1973).

Ratios of As/Se and S/Se were used to investigate coal combustion signatures (Keeler and Samson, 1989). The As/Se ratio in coal combustion emissions is typically less than or equal to one whereas an As/Se ratio greater than one is suggestive of smelter emissions, as determined from fine particulate samples from New York state (Olmez,

1998; Yoo, 2006). In addition to the Zn smelters previously mentioned, there are also several Ni and Cu smelters in Ontario (e.g. Noranda and Falconbridge) (Annual survey of U.S. and Canadian smelters). Selenium is also emitted from non-ferrous metal smelting as well as oil and wood combustion, and on a global basis coal combustion is the largest anthropogenic source of Se (Wen and Carignan, 2007). Only 23% of the Underhill daily-event precipitation samples contained As/Se ratios greater than one, demonstrating the dominance of coal combustion on the As and Se levels in precipitation at Underhill (As/Se slope = 0.34; R^2 = 0.54; $p < 0.001$; Figure 3.SI-3). The total Hg deposition measured in these samples accounted for only 16% of the total Hg deposition measured during the 12-year period.

The S/Se ratio can also be used to identify coal combustion emissions as well as suggest the distance to coal-fired utility boilers. Sulfur and Se are emitted from various combustion sources (Grahame and Hidy, 2004). Sulfur is dominantly emitted from coal combustion sources as SO_2 and is converted to sulfate (SO_4^{2-}) slowly during transport (Tuncel et al., 1985). Selenium, on the other hand, is emitted from coal combustion predominantly in the gas phase but quickly binds to particles or is converted to submicron sized particles following emission (Tuncel et al., 1985; Wen and Carnigan, 2007). Consequently, near CFUBs the particulate S/Se ratio is typically much less than 1,000 and increases with distance from the source as emitted SO_2 is converted to sulfate (Tuncel et al., 1985). The particulate S/Se ratio hypothetically reaches a steady-state value around 3,000 in rural locations where there is an absence of local SO_2 emissions (Tuncel et al., 1985). The Underhill samples followed this prediction (S/Se slope = 2630; R^2 = 0.75; $p < 0.001$; Figure 3.SI-3). A weak relationship was observed in the Underhill

precipitation data with the estimated particulate S/Se ratio for oil combustion emissions (Olmez et al., 1988; Polissar et al., 2001) (Figure 3.SI-3). While elemental ratios provided insight for potential sources contributing to deposition at Underhill it was also clear that more sophisticated multivariate techniques were needed to apportion the Hg deposition to specific sources.

3.3.3 1995-2006 PMF Model Results

PMF resolved a five factor solution (Table 3.1; Figure 3.2) for Underhill precipitation samples that were identified as: (1) mixed smelter and incinerator, (2) oil combustion (3), phosphorus, (4) iron-steel manufacturing, and (5) coal combustion. Based upon the bootstrapping analysis and the relative attribution of Hg deposition to the aforementioned PMF factors, it was determined that three of the five source categories contributed significantly to Hg deposition: smelter/incinerator (12.7%), phosphorus (26.5%), and coal combustion (60.7%). PMF was able to reproduce 78% of the total measured Hg deposition. The remaining 22% may represent sources of Hg not accounted for by the model, which could include contributions from the global background. A regression of PMF observed versus predicted values had a slope of 0.63, an intercept of 0.02, and an R^2 of 0.68. The scaled residuals (difference between observed and predicted deposition amount, scaled by the uncertainty) for modeled Hg deposition were normally distributed and 98% of values were between -3 and +3, the suggested range for well-modeled data in PMF (Norris et al., 2008).

The mixed smelter/incinerator factor contained the highest loadings of Cd, Zn, Pb, and Cu. Metal smelting and incineration influences were previously observed in atmospheric samples at Underhill (Polissar et al., 2001), but as suspected based on the

71

Zn/Pb ratios, PMF was unable to distinguish the two sources due to common elements in their emissions. The percent contribution to Hg wet deposition from the smelter/incinerator factor was greatest in the winter (21% in PMF) and lowest in the summer (11% in PMF). Precipitation events with As/Se ratios greater than one predominantly occurred during winter months under northerly flow, demonstrating the impact of Canadian smelters during the winter season and adding support for the identification of this source type.

The oil combustion factor had the highest loading of V with additional contributions from Cd, S, Cr, Zn, As, and Se. Interestingly, this factor did not significantly contribute to Hg deposition, which follows our understanding that much lower Hg concentration are found in residual oil than in coals burned in utility boilers (Olmez et al. 1998). The seasonal variability in La/V ratios suggested the importance of V emissions during fall and winter months due to increased residual oil-burning in the Northeast states for heating. Hg deposition amounts are substantially lower during the cold seasons due, in part, to inefficient scavenging of atmospheric Hg(II) by snowfall (Burke et al. 1995; Gratz et al., 2009); thus an insignificant contribution from residual oil combustion to Hg wet deposition is reasonable.

The phosphorus source contained significant contributions from P, Mg, Mn, and K (Figure 3.2). It is not certain precisely what this factor represents, but the following sources are hypothesized. Firstly, biomass burning is known to release P and K to the atmosphere (Mahowald et al., 2008) and there are several wood-burning industrial/commercial boilers in the Northeast states (Figure 3.1). Polissar et al. (2001) previously showed that wood smoke with high loadings of K contributed to $14.5 \pm 5\%$ of

72

PM$_{2.5}$ at the Underhill site, with the largest source contributions occurring in spring during transport from southeastern Quebec and northern New England. While Hg emissions from wood-fired commercial/industrial and electric utility boilers were estimated to account for ~1% of the Northeast regional mercury emissions inventory (NEIWPCC, 2007), wood smoke at Underhill could also be associated with residential wood burning and forest fires (Polissar et al., 2001).

The phosphorus factor in PMF could also represent the increasing use of waste from wood-fired boilers, paper mills, and waste water treatment plants as fertilizer in order to enrich soils with P and K (Vance, 1996; Pitman, 2006). The majority of boiler ash and wastewater sewage sludge in the U.S. is sent to landfills or incinerated; however in the Northeast states ~80% of these industrial and wastewater byproducts are converted to "biosolids" and other organic residuals that are land applied as fertilizer (Erich and Ohono, 1992; Vance, 1996). Following application of these substances to the soil surface, biosolids have been detected in downwind aerosol samples under wind speeds > 5 m/s (Baertsch et al., 2007). However, the phosphorus factor in PMF does not contain significant contributions from common crustal elements (e.g. La or Ce) that would support the hypothesis that wind blown soil particles were transported to the Underhill site. It should be noted that biosolids may also be injected into the soil which would affect the ambient air only as the soil is tilled. Land application of biosolids has not previously been assumed to be a significant source of Hg to the regional total maximum daily load (NEIWPCC, 2007), but given that primary biogenic emissions are a reported source of P and K to the atmosphere (Mahowald et al., 2008), and there is a strong relationship between Hg and these elements, it seems plausible that the release of

biogenic aerosols from vegetation treated with biosolids could be a source of P, K, and Hg to the atmosphere. The amount of Hg in wastewater treatment facility sewage sludge has been greatly reduced in the Northeast since 2004 due to increased use of dental amalgam separators (NESCAUM, 2007; King et al., 2008). However, the annual contribution from the phosphorus source to Hg deposition did not significantly decline between 1995 and 2006 or between 2004 and 2006 suggesting these recent reductions were not evident in the Underhill precipitation samples.

The seasonality of the phosphorus source contribution to Hg wet deposition was also investigated. This source contributed to ~30% of Hg deposition in the spring, fall, and winter and was markedly lower in the summer (~19%). This pattern could be explained by seasonal differences in emissions from the aforementioned sources, but may also suggest seasonal variability in transport pathways to the Underhill site.

PMF calculated a factor with the highest loadings of iron-steel manufacturing elements (Mg, Cr, Mn, Al, Fe and Co) (Machemer, 2004). The elevated loadings of Al on the this factor may also reflect the emissions from aluminum production facilities in Kentucky, Indiana, Ohio, and West Virginia (U.S. EPA 2002 NEI) that are in close proximity to many of the major iron-steel manufacturers. The highest loadings of La and Ce were also found on the iron-steel factor, and enrichments of rare earth elements such as La and Ce have been observed in emissions from the iron-steel facilities (Geagea et al., 2007).

Finally, PMF calculated a distinct source factor characterized by the highest contributions of S, As, and Se which was determined to signify emissions from coal combustion (Grahame and Hidy, 2004). Furthermore, PMF attributed ~60% of the total

74

Hg deposition to this factor. The percent contribution to Hg deposition from coal combustion was highest in the summer (70%) and lowest in the winter (50%). This can in part be attributed to meteorological transport patterns at the Underhill site. Southwesterly flow accompanied by warm temperatures and rainfall occurs during the summer, and these conditions produce the highest Hg wet deposition at the Underhill site (Gratz et al., 2009). Coal combustion was consistently calculated to be the largest source contributor, with 50-70% of the total annual Hg deposition from coal-fired utility boilers each year. These results are consistent with the findings of Gratz et al. (2009) that total annual Hg wet deposition has not changed from 1995 to 2006 due to consistent transport of Hg from the high emission source areas in the Midwest and East Coast where the density of coal-fired utility boilers is largest (Figure 3.1).

These source apportionment results can be compared to recently reported analysis of precipitation samples collected in Steubenville, OH (Keeler et al., 2006), which is in close proximity to various anthropogenic sources. Keeler et al. (2006) employed similar source apportionment techniques to examine two years of precipitation samples at the highly industrialized Steubenville site. Approximately 70% of Hg wet deposition at Steubenville was attributed to coal-fired utility boiler emissions, a source signature which was identified based on elevated contributions from S and Se. The remaining Hg wet deposition was attributed to iron-steel manufacturing (identified by loadings of Mn, Fe, and Cr), a phosphorus source (with high loadings from Mg, Mn, Fe, and Sr), waste incineration (with elevated Cd and S) and a nickel source. These source categories are similar to what was identified in the Underhill precipitation data. The most interesting

similarity between the remote Underhill site and the industrial Ohio location is the dominance of coal combustion emissions to Hg wet deposition at both locations.

3.3.4 1995-2000 and 2001-2006 PMF Model Results

Although Hg deposition did not decline from 1995 to 2006, a significant increase in precipitation amount occurred in the second half of the study (2001-2006) which led to a decline in the volume-weighted mean (VWM) Hg concentration (Gratz et al., 2009). To further explore the finding that Hg deposition did not decline in conjunction with the decrease in VWM concentration due to consistent transport from the Midwest and East Coast source regions (Gratz et al., 2009), the two six-year periods (1995-2000 and 2001-2006) of Hg and trace element deposition were also modeled separately using PMF (Tables 3.SI-2 and 3.SI-3). From 1995 to 2000, PMF identified the same five factors and comparable trace element loadings as those identified in the 1995-2006 data. Similarly, source factor contributions to Hg deposition were significant only for the smelter/incinerator, phosphorus, and coal combustion factors. PMF attributed a small amount of Hg deposition to iron-steel manufacturing from 1995 to 2000, but the contribution (8.2%) was not significant according to the bootstrap analysis. The percent contribution to Hg deposition from the smelter/incinerator, phosphorus, and coal combustion factors were 26.0%, 8.6% and 57.1%, respectively.

From 2001 to 2006, PMF only calculated four factors: mixed smelter and incinerator, phosphorus, iron-steel manufacturing, and coal combustion. The trace elements that apportioned to the oil combustion factor in 1995-2000 were predominantly distributed among the incinerator/smelter and coal combustion factors in the 2001-2006 analysis, which is reasonable based on knowledge of source emissions of these elements.

Hg deposition was only significantly attributed to the phosphorus (30.4%) and coal combustion (64.7%) sources in the 2001-2006 data, while the contributions from incinerator/smelter (3.7%) and iron-steel (1.2%) were insignificant in the bootstrap analysis. As hypothesized, PMF could no longer identify a contribution to Hg deposition from waste incineration. The determination of coal combustion emissions as the dominant contributor to Hg deposition was, however, consistent between the two six-year periods.

3.3.5 QTBA of Major Trace Elements

Application of the PMF model to the daily-event deposition data provided an estimate of the contributions of the major source types influencing wet deposition at Underhill. Key trace elements identified by the PMF model were further examined using QTBA to identify the likely locations of the sources contributing to these species. For example, Fe and Mg deposition amounts were selected to explore the source region associated with iron-steel manufacturing. QTBA suggests that the dominant sources of Fe and Mg are located in the Midwest, particularly in Ohio, southeast Michigan, western Pennsylvania, and southern Ontario (Figure 3.3), consistent with known locations of iron-steel manufacturing plants in the region (Figure 3.1).

In contrast, QTBA clearly indicated that the highest contributions to P and K were associated with east-southeasterly flow (Figure 3.3), suggesting a dominance of New England sources of these elements. These findings are consistent with the location of many of the region's wood-fired utility boilers (Figure 3.1), as well as the hypothesized contributions from the application of boiler ash and sewage sludge as fertilizer in the Northeast States. The results of QTBA on P and K may also suggest a marine source of

77

these elements (Figure 3.1), but lacking measurements of other common marine tracers such as Na and Cl it is unknown at this time whether this could be a likely source of P and K to Underhill.

QTBA calculated that Pb deposition was contributed from several sources or source regions (Figure 3.4). The contribution from the Midwest (Ohio and Pennsylvania) coincides with the location of many coal-fired utility boilers as well as Fe-steel production, while the contributions north of the site point to the location of Canadian smelters. The elevated contribution from eastern New York is likely due to the large cement production facilities in the Albany and downstate areas (Figure 3.1).

The contribution field for Vanadium deposition (Figure 3.4) clearly highlights the area along the east coast through New York and New Jersey where many of the major oil-fired utility boilers are located and where residual oil burning is common. Vanadium deposition additionally shows a fairly strong Midwestern contribution related to coal combustion emissions (Tuncel et al., 1985; Grahame and Hidy, 2004). Although molybdenum (Mo) was not used in the PMF model due to high analytical uncertainty associated with this element, it is a known tracer of oil-burning and thus was plotted in QTBA (Figure 3.4) to further identify the location of this source contribution. Its spatial distribution is similar to that for V in QTBA, with contributions along the East Coast and into the Northeast likely due to oil-fired utility boiler and residual oil burning emissions.

Finally, QTBA suggests a consistent contribution from the Midwestern U.S. to S and Se deposition in the Underhill precipitation data (Figure 3.4). These two elements are known tracers of coal combustion and the QTBA contribution fields point to the locations of the region's largest density of coal-fired utility boilers. The application of

QTBA to the aforementioned trace elements shows coherence with the known locations of major emission point sources, demonstrating that QTBA is capable of distinguishing between source regions for different elements and is a valuable tool for examining source contributions in event precipitation samples.

3.3.6 QTBA of Hg Deposition

The Hg deposition pattern from 1995 to 2006 in QTBA (Figure 3.5) is highly similar to the deposition patterns for S and Se (Figure 3.4) with the most likely source regions located in the Midwest and Ohio River Valley. This is consistent with the grouping of these elements within PMF. Contributions to Hg deposition can be observed to the south and southeast of the site similar to the regions identified for Pb and P deposition within QTBA; however the strong relationship between Hg, S and Se in PMF suggests that the dominant source region is located southwest of the Underhill site. The consistent pattern of Hg deposition with known coal-combustion tracers such as S and Se supports the hypothesis that coal-fired utility boilers are the largest sources of Hg in Underhill precipitation. The QTBA plots of Hg deposition in the two six year periods (1995-2000 and 2001-2006) also identify the Midwest as the dominant source region of Hg in Underhill wet deposition (Figure 3.5).

Finally, to connect the source apportionment results with the meteorological transport and likely source regions, the contributions to event Hg deposition amounts from the individual PMF source factors were also modeled as input to QTBA (Figure 3.6). The contribution to Hg deposition from the PMF smelter/incinerator factor shows that the likely sources are located in Midwest U.S., the Northeast U.S., and north of the Underhill site in Canada. This contribution to Hg deposition is similar to the regions

identified for Pb deposition in QTBA and coincides with the high loadings of Pb deposition on the PMF smelter/incinerator factor. These source regions are also suggestive of the locations of major metal smelters in the Midwest and in Canada, as well as the locations of municipal waste incinerators in the Northeast states (Figure 3.1).

Similarly to the QTBA plots of P and K deposition, the Hg deposition associated with the phosphorus source also suggests predominantly southeasterly transport from the New England coast, confirming a distinct transport direction associated with the phosphorus source. In this region, the most likely point sources of Hg with additional contributions of P and K are wood-fired industrial/commercial boilers (Figure 3.1). PMF and QTBA were collectively able to identify this source type and its likely location.

The contribution to Hg deposition from the PMF coal combustion factor also demonstrated a consistent pattern with the key elements in this source type. The PMF contribution to Hg deposition from coal combustion suggests transport of emissions from the Midwest. The contours associated with the highest Hg deposition from the coal combustion factor follows almost the same pattern as S and Se, confirming a common source of these elements as well as the use of S and Se as tracers of coal combustion.

Although PMF and QTBA were able to identify the likely compositions and locations of the smelter/incinerator and phosphorus sources, the contribution from these sources to Hg deposition was substantially smaller than the contribution from coal combustion. This is consistent with meteorological analysis at the Underhill site which demonstrated that the highest Hg wet deposition was observed with southwesterly transport along with rainfall and warm temperatures, whereas northerly and easterly transport were more likely associated with cold temperatures and snow or mixed

precipitation which are less effective at removing Hg from the atmosphere (Gratz et al., 2009).

3.4 Conclusions

This manuscript presents the application of source apportionment and hybrid-receptor models to a long-term precipitation dataset. PMF attributed Hg deposition measured at this remote location to source factors identified as coal-fired utility boilers, a combination of non-ferrous metal smelters and waste incinerators, and a mixture of wood-fired boilers and the application of boiler ash and sewage sludge as fertilizer. The PMF results further suggest that emissions from coal-fired utility boilers have consistently contributed to ~60% of Hg wet deposition. Although waste incineration was previously one of the largest anthropogenic sources in the U.S., the contribution from this source to Hg wet deposition was not substantial at Underhill. A strong contribution to Hg wet deposition from waste incineration should not be expected at Underhill because in addition to the restrictions placed on waste incinerator emissions during the first half of the Underhill study, the dominance of RGM in waste incinerator Hg emissions is not conducive to Hg transport to the remote monitoring location.

QTBA analysis of Hg and trace metal deposition was consistent with the known locations of major source types, identifying smelter/incinerator emissions from Canada as well as the Midwest and Northeast U.S., and distinct contributions from wood-fired utility boilers and fertilizer application from the Northeast states. QTBA also accurately identified the dominant locations of coal-fired utility boilers in the Midwestern U.S. The dominant contribution from this source region to the observed Hg deposition at Underhill is consistent with past findings that the highest levels of Hg deposition at Underhill occur

with southwesterly transport. The combined PMF and QTBA analysis provides strong

corroborative evidence to support the finding that total annual Hg wet deposition at

Underhill from 1995 to 2006 was due to consistent transport of Hg emissions from the

high emission source area in the Midwest where the density of coal-fired utility boilers is

greatest.

References

Annual survey of U.S. and Canadian Smelters (http://costs.infomine.com/costdatacenter/smeltingcosts.aspx).

Baertsch, C., Paez-Rubio, T., Viau, E., Peccia, J., 2007. Source tracking aerosols released from land-applied class B biosolids during high-wind events. Applied and Environmental Microbiology 73(14), 4522-4531.

Burke, J., Hoyer, M., Keeler, G.J. and Scherbatskoy, T. 1995. Wet deposition of mercury and ambient mercury concentrations at a site in the Lake Champlain Basin. Water, Air and Soil Pollution 80, 353-362.

Burke, J.M., 1998. An investigation of source-receptor relationships for atmospheric mercury in the Great Lakes Region using receptor modeling techniques. Ph.D. Dissertation, University of Michigan.

Butler, T.J., Cohen, M.D., Vermeylen, F.M., Likens, G.E., Schmeltz, D., Artz, R.S., 2008. Regional precipitation mercury trends in the eastern USA, 1998-2005: Declines in the Northeast and Midwest, no trend in the Southeast. Atmospheric Environment 42, 1582-1592.

Carpi, A., 1997. Mercury from combustion sources: A review of the chemical species emitted and their transport in the atmosphere. Water, Air, and Soil Pollution 98, 241-254.

Cohen, M.D., Artz, R.S., Draxler, R.R., 2007. Report to Congress: Mercury Contamination in the Great Lakes. NOAA Air Resources Laboratory, Silver Spring, MD.

Draxler, R.R. and Hess G.D., 1997. Description of the HYSPLIT_4 Modeling System. NOAA TECHNICAL MEMORANDUM ERL ARL-224.

Dvonch, J.T., Graney, J.R., Marsik, F.J., Keeler, G.J., Stevens, R.K., 1998. An investigation of source-receptor relationships for mercury in south Florida using event precipitation data. The Science of the Total Environment, 213, 95-108.

Dvonch, J.T., Graney, J.R., Keeler, G.J., Stevens, R.K., 1999. Use of Elemental Tracers to Source Apportion Mercury in South Florida Precipitation. Environmental Science and Technology 33, 4522-4527.

Environment Canada 2007 National Pollutant Release Inventory (NPRI) (www.ec.gc.ca/inrp-npri/).

Erich, M.S. and Ohno, T., 1992. Phosphorus availability to corn from wood ash-amended soils. Water, Air, & Soil Pollution 64, 475-485.

Evers, D.C., Han, Y-J., Driscoll, C.T., Kamman, N.C., Goodale, M.W., Lambert, K.F., Holsen, T.M., Chen, C.Y., Clair, T.A., Butler, T., 2007. Biological Mercury Hotspots in the Northeastern United States and Southeastern Canada. BioScience 57, 29-43.

Gao, N., Gildemeister, A.E., Krumhansl, K., Lafferty, K., Hopke, P.K., Kim, E., Poirot, R.L., 2006. Sources of Fine Particulate Species in Ambient Air over Lake Champlain Basin, VT. Journal of Air & Waste Management Association 56, 1607-1620.

Geagea, M.L., Stille, P., Perrone, Th., 2007. REE characteristics and Pb, Sr, and Nd isotopic compositions of steel plant emissions. Science of the Total Environment 373, 404-419.

Godish, T. *Air Quality, 4th Edition*. CRC Press: Boca Raton 2004.

Grahame, T. and Hidy, G., 2004. Using factor analysis to attribute health impacts to particulate pollution sources. Inhalation Toxicology, 16 (suppl. 1), 143-152.

Graney, J.R., Halliday, A.N., Keeler, G.J., Nriagu, J.O., Robbins, J.A., Norton, S.A., 1995. Isotopic record of lead pollution in lake sediments from the northeastern United States. Geochimica et Cosmochimica Acta, 59(9), 1715-1728.

Gratz, L.E., Keeler, G.J., Miller, E.K. 2009. Long-term relationships between mercury wet deposition and meteorology. Atmospheric Environment 43, 6218-6229.

Greenberg, R.R., Gordon, G.E., Zoller, W.H., Jacko, R.B., Neuendorf, D.W., Yost, K.J., 1978. Composition of particles emitted from the Nicosia Municipal Incinerator. Environmental Science and Technology 12(12), 1329-1332.

Hammerschmidt, C.R. and Fitzgerald, W.F., 2006. Methylmercury in Freshwater Fish Linked to Atmospheric Mercury Deposition. Environmental Science and Technology 40, 7764-7770.

Hammond, D.M., Dvonch, J.T., Keeler, G.J., Parker, E.A., Kamal, A.S., Barres, J.A., Yip, F.Y., Brakefield-Caldwell, W., 2008. Sources of ambient fine particulate matter at two community sites in Detroit, MI. Atmospheric Environment 42, 720-732.

Handbook of Chemistry and Physics (http://www.speclab.com).

Kahl, J.D. and Samson, P.J., 1986. Uncertainty in Trajectory Calculations Due to Low Resolution Meteorological Data. Journal of Climate and Applied Meteorology 25, 1816-1831.

Keeler, G.J. and Samson, P.J., 1989. Spatial representativeness of trace element ratios. Environmental Science and Technology 23, 1358-1364.

Keeler, G.J.; Gratz, L.E.; Al-Wali, K., 2005. Long-term atmospheric mercury wet deposition at Underhill, Vermont. Ecotoxicology 14, 71-83.

Keeler, G.J., Landis, M.S., Norris, G.A., Christianson, E.M., Dvonch, J.T., 2006. Sources of mercury wet deposition in Eastern Ohio, USA. Environmental Science and Technology 40, 5874-5881.

King, S., Miller, P., Goldberg, T., Graham, J., Hochbrunn, S., Wienert, A., Wilcox, M., 2008. Reducing mercury in the Northeast United States. Air & Waste Management Association (http://www.neiwpcc.org/mercury/mercury-docs/kingNEmercuryprogress.pdf).

Kitto, M.E., Anderson, D.L., Gordon, G.E., Olmez, I., 1992. Rare earth distributions in catalysts and airborne particles. Environmental Science and Technology 26, 1368-1375.

Kitto, M.E., 1993. Trace-element patterns in fuel oils and gasolines for use in source apportionment. Journal of Air and Waste Management, 43, 1381-1388.

Krachler, M., Mohl, C., Emons, H., Shotyk, W., 2003. Two thousand years of atmospheric rare earth element (REE) deposition as revealed by an ombotrophic peat bog profile, Jura Mountains, Switzerland. Journal of Environmental Monitoring, 5(1), 111-121.

Landis, M.S. and Keeler, G.J., 1997. Critical Evaluation of a Modified Automatic Wet-Only Precipitation Collector for Mercury and Trace Element Determinations. Environmental Science and Technology 31, 2610-2615.

Lin, C. and Pehkonen, S.O., 1999. The chemistry of atmospheric mercury. Atmospheric Environment 33, 2067-2079.

Liu, B., 2007. Atmospheric mercury speciation in urban air: Identifying the relative importance of local anthropogenic sources in Detroit, Michigan. Ph.D. Dissertation, University of Michigan.

Liu, B., Keeler, G.J., Dvonch, J.T., Barres, J.A., Lynam, M.M., Marsik, F.J., Morgan, J.T., 2007. Temporal variability of mercury speciation in urban air. Atmospheric Environment, 41, 1911-1923.

Liu, W., Hopke, P.K., Han, Y., Yi, S., Holsen, T.M., Cybart, S., Kozlowski, K., Milligan, M., 2003. Application of receptor modeling to atmospheric constituents at Potsdam and Stockton, NY. Atmospheric Environment 37, 4997-5007.

Lucey, D., Hadjiiski, L., Hopke, P.K., Scudlark, J.R., Church, T., 2001. Identification of sources of pollutants in precipitation measured at the mid-Atlantic US coast using

potential source contribution function (PSCF). Atmospheric Environment 35, 3979-3986.

Machemer, S.D., 2004. Characterization of airborne bulk particulate from iron and steel manufacturing facilities. Environmental Science and Technology 38, 381-389.

Mahowald, N., Jickells, T.D., Baker, A.R., Artaxo, P., Benitez-Nelson, C.R., Bergametti, G., Bond, T.C., Chen, Y., Cohen, D.D., Herut, B., Kubilay, N., Losno, R., Luo, C., Maenhaut, W., McGee, K.A., Okin, G.S., Siefert, R.L., Tsukuda, S., 2008. Global distribution of atmospheric phosphorus sources, concentrations and deposition rates, and anthropogenic impacts. Global Biogeochemical Cycles 22, GB4026.

Mamane, Y. and Pirrone, N. Vanadium in the atmosphere. In *Vanadium in the Environment Part 1: Chemistry and Biochemistry*; Nriagu, J.O., Ed; John Wiley & Sons, Inc.: New York 1998; pp 37-72.

Morishita, M., Keeler, G.J., Wagner, J.G., Harkema, J.R., 2006. Source identification of ambient PM2.5 during summer inhalation exposure studies in Detroit, MI. Atmospheric Environment 40, 3823-3834.

New England Interstate Water Pollution Control Commission (NEIWPCC), 2007. Northeast Regional Mercury Total Maximum Daily Load (http://www.neiwpcc.org/mercury/mercury-docs/FINAL%20Northeast%20Regional%20Mercury%20TMDL.pdf).

Norris, G., Vedantham, R., Wade, K., Brown, S., Prouty, J., Foley, C., 2008. EPA Positive Matrix Factorization (PMF) 3.0 Fundamentals & User Guide. U.S. Environmental Protection Agency.

Northeast States for Coordinated Air Use Management (NESCAUM), 2005. Inventory of Anthropogenic Mercury Emissions in the Northeast. November 30, 2005 Report (http://www.nescaum.org/documents/inventory-of-anthropogenic-mercury-emissions-in-the-northeast/).

Northeast States for Coordinated Air Use Management (NESCAUM), 2007. Northeast States Succeed in Reducing Mercury in the Environment, October 24, 2007 Report Summary (http://www.nescaum.org/documents/northeast-states-succeed-in-reducing-mercury-in-the-environment/).

Olmez, I., Gordon, G.E., 1985. Rare Earths: Atmospheric signatures for oil-fired power plants and refineries. Science, 229, 966-968.

Olmez, I., Sheffield, A.E., Gordon, G.E., Houck, J.E., Pritchett, L.C., Cooper, J.A., Dzubay, T.G., Bennett, R.L., 1988. Compositions of particles from selected sources in Philadelphia for receptor modeling applications. JAPCA, 38, 1392-1402.

Olmez, I., Ames, M.R., Gullu, G., 1998. Canadian and U.S. sources impacting the mercury levels in fine atmospheric particulate material across New York State. Environmental Science and Technology, 32, 3048-3054.

Paatero, P., 1997. Least squares formulation of robust non-negative factor analysis. Chemometrics and Intelligent Laboratory Systems 37, 23-35.

Pitman, R.M., 2006. Wood ash use in forestry – a review of the environmental impacts. Forestry 79(5), 563-588.

Poirot, R.L., Wishinski, P.R., Hopke, P.K., Polissar, A.V., 2001. Comparative Application of Multiple Receptor Methods to Identify Aerosol Sources in Northern Vermont. Environmental Science and Technology 35, 4622-4636.

Polissar, A.V., Hopke, P.K., Poirot, R.L., 2001. Atmospheric Aerosol over Vermont: Chemical Composition and Sources. Environmental Science and Technology 35, 4604-4621.

Rahn, K.A., Lowenthal, D.H., 1984. Elemental Tracers of Distant Regional Pollution Aerosols. Science 223(4632), 132-139.

Schroeder, W.H., Munthe, J., 1998. Atmospheric mercury - An overview. Atmospheric Environment 32, 809-822.

Schuhmacher, M., Domingo, J.L., Garreta, J., 2004. Pollutants emitted by a cement plant: health risks for the population living in the neighborhood. Atmospheric Environment, 95, 198-206.

Seigneur, C., Lohman, K., Vijayaraghavan, K., Jansen, J., Levin, L., 2006. Modeling atmospheric mercury deposition in the vicinity of power plants. Journal of Air and Waste Management 56, 743-751.

Tuncel, S.G., Olmez, I., Parrington, J.R., Gordon, G.E., 1985. Composition of fine particle regional sulfate component in Shenandoah Valley. Environmental Science and Technology, 19, 529-537.

U.S. Environmental Protection Agency (U.S. EPA), 1997. Mercury Study Report to Congress, Volume 2. EPA-452/R-97-003; Office of Air Quality Planning and Standards, Office of Research and Development: Washington DC.

U.S. Environmental Protection Agency (U.S.EPA) 2002 National Emissions Inventory (NEI) on Planet Hazard (http://www.planethazard.com).

U.S. Environmental Protection Agency (U.S.EPA) 2005 National Emissions Inventory (NEI) Data and Documentation (www.epa.gov/ttnchie1/net/2005inventory.html).

Vance, E.D., 1996. Land application of wood-fired and combination boiler ashes: An overview. Journal of Environmental Quality 25, 937-944.

Wen, H. and Carignan, J., 2007. Reviews on atmospheric selenium: Emissions, speciation, and fate. Atmospheric Environment 41, 7151-7165.

White, E.M., Keeler, G.J. and Landis, M.S. 2009. Spatial variability of mercury wet deposition in Eastern Ohio: Summertime meteorological case study analysis of local source influences. Environmental Science and Technology 43, 4946-495.

White, E.M., 2009. Source attribution, physicochemical properties and spatial distribution of wet deposited mercury to the Ohio River Valley. Ph.D. Dissertation, University of Michigan.

Yoo, S-J., 2006. Source apportionment of mercury in ambient air and in precipitation at New England region using hybrid receptor model. Ph.D. Dissertation, University of Michigan.

Zoller, W., 1973. Sources and distribution of vanadium in the atmosphere. Advances in Chemistry Series 123, 31-47.
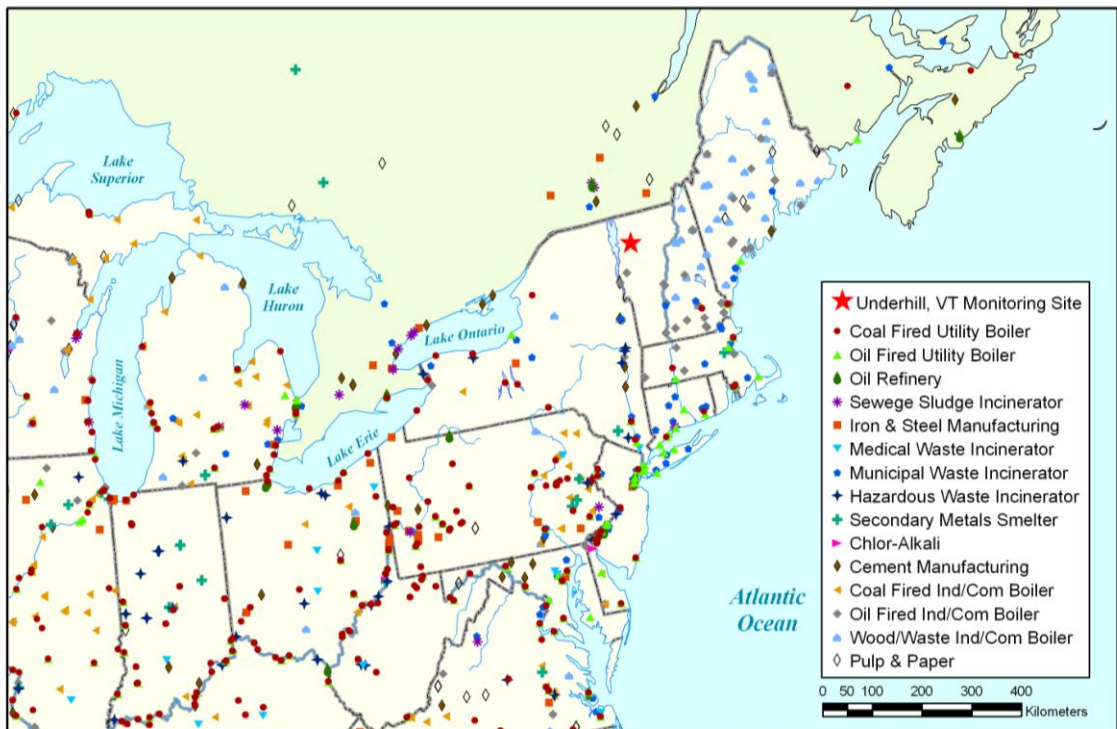
Figure 3.1: Location of the Underhill, VT monitoring site and major mercury point sources emitting ≥ 0.1 kg/yr (2005 U.S. EPA NEI; 2007 Environment Canada NPRI). Source categories for U.S. sources correspond to the MACT source category.
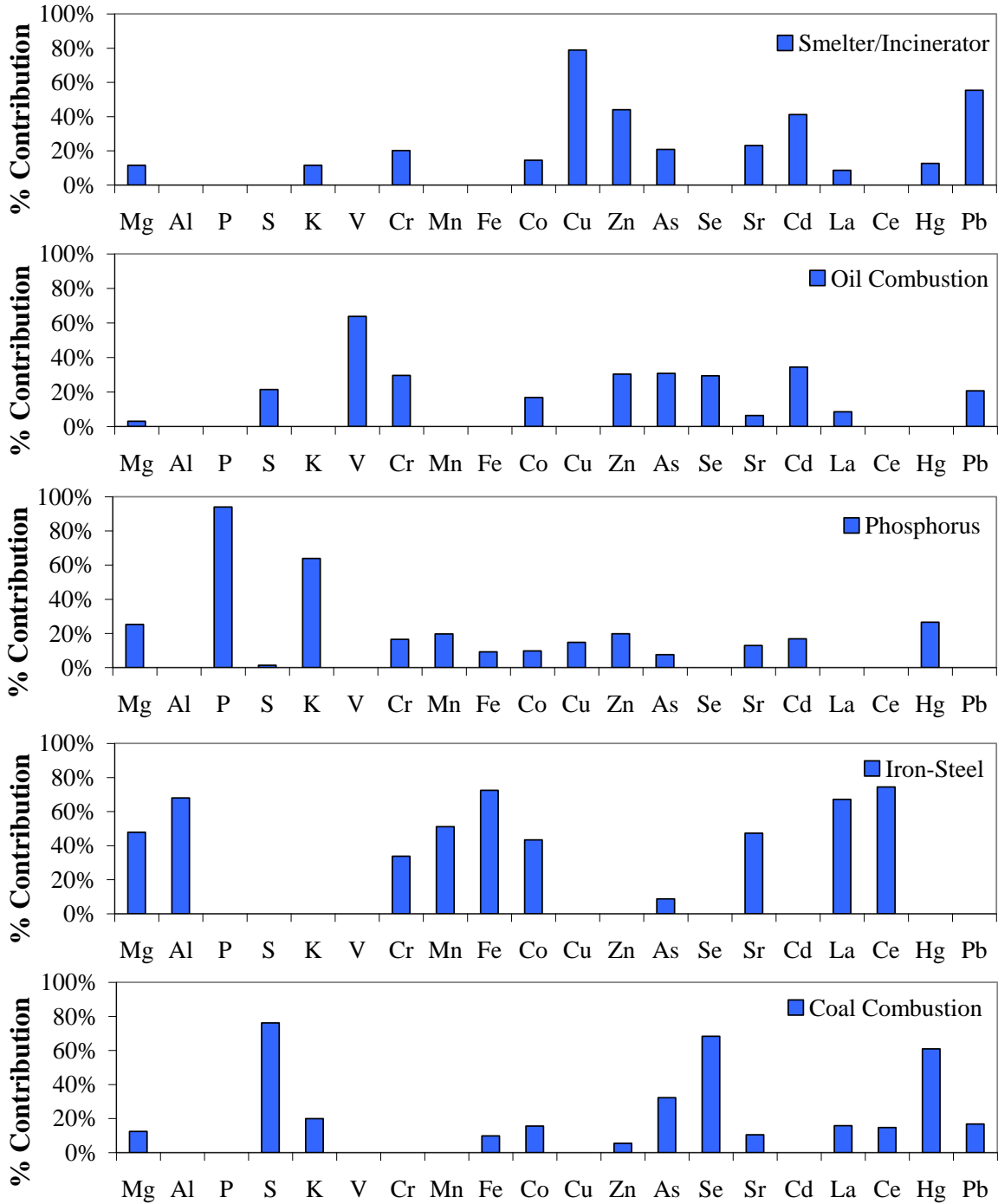
Figure 3.2: Percent of the total modeled deposition of each element attributed to the to the PMF factors.
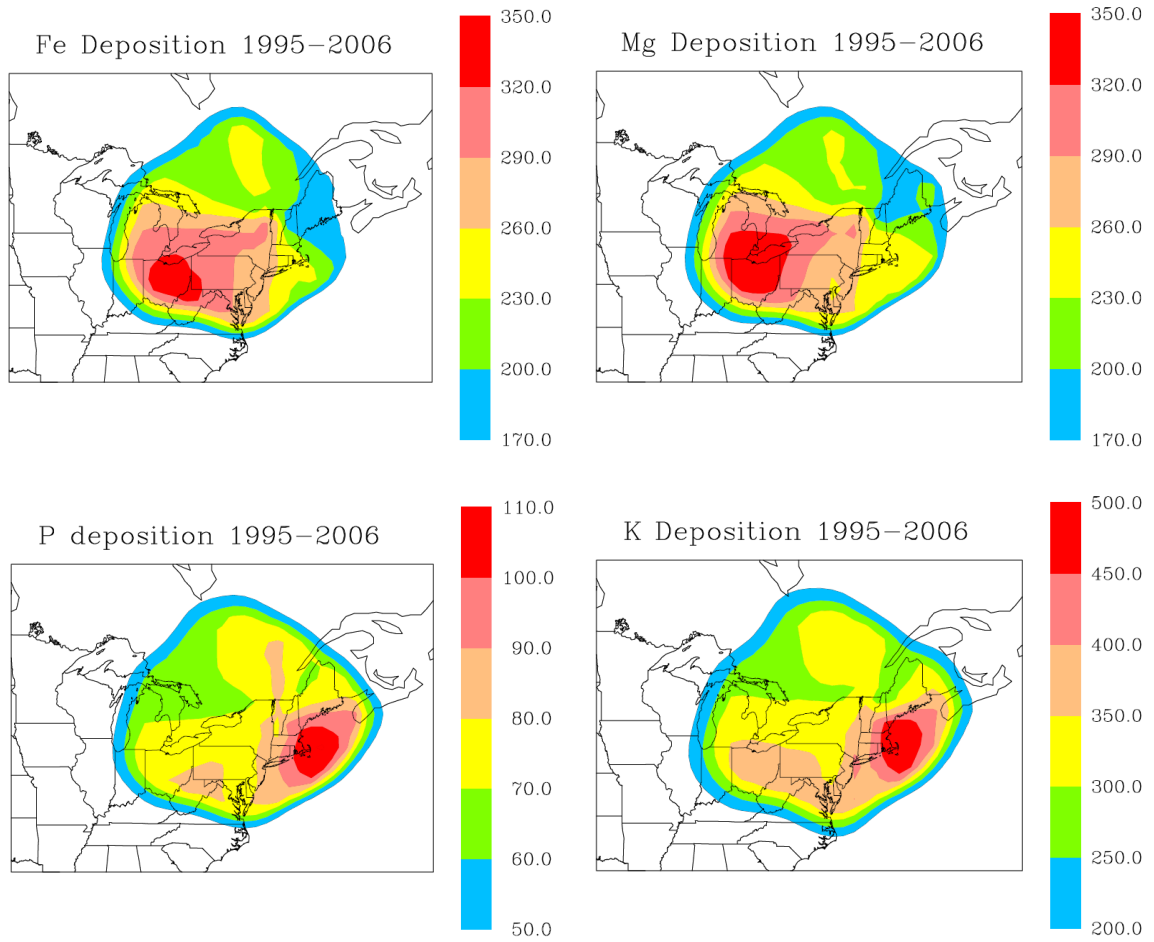
Figure 3.3. QTBA plots of Fe, Mg, P and K wet deposition at Underhill, VT from 1995 to 2006. Contours for all elements are in units of μg/m^2.
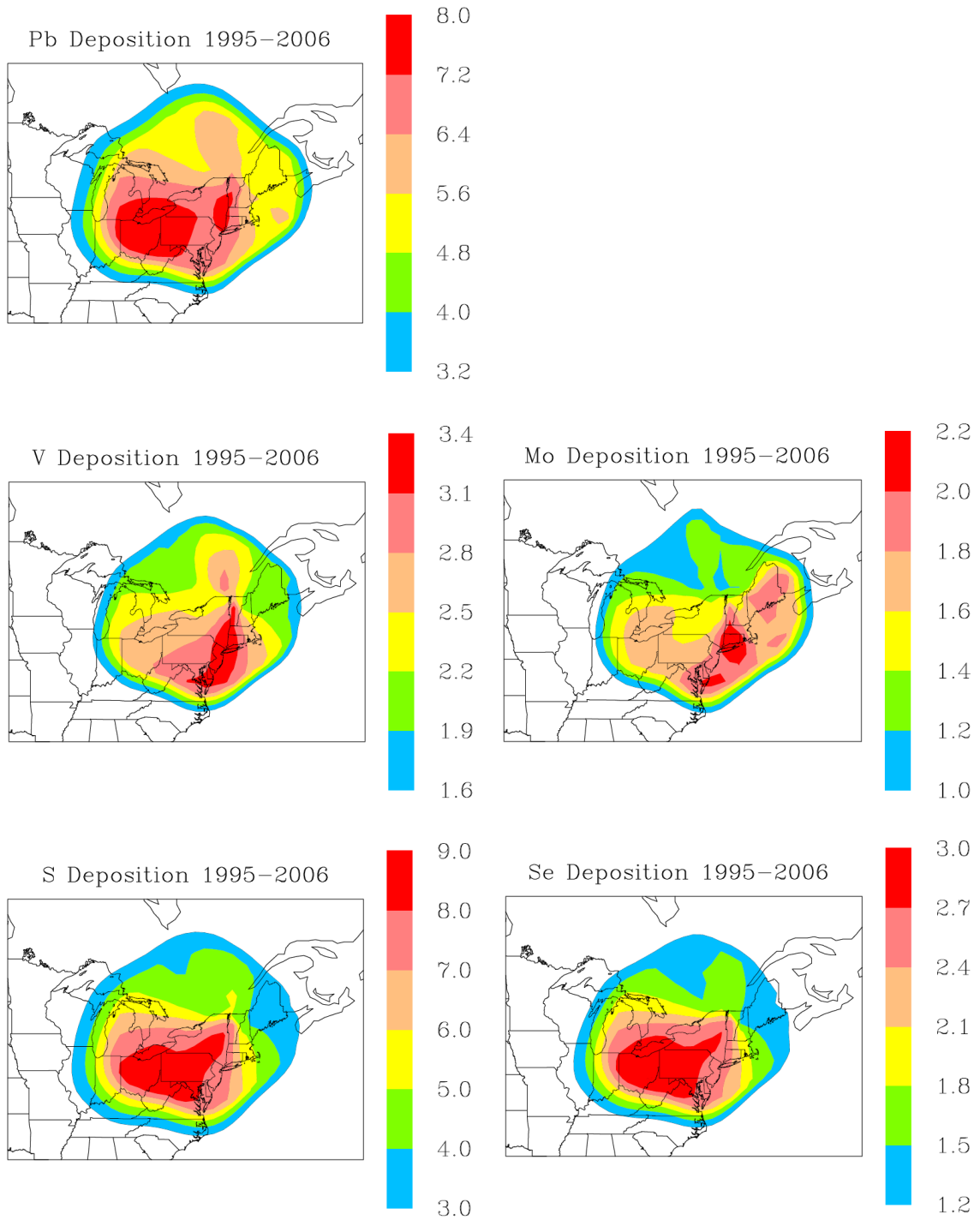
Figure 3.4. QTBA plots of Pb, V, Mo, S and Se wet deposition at Underhill, VT from 1995 to 2006. Contours for all elements are in units of μg/m², with the exception of S which is in units of mg/m².
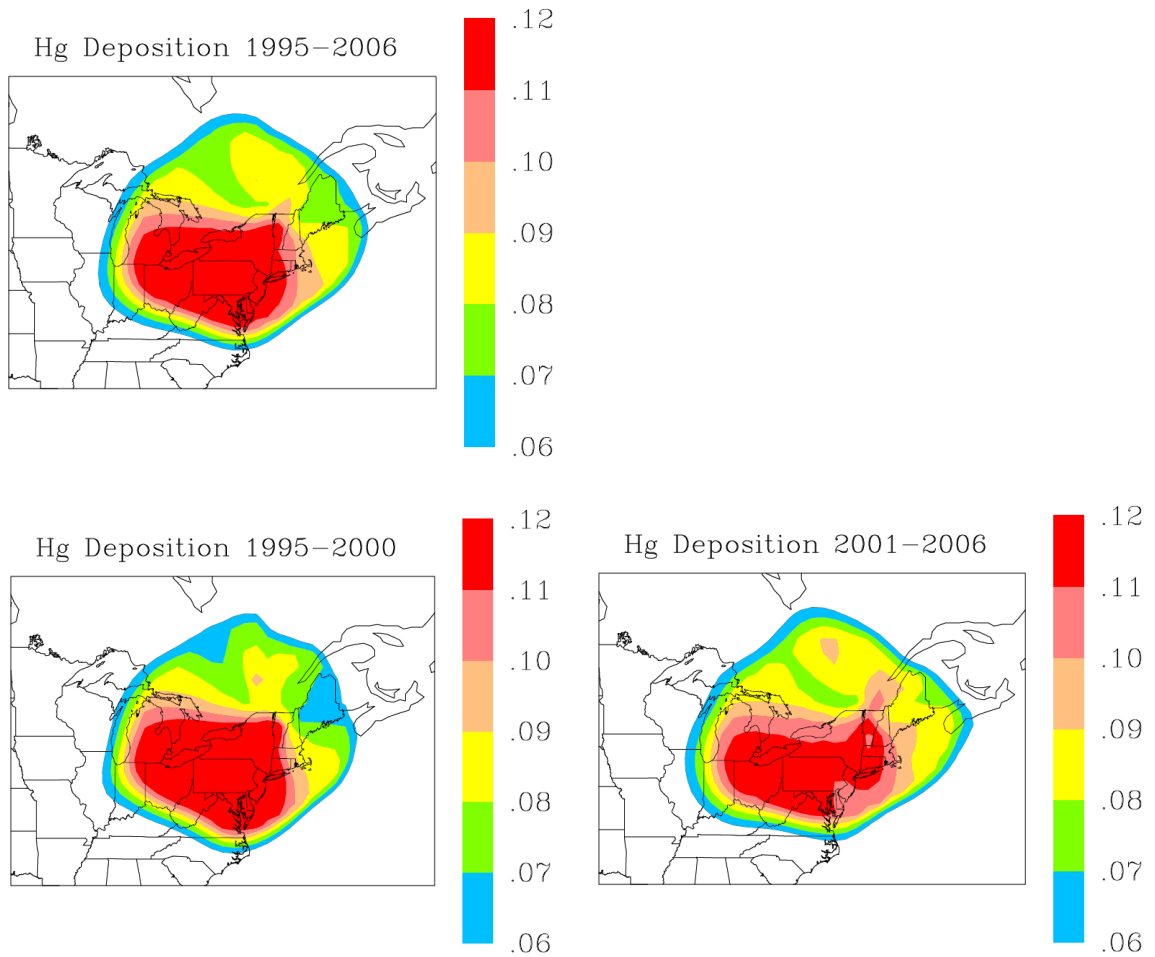
Figure 3.5. QTBA plots of Hg wet deposition at Underhill, VT from 1995-2006, 1995-2000, and 2001-2006. Contours are in units of μg/m^2.
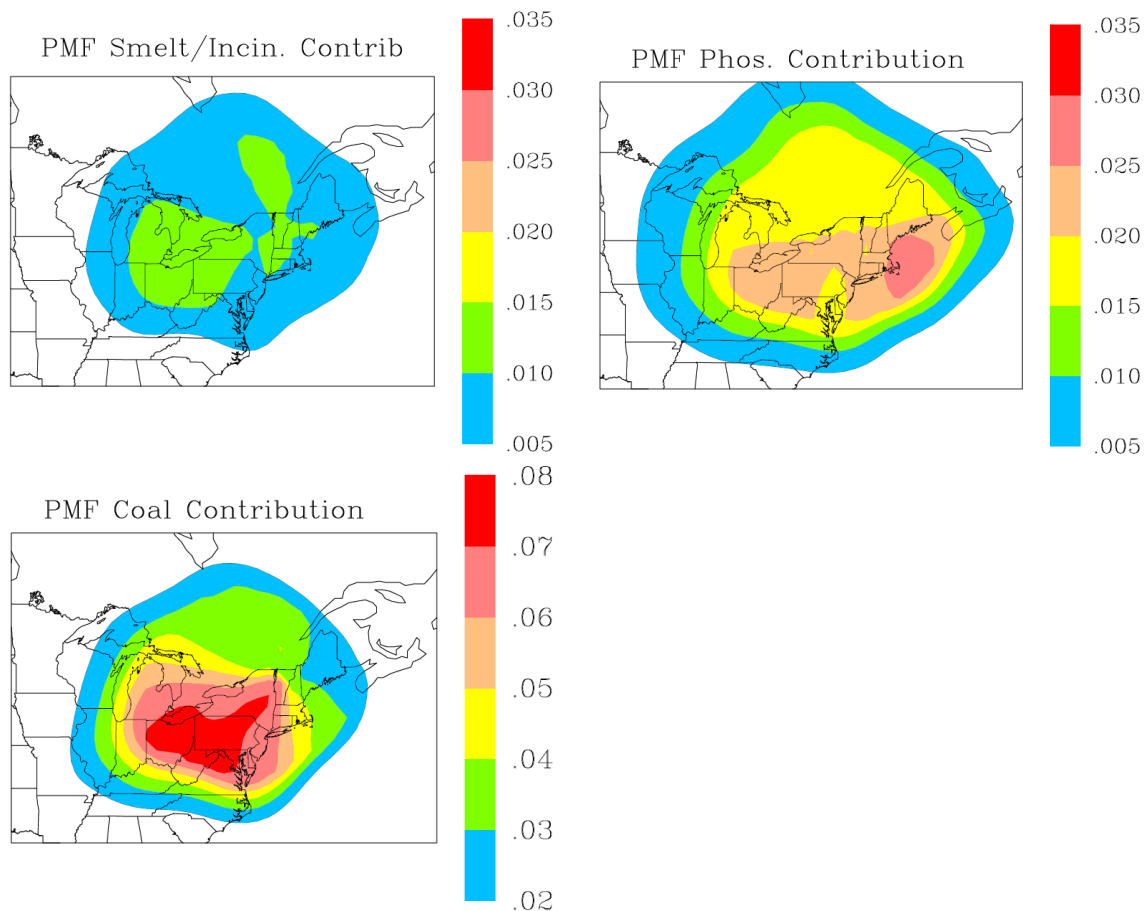
Figure 3.6. QTBA plots of PMF factor contributions to Hg wet deposition at Underhill, VT from 1995-2006. Contours represent μg/m^2 of Hg. Note the different scale on the Smelter/Incinerator and Phosphorus contribution plots compared to the Coal Combustion contribution plot.

Table 3.1: PMF source factor profiles for Underhill precipitation samples from 1995 to 2006. The highest contribution from each element is shown in bold.

	Smelter/ Incinerator	Oil Combustion	Phosphorous	Iron-Steel	Coal Combustion	% of Deposition Explained
Mg	26.2	6.8	57.2	**108.4**	28.3	89%
Al	*	*	*	**160**	*	58%
P	*	*	**64**	*	*	82%
S	*	1173	72	*	**4165**	91%
K	*	*	**160.0**	*	49.9	61%
V	*	**1.39**	*	*	*	57%
Cr	0.14	0.20	0.11	**0.23**	*	79%
Mn	*	*	3.07	**8.00**	*	46%
Fe	*	*	20	**160**	22	82%
Co	0.03	0.04	0.02	**0.09**	0.03	87%
Cu	**11.3**	*	2.1	*	*	60%
Zn	**18.7**	12.9	8.4	*	2.3	71%
As	0.20	0.29	0.07	0.08	**0.31**	86%
Se	*	0.52	*	*	**1.21**	84%
Sr	0.88	0.24	0.49	**1.80**	0.40	90%
Cd	**0.18**	0.15	0.07	*	*	70%
La	0.02	0.02	*	**0.16**	0.04	89%
Ce	*	*	*	**0.32**	0.06	81%
Hg	0.01	*	0.02	*	**0.05**	78%
Pb	**2.9**	1.09	*	*	0.9	78%
% Hg	**12.7%**	*	**26.5%**	*	**60.7%**	

*not significant at 95% confidence interval
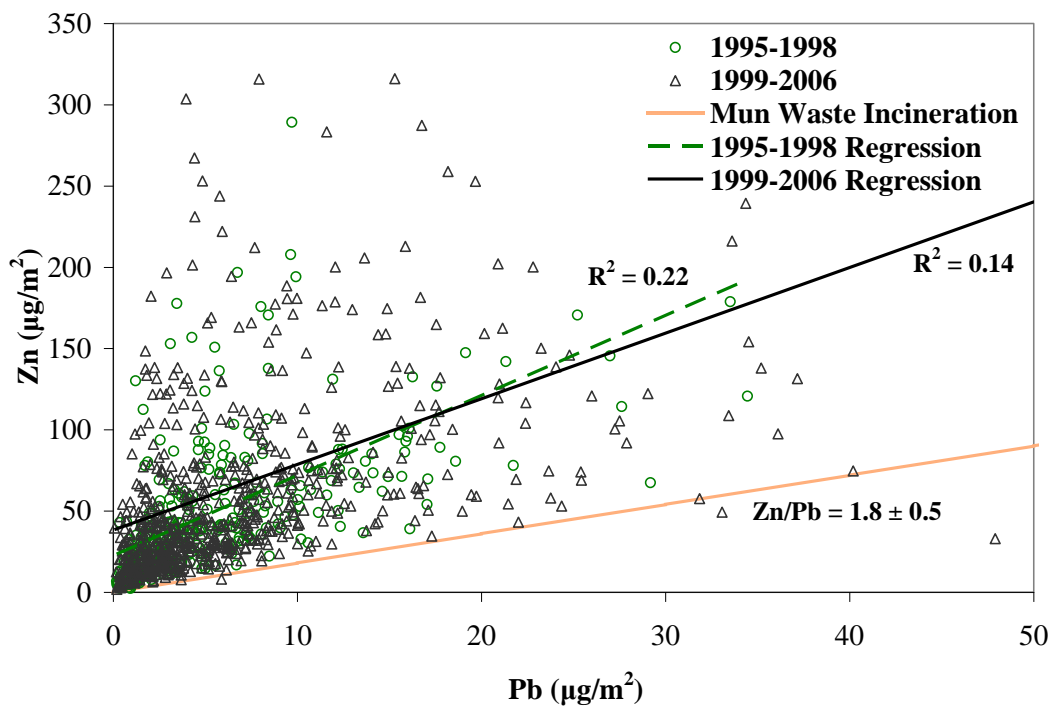
(a)
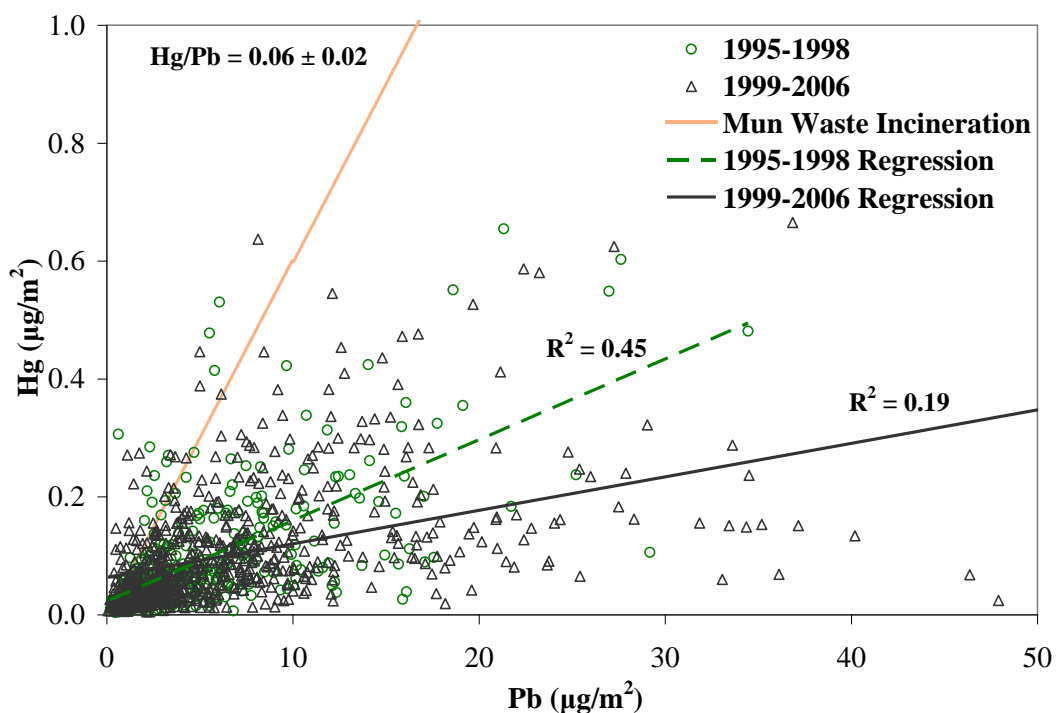
(b)

Figure 3.SI-1: Regressions of (a) Zn vs Pb and (b) Hg vs Pb in Underhill, VT precipitation samples with respect to observed values in municipal waste incinerator emissions.
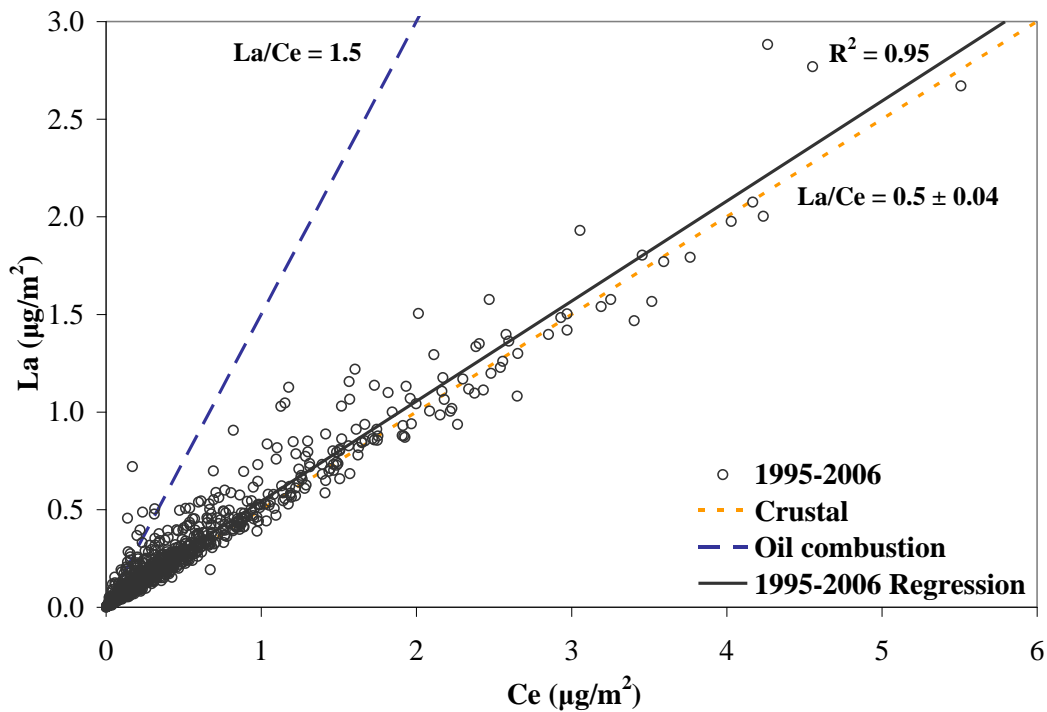
(a)
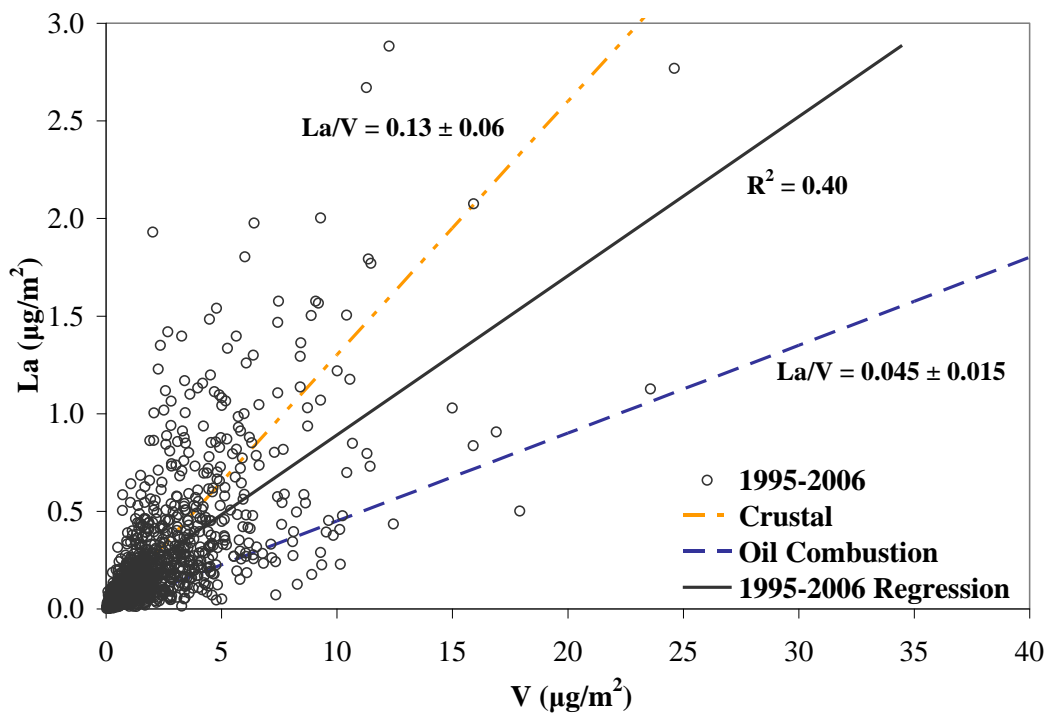
(b)

Figure 3.SI-2: Regressions of (a) La vs Ce and (b) La vs V in Underhill, VT precipitation samples with respect to observed values in crustal material and oil combustion emissions.
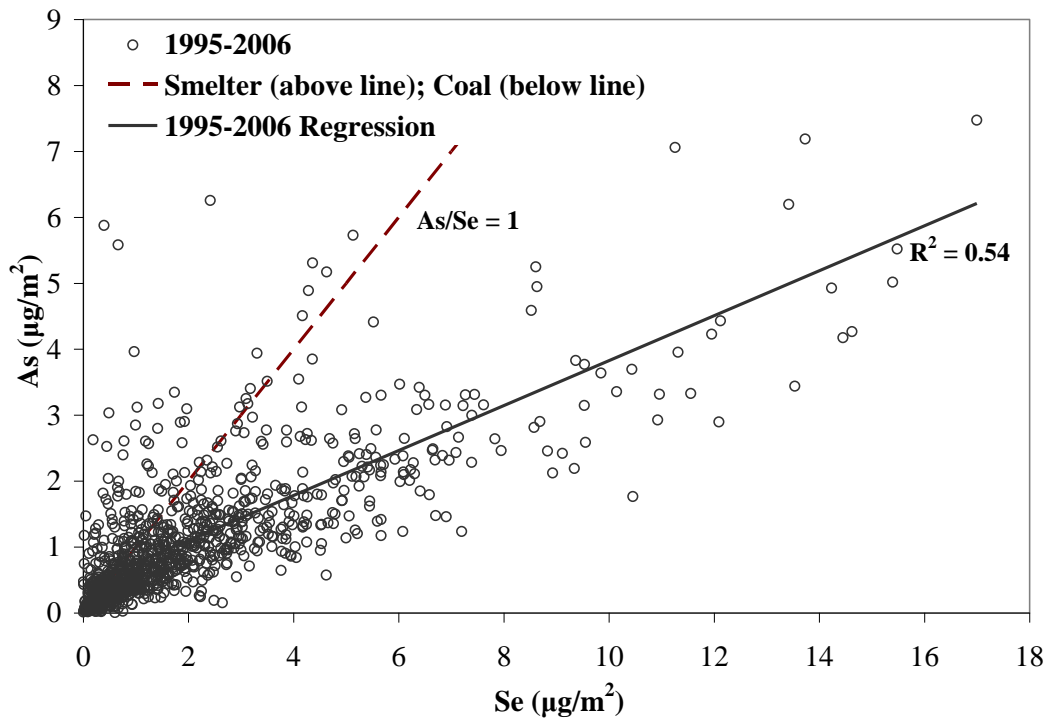
(a)
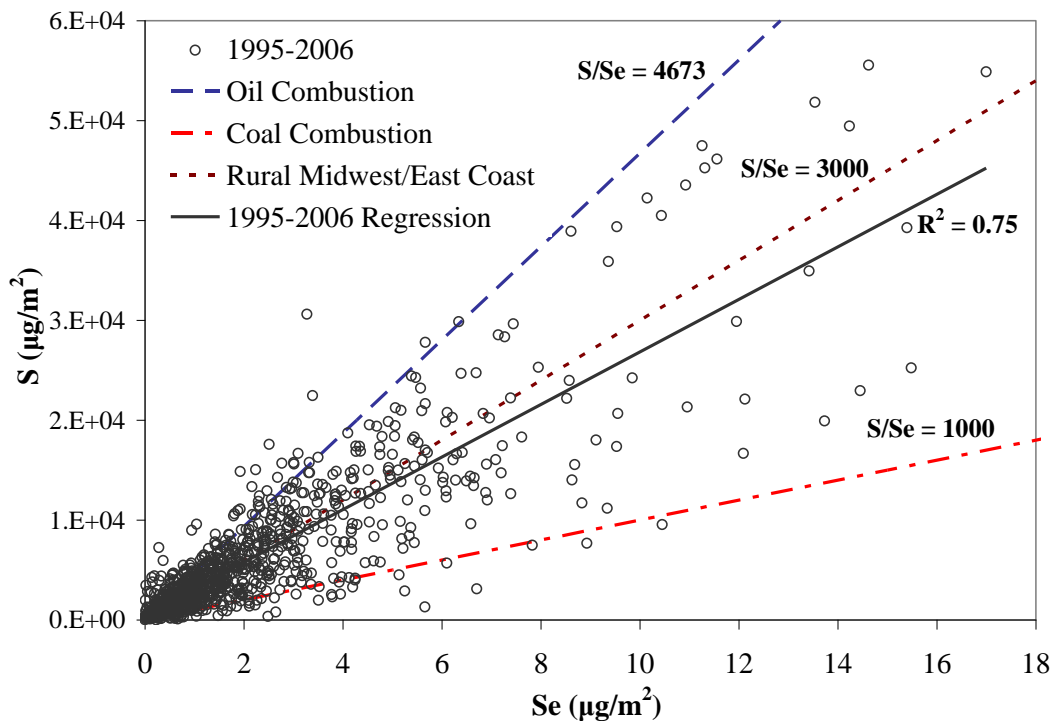
(b)

Figure 3.SI-3: Regressions of (a) As vs Se and (b) S vs Se in Underhill, VT precipitation samples with respect to observed ratios in emissions from (a) coal combustion and metal smelting, and (b) oil and coal combustion.

Table 3.SI-1. Average analytical uncertainty for trace elements analyzed using ICP-MS. Reported values are the average relative standard deviations (RSD) in % for each element, where the RSD is the standard deviation of the three replicate analysis of each sample.

Element	Symbol	RSD (%)
Magnesium	Mg	2.9
Aluminum	Al	2.8
Phosphorus	P	7.0
Sulfur	S	3.0
Potassium	K	4.1
Vanadium	V	3.8
Chromium	Cr	5.7
Manganese	Mn	4.2
Iron	Fe	3.7
Cobalt	Co	11.2
Copper	Cu	3.3
Zinc	Zn	3.5
Arsenic	As	10.7
Selenium	Se	22.7
Strontium	Sr	2.0
Cadmium	Cd	4.3
Lanthanum	La	2.9
Cerium	Ce	2.7
Lead	Pb	3.1

Table 3.SI-2: PMF source factor profiles for Underhill precipitation samples from 1995 to 2000. The highest contribution from each element is shown in bold.

	Smelter/ Incinerator	Oil Combustion	Phosphorous	Iron-Steel	Coal Combustion	% of Deposition Explained
Mg	37.2	*	41.2	**133.6**	9.0	87%
Al	57	*	*	**199**	*	76%
P	*	*	**69**	*	*	86%
S	*	1500	*	*	**3912**	95%
K	*	25.9	**150.5**	59.0	30.7	80%
V	*	**1.79**	*	*	*	69%
Cr	**0.35**	0.13	*	0.27	*	79%
Mn	*	*	4.96	**9.32**	*	60%
Fe	17	*	5	**210**	25	86%
Co	0.04	0.04	0.01	**0.11**	0.02	94%
Cu	**7.7**	*	0.7	*	*	58%
Zn	**34.5**	8.4	*	*	*	71%
As	0.19	**0.35**	0.05	0.13	0.21	85%
Se	0.08	0.54	*	*	**1.10**	86%
Sr	0.61	0.53	0.28	**2.23**	*	90%
Cd	**0.20**	0.16	0.04	*	*	79%
La	*	0.05	*	**0.19**	*	87%
Ce	*	*	*	**0.38**	0.03	83%
Hg	0.02	*	0.01	*	**0.04**	75%
Pb	0.7	**2.0**	*	0.4	0.7	76%
% Hg	**26.0%**	*	**8.6%**	*	**57.1%**	

*not significant at 95% confidence interval

Table 3.SI-3: PMF source factor profiles for Underhill precipitation samples from 2000 to 2006. The highest contribution from each element is shown in bold.

	Smelter/ Incinerator	Phosphorous	Iron-Steel	Coal Combustion	% of Deposition Explained
Mg	*	53.97	**120.6**	41.18	85%
Al	34	11	**117**	*	76%
P	*	**61**	*	*	81%
S	*	234	297	**4846**	87%
K	*	**218.6**	*	51.7	75%
V	0.19	*	0.27	**1.37**	80%
Cr	**0.29**	0.05	0.18	0.08	81%
Mn	*	4.20	**9.08**	1.60	62%
Fe	10	13	**121**	15	87%
Co	0.04	0.02	**0.10**	0.06	81%
Cu	**16.3**	2.3	*	*	60%
Zn	**24.5**	7.1	*	13.8	77%
As	0.25	0.06	0.07	**0.62**	88%
Se	0.10	*	*	**1.67**	84%
Sr	0.60	0.56	**2.02**	0.75	88%
Cd	0.24	0.06	*	0.19	73%
La	0.01	*	**0.18**	0.05	87%
Ce	*	*	**0.34**	0.04	82%
Hg	*	0.02	*	**0.05**	66%
Pb	**4.13**	*	0.3	1.93	84%
% Hg	*	30.4%	*	**64.7%**	

*not significant at 95% confidence interval

CHAPTER 4

Atmospheric Mercury Transport Across Southern Lake Michigan: Influence from the Chicago/Gary Urban Area

Abstract

Quantifying the local and regional impacts of mercury (Hg) emissions from major urban and industrial areas is critical in order to further understand Hg cycling in the environment. The Chicago/Gary area is one such location in which Hg emissions from industrial sources are significant and regional Hg transport needs to be further examined. Speciated atmospheric Hg was measured in Chicago, IL and Holland, MI from July to November 2007 to obtain a better characterization of the impact of Chicago/Gary on southwest Michigan and improve our understanding of the transport and deposition of Hg species. The mean fine particulate bound mercury (Hg_p) concentration was ~1.5 times higher while gaseous elemental mercury (Hg^0) and divalent reactive gaseous mercury (RGM) concentrations were ~2 times higher in Chicago than in Holland. Meteorological analysis indicated that southwest transport to the Holland site from Chicago/Gary occurred frequently during the study, leading to 6% and 8% increases in Hg^0 and Hg_p concentrations, respectively, and a five-fold increase in RGM concentrations in Holland. Two transport case studies are presented using speciated Hg data from Holland and Chicago along with dispersion modeling to further demonstrate the impact of Chicago/Gary sources on southeast Michigan and to elucidate the role of

direct transport and dispersion of Hg emissions. Results suggest that ~52% of the observed RGM peaks in Holland could be attributed to direct transport of primary Hg emissions from Chicago with the remainder associated with Hg^0 oxidation during transport over the lake. The presented analyses demonstrate the spatial scale of impact of speciated Hg emissions from a large urban area on a more remote downwind location.

4.1 Introduction

Mercury (Hg) is a hazardous neurotoxin released to the environment by a variety of natural and anthropogenic sources. It is a pollutant of great public health concern because of its ability to bioaccumulate within the aquatic food chain (U.S. EPA, 1997). The Great Lakes were targeted under the Great Waters Provision of the Clean Air Act Amendments of 1990 as an area in which monitoring of Hg transport and deposition was needed due to elevated Hg levels in the aquatic ecosystem (U.S. EPA, 1994). Atmospheric deposition now is widely recognized as the dominant mechanism for Hg inputs to Lake Michigan (Mason and Sullivan, 1997; Landis and Keeler, 2002), and previous studies have demonstrated the substantial contributions from sources in the Chicago/Gary urban area to atmospheric Hg in the region (Landis et al., 2002; Landis and Keeler, 2002; Vette et al, 2002). Defining the local and regional impacts of atmospheric Hg emissions from major urban and industrial sources in the Chicago/Gary urban area is critical to improving our understanding of atmospheric Hg transport and deposition in the Great Lakes region.

Hg displays complex chemistry in the atmosphere that allows it to deposit locally (White et al., 2009) as well as be transported regionally (Gratz et al., 2009) and globally

(Jaffe et al., 2005; Weiss-Penzias et al., 2006), leading to great challenges in understanding the biogeochemical cycling of Hg. Hg is emitted to the atmosphere in three main forms: gaseous elemental Hg (Hg^0), fine particle bound Hg (Hg_p), and divalent reactive gaseous Hg (RGM). Hg^0 is not very water soluble or particle-reactive and thus can be transported great distances before being deposited, whereas the reactive forms, Hg_p and RGM (collectively Hg(II)), are very water soluble and tend to deposit close to sources (Schroeder and Munthe, 1998). Atmospheric reactions that convert Hg between its reactive (Hg(II)) and nonreactive (Hg^0) forms (Seigneur et al., 1994; Lin and Pehkonen 1997; Lin and Pehkonen 1999), as well as the deposition and re-emission of Hg from terrestrial and aquatic surfaces (Schroeder and Munthe, 1998; Gustin et al., 2008) create further challenges in understanding Hg chemistry and transport.

The Chicago/Gary urban area lies on the southwestern shore of Lake Michigan (Figure 4.1). This region is defined by 14 counties in northeastern Illinois, northwestern Indiana, and southeastern Wisconsin (U.S. Census Bureau). The major Hg emission point sources in this area include secondary metal smelters, iron-steel manufacturers, and coal- and oil-fired utility boilers. Coal-combustion is the largest anthropogenic emitter of total Hg in the region as well as in the United States (U.S. EPA 2005 NEI). Nine coal-fired utility boilers (CFUBs) contribute ~75% of the total Hg emissions from the Chicago/Gary area and collectively emit nearly 3 tons per year (tpy) of Hg (U.S. EPA 2005 NEI). Nationally, CFUBs emit ~50 tpy of Hg (U.S. EPA, 1997; Cohen et al., 2007; Butler et al., 2008). Emissions from CFUBs are typically ~50-80% Hg(II), and ~20-50% Hg^0 (Carpi, 1997; Seigneur et al., 2006). Additionally, because Hg_p is more easily removed by filters and other control equipment in the stack, it is expected to comprise

less than 5% of total Hg emissions from combustion and therefore Hg(II) emissions from combustion should be predominantly RGM (Carpi, 1997).

The Lake Michigan Mass Balance Study (LMMBS) and the Atmospheric Exchange Over Lakes and Oceans Study (AEOLOS) were initiated in 1994 to identify the major Hg sources in the region and to quantify deposition from these sources to the Lake Michigan Basin (Landis et al., 2002; Landis and Keeler, 2002; Vette et al., 2002; McCarty et al., 2004). Results of land-based and over-water measurements of total vapor phase atmospheric Hg, Hg wet deposition, and Hg concentrations in the water column suggested that atmospheric deposition was responsible for ~80% of inputs to Lake Michigan (Landis and Keeler, 2002). These analyses also suggested that the Chicago/Gary urban area contributed to ~20% of the annual atmospheric Hg deposition to Lake Michigan (Landis and Keeler, 2002). Furthermore, the highest levels of Hg deposition in southwest Michigan occurred with transport from the Chicago/Gary area, particularly with rapid transport where less Hg was deposited close to sources (Landis et al., 2002). These studies provided valuable insight into the importance of atmospheric transport and deposition of Hg; however, our understanding was limited due to the lack of methods to continuously measure speciated atmospheric Hg, or most importantly RGM, the highly-soluble form of Hg in industrial emissions that is readily removed from the atmosphere.

Since the LMMBS and AEOLOS, development of speciated Hg systems has made it possible to continuously monitor gaseous elemental Hg (Hg^0), particulate Hg (Hg_p), and RGM. In this study, speciated atmospheric Hg was measured in Chicago, IL and Holland, MI from July to November 2007. These measurements are useful for

understanding atmospheric Hg chemistry and differentiating between local and regional source impacts due to the different behaviors of Hg(II) and Hg^0 (Lynam and Keeler, 2005; Liu et al., 2007; Liu et al., 2010). This manuscript presents a summary of the 2007 speciated Hg measurements along with meteorological transport modeling of the dominant flow patterns influencing the monitoring sites over the course of the study. Additionally, two case studies are presented which demonstrate the transport of Chicago/Gary source emissions across southern Lake Michigan. This work offers a valuable perspective on speciated Hg transport in the Lake Michigan basin and further quantifies the impact of Chicago/Gary sources on southwest Michigan.

4.2 Methodology

4.2.1 Site Descriptions

The Chicago, IL site was located at the University of Chicago Kersten Physics building (41.79 N, 87.60 W) in southern downtown Chicago ~2 km west of Lake Michigan. This site was chosen because of its proximity to emission point sources southwest of Chicago and along southern Lake Michigan in the Chicago/Gary industrial region (Figure 4.1). Holland, MI is on the eastern shore of Lake Michigan, ~162 km northeast of Chicago. The Holland, MI site was located at the Michigan Department of Environmental Quality (MDEQ) monitoring station in Holland (42.77 N, 86.15 W), ~5 km east of Lake Michigan. The site was south and west (i.e. upwind) of major local sources so that there was minimal influence from those sources during west-southwest transport from the Chicago area (Figure 4.1).

4.2.2 Data Collection

Atmospheric monitoring at the Chicago, IL and Holland, MI sites commenced on July 1, 2007 and continued through November 8, 2007. Speciated ambient Hg measurements were made simultaneously at the two sites using the Tekran® 2537A/1130/1135 automated Hg sampling system. Data was collected semi-continuously on 2-hour intervals, consisting of a one-hour sampling period followed by a one-hour analysis period. Personnel from the University of Michigan Air Quality Laboratory (UMAQL) visited the sites weekly to conduct maintenance on the Tekran® system, which included performing internal automated calibrations of the 2537A analyzer, replacing inlet filters, and changing the KCl-coated annular denuder. The 1130 inlet assembly was changed bi-weekly and the 1135 particulate filter (RPF) was replaced every two months. The detection limit for the Tekran 2537A Hg^0 measurements is 0.06 ng/m^3 (Tekran, 2001; Poissant et al., 2005; Liu et al., 2007). The detection limit for RGM and Hg_p was determined by three times the standard deviation of the system blank over the course of the study, where the system blank is the third zero air flush at the start of the analysis period (Liu et al., 2007). The detection limit for RGM and Hg_p was 1.7 pg/m^3 in Chicago and 0.6 pg/m^3 in Holland.

Meteorological and criteria gas measurements were also collected at the Chicago and Holland sites. Meteorological parameters were measured at Chicago using the Vaisala® Weather Transmitter WXT510. Hourly ozone concentrations in Chicago were measured using a Dasibi 1008-RS ozone analyzer and the data was provided by the Illinois Environmental Protection Agency Cook County Branch. The MDEQ provided meteorological data at the Holland site for the entire monitoring period and ozone data

from July 1 to September 30, 2007. The UMAQL collected ozone measurements from October 1 to November 8, 2007 and SO_2 measurements from July 28 to November 8, 2007 at the Holland site using TEI 49C and TEI 43C analyzers, respectively.

4.2.3 Meteorological Back-Trajectories

Air mass transport to the Chicago and Holland sites was modeled using the Hybrid Single-Particle Lagrangian Integrated Trajectory (HYSPLIT) Model Version 4.8 (Draxler and Hess, 1997; Draxler and Hess, 1998). HYSPLIT back-trajectories were calculated using the National Weather Service's National Center for Environmental Prediction (NCEP) Eta Data Assimilation System (EDAS) 40 km gridded meteorological data. All data was obtained from the National Oceanic and Atmospheric Administration's Air Resources Laboratory (NOAA-ARL). The trajectories were calculated starting every two-hours corresponding to the speciated ambient Hg measurements. The starting height was set to one-half of the mixed layer depth as determined by the HYSPLIT model in order to best represent transport within the boundary layer. Cluster analysis was performed using Ward's Minimum-Variance method (Ward, 1963; Landis et al., 2002).

4.2.4 Dispersion Modeling

The HYSPLIT model was also used to calculate the dispersion of pollutants from the Chicago source region for the case studies. Determining the fraction of primary RGM emissions reaching the downwind Holland site after transport and dispersion was of main interest in both selected case studies. HYSPLIT uses the gridded meteorological data to calculate atmospheric advection and dispersion of pollutants released from a given location (Draxler and Hess, 1998). Plume dispersion was modeled using horizontal top-

hat puff and vertical particle equations, as described in Draxler and Hess (1998). A Gaussian puff model can also be applied to horizontal dispersion, but requires longer computation time and produces similar results to the top-hat calculations (Draxler and Hess, 1998). Concentrations were calculated over a horizontal grid of 0.1 degrees latitude by 0.1 degrees longitude (~10km). Atmospheric reactions during transport were not included in this preliminary dispersion model exercise.

To provide geographical reference for emissions from the Chicago/Gary industrial area, and because CFUBs are the largest emitters of atmospheric Hg in the region, the modeled puff was released from the location of a CFUB in Joliet, IL that is ~50 km southwest of the Chicago site and is the largest Hg emission point source in the Chicago/Gary area (U.S. EPA 2005 NEI). The puff was released continuously at one mass unit per hour from the stack height for this facility (137 m above ground level (AGL)) and the plume dispersion was examined from 0-500m AGL. While there are a range of sources in the Chicago/Gary area which emit varying amounts and fractions of Hg^0 and Hg(II), because CFUBs contribute to such a high percentage (~75%) of the total Hg emissions from the region, the speciated emissions of a typical CFUB were assumed as a reasonable first approximation.

Dry deposition occurs in the HYSPLIT model only when the puff or particle is within the surface layer (Draxler and Hess, 1998). A deposition velocity of 0.006 m/s was selected to represent a typical RGM deposition velocity under relatively stable atmospheric conditions (Marsik et al., 2007). It is acknowledged that the dry deposition velocity can fluctuate diurnally as well as over land and water due to variability in atmospheric turbulence and stability (Malcolm and Keeler, 2002; Zhang et al., 2003;

Marsik et al., 2007); however, it was not possible to vary the velocity within a given model simulation and transport over Lake Michigan was of the greatest interest here. Wet deposition was not included in the model as it did not rain during the chosen short duration case studies.

4.3 Results and Discussion

4.3.1 Speciated Hg Measurements

The distribution and range in speciated ambient Hg concentrations demonstrate the impact of urban/industrial sources on the Chicago monitoring site, as concentrations in Holland did not display the same degree of variability due to the relatively few local sources impacting the site (Table 4.1; Figure 4.2). The semi-continuous concentrations of Hg^0, Hg_p, and RGM were significantly different between the urban Chicago and semi-rural Holland sites (Kruskal-Wallis, $p<0.001$). The mean Hg^0 and RGM in Chicago were approximately two times greater than in Holland while the mean Hg_p in Chicago was nearly 1.5 greater than in Holland.

Elemental Hg concentrations in Holland displayed a relatively narrow distribution with a maximum concentration of 6.0 ng/m^3 but a 75th percentile value of only 1.4 ng/m^3 (Table 4.1). In contrast, Hg^0 in Chicago had a much wider distribution with concentrations reaching as high as 16.5 ng/m^3. Although the median Hg^0 concentration (1.9 ng/m^3) in Chicago was only marginally above the value suggested for the global background in the Northern Hemisphere (1.5 – 1.7 ng/m^3) (Lindberg et al., 2007) and the 75th percentile Hg^0 concentration was 2.8 ng/m^3 (Table 4.1), it was not uncommon for concentrations to reach values near 10 ng/m^3 and remain there for entire sampling periods (Figure 4.2).

The mean RGM concentration in Chicago was actually larger than the 75th

percentile of RGM (Table 4.1) due to the numerous peaks in RGM concentration that

were well above the median value caused by nearby sources in Chicago (Figure 4.2).

The impact of a local source was particularly evident in the maximum RGM

concentration observed during the sampling period at Chicago (2.7 ng/m^3) which

occurred in the early morning hours in conjunction with elevated Hg^0 (4.8 ng/m^3) and

Hg_p (180 pg/m^3). In contrast, RGM concentrations in Holland displayed a much

narrower distribution with a maximum concentration of 137 pg/m^3 (Table 4.1).

The mean Hg_p in Chicago was also greater than the 75th percentile value due largely

to the impact of local sources. The median Hg_p concentrations were comparable between

Chicago and Holland, but once again the range in concentration was much larger at the

Chicago site as evidenced by the more dramatic peaks in concentration (Figure 4.2).

The range and variability in RGM concentrations at Chicago and Holland during

the summer 2007 study were much greater than Hg_p. This appears consistent with past

observations that when ambient temperatures are elevated, such as during the summer

months, Hg(II) tends to exist primarily in the gas phase (RGM), whereas in colder winter

months there is a greater propensity for reactive Hg to partition the condensed phase and

bind to particles (Hg_p) (Lynam and Keeler, 2005; Liu et al. 2010). In Chicago different

ranges in RGM and Hg_p concentrations is likely also due to the dominance of RGM over

Hg_p in combustion emissions (Carpi, 1997). The summary statistics for Hg^0, RGM, and

Hg_p (Table 4.1) demonstrate that speciated ambient Hg concentrations at both sites, and

particularly in Chicago, were not normally distributed and thus non-parametric statistics

will primarily be used in subsequent statistical discussions.

There are several time periods in which concentrations at the two sites were elevated at similar times (Figure 4.2). In Chicago, the largest peaks in Hg^0, RGM, and Hg_p occurred predominantly during the evening and early morning hours (19:00 – 7:00 EST) (Figure 4.3). Additionally, ozone concentrations, which reached up to 89 ppb during the study, were typically < 30 ppb during these periods of peak Hg concentrations. These observations suggest the effect of the nighttime boundary layer containing local emissions near the site as ozone is a secondary pollutant and should not be elevated under local source influences. Daytime RGM and Hg_p peaks occurred at Chicago as well, but were typically observed as sudden sharp increases under southeasterly transport from Chicago/Gary sources.

Elevated Hg^0 concentrations in Holland occasionally occurred during the night and early morning hours under northerly or easterly flow (Figure 4.1). During these nighttime periods of elevated Hg^0, ozone concentrations were typically < 40 ppb. Acknowledging that hourly ozone concentrations up to 123 ppb were observed at the Holland site over the course of the study, with elevated concentrations typically occurring in the afternoon hours (13:00 – 19:00 EST) due to daytime photochemical activity, the reduced ozone concentrations that accompanied elevated Hg^0 during night and early morning hours seem to suggest the transport of local source emissions within the nocturnal boundary layer to the Holland site at these times. Peak Hg_p concentrations at Holland occurred during both day and nighttime hours, but most noticeable was the increased frequency of high Hg_p concentrations in October and November (Figure 4.2) with temperatures less than 20°C (68°F) suggesting the increased preference for Hg(II) to bind to particles under cooler temperatures. Unlike Hg^0 and Hg_p, elevated RGM

concentrations in Holland occurred almost entirely during daytime hours (11:00 – 19:00 EST) (Figure 4.3). These concentrations also typically occurred with southwesterly transport and temperatures > 15°C (59°F). During these periods, ozone and SO_2 concentrations were on average 60 ppb and 6.1 ppb, respectively. It is evident that elevated RGM concentrations in Holland were often strongly related to daytime photochemistry as well as transport from the Chicago/Gary region. These relationships are explored in greater detail through the meteorological trajectory clusters and the case studies presented below.

4.3.2 Meteorological Back-Trajectory Cluster Analysis

Cluster analysis was performed on 24-hour HYSPLIT back-trajectories corresponding to the semi-continuous hourly ambient Hg measurements at the Chicago and Holland sites to investigate how different transport regimes affect Hg concentrations at the two locations. One-day back-trajectories are adequate to describe the transport between the sites, as their separation is only ~162 km, while also accounting for transport from other major regional urban areas such as St. Louis, MO and Detroit, MI. Nine clusters were computed for each site, explaining 80% of the variance in each dataset. Wilcoxon and Kruskal-Wallis tests indicated that the Hg^0, Hg_p, and RGM concentrations at each site were significantly different by cluster.

In Chicago, the highest median Hg concentrations were associated with southeasterly flow from the highly industrialized Chicago/Gary urban area (Figure 4.4b; Table 4.2). This cluster includes ~17% of the Chicago trajectories. Under this transport regime, the median Hg^0 was 49% greater while Hg_p and RGM were each more than two times greater than the median concentrations in the other eight clusters. In this

113

southeasterly cluster, all three Hg species had significant positive correlations with each other but were negatively correlated with ozone, suggesting that direct Hg emissions were impacting the site with southeast flow. Chemical conversion between Hg^0 and RGM is thought to be fairly slow; thus, near a Hg emission source these species should be positively correlated. Additionally, because ozone is a regionally transported secondary pollutant, it will not be present in primary emissions but rather produced downwind through reactions involving emitted ozone precursors. Therefore, ozone should be negatively correlated with Hg concentrations under the influence of local source emissions (Sillman et al., 2007). The lowest median Hg concentrations were observed with northerly transport, often with flow across the lake (Table 4.2; Figures 4.4d & 4.4i).

In Holland, the highest Hg concentrations were observed under south-southwesterly flow (Table 4.3; Figures 4.5c & 4.5d). The trajectories with this flow were grouped into two clusters which comprised ~27% of all the trajectories examined. The median Hg^0 and Hg_p concentrations in these two clusters were 6% and 8%, greater, respectively, than the median concentrations observed under all of the other modeled transport regimes; however, the Hg_p enhancement was not statistically significant. Most interestingly, the median RGM concentration under south-southwesterly flow was five times greater than the median RGM concentration of the other modeled transport regimes. In the event of photochemical oxidation, Hg^0 and RGM should be negatively correlated while ozone and RGM should be positively correlated, whereas under direct transport the Hg species should be positively correlated with one another but negatively correlated with ozone because ozone is a secondary pollutant (Sillman et al., 2007).

Under south-southwesterly flow at Holland (clusters 5c and 5d), RGM was significantly positively correlated with ozone ($p<0.0001$). However, in cluster 5c Hg^0 was not significantly correlated with RGM or ozone. In cluster 5d Hg^0 was negatively correlated with RGM ($R_S = -0.32$, $p = 0.001$) and ozone ($R_S = -0.24$, $p = 0.02$), but the correlation coefficients were small. These varying relationships between Hg species and ozone suggest the combination of direct transport and chemical activity under south-southwesterly flow.

In contrast, under northerly flow at Holland (Table 4.3; Figures 4.5f & 4.5i) a positive correlation between RGM and Hg^0 suggests the dominance of direct Hg emission from sources north of the site (Sillman et al., 2007). The median concentrations of Hg^0, Hg_p, and RGM in these clusters were significantly less (11%, 32%, and 83%, respectively) than the median concentrations observed under southwest flow.

4.3.3 Case Studies and HYSPLIT Dispersion Modeling

In addition to quantifying the influence of Chicago sources on Holland for the study period, two case studies were also selected to more closely examine transport over Lake Michigan from Chicago to Holland. Further application of the HYSPLIT model was used to (a) support the upwind air mass history suggested by the measurements, and (b) estimate the amount of RGM directly transported to Holland from that which was produced through Hg^0 oxidation following transport.

Studies have demonstrated the unique meteorological system that develops with transport over large lakes and consequently impacts atmospheric mixing and chemistry during transport (Lyons and Cole, 1975; Sillman et al., 1993; Dye et al., 1995). These conditions, along with increased photochemical activity during the summer months, can

lead to significantly elevated ozone concentrations at locations along the Lake Michigan

shoreline (Lyons and Cole, 1975; Sillman et al., 1993; Dye et al., 1995). Over the surface

of Lake Michigan, highly stable atmospheric layers tend to form due to cool water

temperatures relative to the overlying air (Lyons and Cole, 1975; Sillman et al., 1993).

These layers are particularly evident in the summertime during both day and nighttime

hours due to elevated atmospheric temperatures at this time of year. Vertical atmospheric

mixing over the lake within these layers is consequently suppressed, allowing pollutants

to be transported across the lake with minimal loss or dispersion. Overnight and in the

early morning hours a land breeze may form, carrying emissions from Chicago sources

over the lake into the stable atmospheric layers (Lyons and Cole, 1975; Dye et al., 1995).

As the sun rises, because the air over the land tends to heat faster than the air over the

water due to differences in their heat capacities, the boundary layer over the land will

tend to rise while the air over the water remains in a stable layer (Dye et al., 1995). The

heating of the land erodes the nocturnal boundary from below and a thermal internal

boundary layer forms from the shoreline inland (Lyons and Cole, 1975). As the day

progresses, the development of a sea-breeze may transport pollutants from the stable

layers over the lake to the shoreline regions where, upon encountering the thermal

internal boundary layer, the pollutants can be mixed down to the surface through

fumigation typically within ~5 km of the shore (Lyons and Cole, 1975; Dye et al., 1995).

Given that this fumigation occurs within the mixed layer (Lyons and Cole, 1975), the

pollutants that are mixed down to the surface near the shoreline should primarily be those

which were transported over the lake with minimal entrainment of constituents of

tropospheric air above the mixed layer, effectively isolating the transport of emissions from Chicago sources.

These meteorological conditions are also likely to affect Hg chemistry, allowing emitted Hg^0 and $Hg(II)$ to be contained within the stable layers over the lake and undergo chemical reactions during transport. Evidence for RGM production in the atmosphere under relatively elevated ozone concentrations (> 60 ppb) have been reported (Keeler and Dvonch, 2005; Liu et al. 2007; Liu et al., 2010). Furthermore, Sillman et al. (2007) reported that anthropogenic NO_x and VOCs in the Great Lakes were important in RGM production from Hg^0, reducing the concentration of chemically produced RGM by 40% when these emissions were turned off in the modeling scenario. The ability to separate the primary emissions of RGM transported from a source and the RGM production through oxidation en route is crucial to quantifying the sources and fate of Hg emitted to the atmosphere.

4.3.3.1 Case Study #1: July 29 – August 3, 2007

From July 29 to August 3, 2007 a high pressure center passed over Lake Michigan (Figure 4.6) and the impact of the clockwise flow on ambient Hg concentrations at the two monitoring sites was evident. On July 29-30, the high-pressure system was positioned northwest of the sites generating north-northeasterly flow from over Lake Michigan before reaching Chicago. Mercury and ozone concentrations remained relatively low at the Chicago site during this 48-hour period, with a median Hg^0 concentration of 1.6 ng/m^3, median RGM and Hg_p concentrations less than 5 pg/m^3, and a maximum ozone concentration of only 38 ppb (Figure 4.7). On July 29 and 30, Holland received easterly transport during the night and early morning hours and northwesterly

117

transport during the day. RGM displayed diurnal variability with elevated daytime concentrations, while Hg^0 and Hg_p concentrations remained relatively constant during this period (~1.3 ng/m^3 and 4 pg/m^3, respectively) (Figure 4.8). The maximum RGM concentration on July 29 at 17:00 EST (53 pg/m^3) occurred under rapid northwest flow with only moderately high ozone concentrations (50 ppb) and slightly elevated SO_2 (7 ppb), suggesting transport of emissions from local sources north of the Holland site. Overnight the wind direction shifted easterly and Hg concentrations were very low. However, Hg^0 and Hg_p rose sharply at 9:00 EST on July 30 to 3.0 ng/m^3 and 18.1 pg/m^3 when the wind direction suddenly shifted from easterly to northwesterly. SO_2 simultaneously rose to 13 ppb, suggesting that these peaks were again likely due to local emissions north of the site (Figure 4.1). As the wind direction continued to shift westerly, Hg^0, Hg_p, and SO_2 concentrations quickly declined while RGM rose in a wide daytime peak (41 pg/m^3), likely due to chemical production.

The high-pressure system progressed eastward over the Chicago and Holland sites on July 31 and August 1. During this period Hg^0 fluctuated greatly in Chicago reaching a maximum of 8.1 ng/m^3. Most of the large Hg^0 peaks occurred in the evening and early morning hours suggesting containment of local emissions within the boundary layer. RGM and Hg_p also moderately increased in Chicago during this time, with peak concentrations of 43 pg/m^3 and 35 pg/m^3, respectively. In Holland Hg^0 and Hg_p did not vary significantly on July 31 and August 1, while RGM displayed smaller daytime elevations than on the previous days. The reduced SO_2 concentrations and elevated ozone during this period suggests that the RGM at Holland was due to chemical production.

By the morning of August 2, the high-pressure system moved east of the sites generating southwesterly flow behind the high. Following behind the high-pressure system, a cold front approached the region from the northwest extending out of a low centered in Canada through the central plains region, further supporting southwesterly flow in advance of the front. As a result of this change in transport direction, the Hg concentrations in Chicago declined, with the exception of a moderate RGM peak (50 pg/m^3) on the afternoon of August 2 during a period of reduced local wind speeds (Figure 4.7). In Holland on the afternoon of August 2, under south-southwesterly flow RGM concentrations reached the maximum for the period (137 pg/m^3; Figure 4.8). The hourly concentrations of ozone and SO$_2$ simultaneously increased in Holland to 115 ppb and 7.6 ppb, respectively. The peak in RGM at Holland on August 2 was ~2.5 times greater than the largest RGM peak observed during the previous four days and appears related to Hg transport from sources in the Chicago/Gary region. On the morning of August 3 the frontal system, which had changed from a cold front to a stationary front, passed over the two sites causing the flow to shift to northwesterly behind it.

The HYSPLIT dispersion model simulation ran from 3Z on August 1 to 9Z on August 3 (Figure 4.9) in order to capture the elevated Hg concentrations in Chicago throughout the day on August 1 (Figure 4.7) followed by the large RGM peak in Holland on August 2 (Figure 4.8). Note that while the model was actually averaged and examined over three hour intervals for the subsequent discussion, six hour average intervals are shown in the figures below to provide a more simplified view of the overall plume transport.

From 3Z to 15Z on August 1, the plume was very concentrated near its source due to stable conditions generated by the high pressure system. From 15Z on August 1 to 3Z on August 2 the plume began to expand northward with little east-west dispersion, suggesting an increase in wind speeds but still a fairly stable atmosphere. Between 3Z and 6Z on August 2 the plume began to disperse over the lake as the high pressure system moved eastward. As the daytime hours began, the plume continued to expand further eastward and higher concentrations within the plume moved closer to the Holland shoreline. The plume first intercepted the Holland site between 9Z and 12Z on August 2, coinciding with the initial rise in RGM concentrations observed at Holland at 12Z (7:00EST). From 12Z through 21Z on August 2, the plume continued on a northeast trajectory, causing continuous transport to Holland throughout the day on August 2. Between 21Z on August 2 and 0Z on August 3, the wind direction shifted westerly in Chicago and the plume began to disperse eastward from the source. The highest concentrations within the plume were also maintained closer to the source. This direction shift continued throughout the remainder of the modeled period, such that by the end of the model simulation (9Z on August 3) the plume was dispersing in a more eastward direction, generally passing south of the Holland site. Coincidentally, the RGM peak in Holland declined sharply between 0Z on August 3 (19:00 EST on August 2) and 6Z on August 3 (1:00 EST) and RGM concentrations were near zero at the end of the modeling period.

The HYSPLIT model simulation clearly depicts the stagnant conditions on August 1 which contained the plume near the Chicago site, followed by southwesterly flow on August 2 that transported emissions to the Holland site (Figure 4.9). The

120

presence of the plume over the Holland site also coincides with the observed RGM peak, which began at 12Z (7:00 EST) on August 2 and continued until 6Z (1:00 EST) on August 3. At the time of the peak RGM concentration in Holland (19:00 EST on August 2; 0Z on August 3) the HYSPLIT model estimates that the concentration near the Holland site was on the order of $1.0E^{-13}$ /m^3. This value represents the amount of emitted mass per m^3 that was transported from the source location to Holland through pure dispersion. The peak RGM concentration measured in Holland on August 2 was 137 pg/m^3 (137 E^{-12} g/m^3). Dividing this concentration by $1.0E^{-13}$ /m^3 gives a mass of 1370 g (1.37 kg) of RGM that would need to be emitted from the source location to achieve the observed RGM concentration through pure dispersion. If one simply assumes continuous total Hg emission at 275 kg/yr from the starting source location (24 hr/day and 365 day/year) this equates to total Hg emissions of ~0.031 kg/hr. Further assuming that 50% of the Hg is emitted as RGM, then RGM is released from the starting location at ~0.016 kg/hr. A total of 45 hours elapsed from the start of the HYSPLIT model simulation to the time of the maximum observed RGM concentration in Holland, so assuming continuous RGM emission of 0.016 kg/hr the source would have emitted ~0.70 kg of RGM over this period. If 1.37 kg of RGM needed to be emitted from this source in order to achieve the observed RGM peak in Holland, then the estimated RGM emissions from this facility (0.70 kg) could account for 52% of the observed RGM peak. Acknowledging that anywhere from 25% (U.S. EPA 2005 NEI) to 80% (Carpi, 1997) of the Hg could be emitted as RGM, by the calculations applied here primary emissions from the source could account for between 25% and 81% of the RGM peak in Holland.

The correlation of RGM with ozone at Holland from 9Z August 1 to 9Z August 3 was significant (R = 0.80; p < 0.001) and the relationship explained 64% of the variance in RGM. Given that ozone is a major oxidant of Hg^0 (Munthe and McElroy, 1992), this may suggest that Hg^0 oxidation is responsible for ~60% of the RGM observed at Holland during the period suggesting that the remaining ~40% would be due to direct transport of primary RGM emissions. Under elevated ozone concentrations, a negative correlation between Hg^0 and ozone may be observed due to Hg^0 oxidation by ozone (Keeler and Dvonch, 2005); however, Hg^0 and ozone were not significantly correlated at Holland during the period. The relative importance of Hg^0 oxidation by ozone can also be estimated by applying a previously reported reaction rate for Hg^0 oxidation by ozone $((7.5 \pm 0.9) E^{-19} cm^3 molecule^{-1} s^{-1}$; Pal and Ariya, 2004). HYSPLIT back-trajectories initiated at the time of the RGM peak in Holland indicate that air mass transport over the lake from Chicago to Holland occurred in six hours. Using the measured concentrations of Hg^0 and ozone in Chicago at that time, it is estimated that Hg^0 oxidation by ozone accounts for 31-40% of the maximum RGM peak. However, there are other potential oxidants of Hg^0 in the atmosphere, such as hydroxyl radicals and halogen compounds (Hynes et al., 2009; Ariya et al., 2009), which would additionally contribute to the fraction of RGM formed in the atmosphere through oxidation. The contributions of these reactions were not estimated here because the aforementioned oxidants were not measured onsite during the study. The stable atmospheric conditions (Figure 4.6), warm temperatures during transport (Figures 4.7 and 4.8), and elevated ozone at the time of the RGM peak in Holland were conducive for chemical reactions within stable layers over

the lake lending support for a larger contribution to RGM from Hg^0 oxidation than from direct dispersion.

4.3.3.2 Case Study #2: August 26 – 29, 2007

The second case study similarly demonstrates rapid southwest flow transporting Hg emissions from the Chicago/Gary urban area to Holland (Figure 4.10). From August 26 until the morning of August 28, Chicago experienced predominantly southeasterly flow with steady wind speeds around 4-5 mph transporting emissions from Chicago/Gary sources. This lead to large and variable peaks in ambient Hg concentrations, where Hg^0 in Chicago reached concentrations up to 6.8 ng/m^3 and RGM and Hg_p rose as high as 412 and 72 pg/m^3, respectively (Figure 4.11).   In the evening hours of August 27 Hg^0 remained high (6.5 ng/m^3) and RGM and Hg_p concentrations initially decreased. Late in the evening (August 28, 1:00 EST) Hg_p increased sharply (193 pg/m^3) while Hg^0 (5.4 ng/m^3) and RGM (62 pg/m^3) also displayed moderate peaks. At this time wind speed also increased slightly from 3 to 4 mph under south-southeasterly flow, suggesting transport of local emissions within the nocturnal boundary. The persistent southeasterly flow, low ozone concentrations, and dramatic peaks in Hg concentrations at various times of day including the night and early morning hours are all suggestive of local source emissions in Chicago.

On August 26 in Holland, north-northwesterly winds during the day likely transported emissions from local sources. At this time RGM increased to 68 pg/m^3, while ozone and SO_2 increased to 44 ppb and 15.2 ppb, respectively (Figure 4.12). The sudden substantial rise in SO_2 under northwesterly flow is highly suggestive of local combustion source emissions. Mercury concentrations and wind speed dropped sharply on the

afternoon of August 26 as the wind direction shifted easterly. On August 27, RGM and

Hg_p peaks were much smaller (18 pg/m^3 and 31 pg/m^3, respectively) under southeasterly

transport and reduced solar insolation. SO_2 concentrations were also much lower on

August 27 (2.1 ppb) than on the previous day.

On August 28, the transport direction shifted to southwesterly and was more rapid

throughout the afternoon, particularly in Holland where local wind speeds were near 8

mph. This transport regime brought elevated Hg concentrations to Holland while RGM

and Hg_p concentrations decreased in Chicago. Hg^0 in Chicago remained between 3-5

ng/m^3 during the day on August 28 (Figure 4.11). In Holland RGM concentrations

reached 112 pg/m^3, which was the maximum for this three day period and ~1.6 times

greater than the RGM peak observed in Holland on August 26 (Figure 4.12). However,

Hg^0 and Hg_p did not vary significantly. SO_2 increased in Holland to 11 ppb at the same

time that RGM concentrations began to increase, but SO_2 then declined steadily through

the afternoon. Interestingly, the SO_2 peak at this time was less than the peak observed on

August 26 under local influences due to the longer transport distance between the source

(Chicago) and receptor (Holland) on August 28. However, the coinciding RGM peak on

August 28 was substantially larger than the peak RGM concentration on August 26,

suggesting a combination of greater Hg emissions from Chicago/Gary sources and/or the

additional potential for chemical RGM production during transport. Ozone also

increased in Holland (90 ppb) simultaneously with RGM concentrations on August 28.

In the evening on August 28 local wind speeds were reduced (~4 mph), local wind

direction shifted slightly from southwesterly to south-southeasterly, and ozone

concentrations declined from 90 ppb to 50 ppb. Consequently, RGM concentrations also declined under weakened transport and reduced photochemical activity.

Early in the morning on August 29 (1:00 – 9:00 EST) winds were southwesterly again at both sites but less rapid than on the previous day. All Hg concentrations in Chicago declined steadily throughout the day on August 29 (Figure 4.11). In Holland under southwest flow overnight, ozone concentrations remained near 50-60 ppb and small peaks in RGM (36 pg/m^3) and SO_2 (8.4 ppb) occurred. This may suggest continued transport from Chicago/Gary sources; however in the absence of photochemistry the overnight RGM peak was ~70% less than the daytime peak on August 28. Hg concentrations generally decreased throughout the day (Figure 4.12) as the flow shifted to a more northerly direction.

The HYSPLIT model simulation was performed from 6Z on August 27 (1:00 EST) to 18Z on August 29 (13:00 EST) in order to capture the elevated Hg concentrations in Chicago throughout the day on August 27, the large RGM peak in Holland on August 28, and the smaller RGM peak in Holland early on August 29. As in case study #1, the plume dispersion was examined on three hour average intervals but Figure 4.13 displays the six-hour average concentrations. From 6Z on August 27 to 6Z on August 28, the plume traveled consistently north-northwestward along the lakeshore. This coincides with the large and variable Hg concentrations observed in Chicago throughout the August 27. The same starting location was used here as in case study #1, but if a similarly large point source closer to Gary, IN is used as the starting location in case study #2 the plume directly intersects the Chicago site and travels northward along the western Lake Michigan shoreline in the same pattern shown in Figure 4.13,

confirming that the speciated Hg measurements in Chicago do reflect Chicago/Gary emissions.

Between 6Z and 12Z on August 28, the plume began to shift eastward over Lake Michigan. It dispersed over northwest Michigan during the day on August 28, primarily intersecting Holland between 18Z (13:00 EST) and 21Z (16:00 EST) and continuing on this path in advance of the ensuing cold front. From 21Z (16:00 EST) on August 28 to 6Z (1:00 EST) on August 29, the plume shifted slightly so that it was passing just north of the Holland site. The plume then moved back southward after 6Z, passing over the Holland site again and continuing southward as the cold front approached the source location on August 29.

The modeled maximum plume concentration over Holland coincided with the maximum observed RGM concentration at the Holland site (112 pg/m^3 at 18Z (13:00 EST) on August 28). The return of the plume back to the Holland site after shifting slightly northward also coincided with the smaller RGM peak observed between 6Z (1:00 EST) and 14Z (9:00 EST) on August 29. The HYSPLIT model calculated that the concentration near the Holland site due to dispersion was on the order of $1.0E^{-13}$ /m^3. Applying the same calculation from case study #1, the point source at the starting location needed to emit 1.12 kg to achieve the maximum observed RGM concentration through dispersion. Assuming the same RGM emission rate (~0.016 kg/hr), over the 36 hours from the start of the simulation to the time of the maximum observed RGM concentration the facility would have emitted ~0.58 kg of RGM. This leads to an estimate that 52% of the measured RGM in Holland could be attributed to direct dispersion of RGM emitted from a source(s) in Chicago with the remainder associated

with oxidation of Hg^0 en route. Acknowledging once again that anywhere from 25% to 80% of the Hg from combustion could be emitted as RGM, direct dispersion may account for 25-80% of the RGM measured in Holland.

A regression of RGM against ozone measurements at Holland from 6Z on August 27 to 18Z on August 29 suggested once again that the two species were significantly correlated ($R = 0.79$; $p < 0.001$) and the relationship explained 62% of the variance in RGM. However, Hg^0 and ozone showed a much weaker relationship ($R = 0.36$; $p = 0.06$). The calculation applied to case study #1 for the oxidation of Hg^0 by ozone over six hours using measured concentrations in Chicago prior to the Holland RGM peak suggested that reaction may account for 21-27% of the RGM produced. However, the half-width of the RGM peak and its timing in the late afternoon suggests the importance of photochemical RGM production during transport, further indicating the potential role of other atmospheric oxidants of Hg^0.

4.4 Conclusions

This study provides valuable insight into the fate of speciated Hg emissions from the Chicago/Gary urban/industrial area and its impacts on southwestern Michigan. Speciated Hg measurements from Chicago, IL and Holland, MI during summer 2007 revealed the differences in ambient Hg concentrations at the urban and rural locations and allowed for examining the transport of Hg emissions within the atmosphere over Lake Michigan. Analysis suggests that RGM concentrations measured in Holland were five times greater under southwesterly flow relative to other transport directions and were significantly less under northerly transport from local sources. Two selected case studies also demonstrated the impact of transport from Chicago/Gary sources to Holland, MI.

HYSPLIT dispersion modeling revealed based on best estimates that dispersion of Chicago/Gary primary source emissions may account for ~52% of RGM concentrations in Holland following transport, with the remainder resulting from Hg^0 oxidation in the atmosphere en route. This estimate was corroborated by a significant relationship between RGM and ozone during the examined case study periods, suggesting the importance of RGM production via Hg^0 oxidation during transport. The application of a comprehensive model which, in addition to atmospheric dispersion also includes detailed atmospheric Hg chemistry and finer scale meteorological inputs could be used in the future to further distinguish between Hg transport and photochemical production across southern Lake Michigan.

References

Ariya, P.A., Peterson,K., Snider, G., Amyot, M., 2009. Mercury chemical transformations in the gas, aqueous and heterogenous phases: State-of-the-art science and uncertainties. In *Mercury Fate and Transport in the Global Atmosphere*; Pirrone, N., Mason, R., Eds; Springer Science + Business Media: New York pp 427-457.

Butler, T.J., Cohen, M.D., Vermeylen, F.M., Likens, G.E., Schmeltz, D., Artz, R.S., 2008. Regional precipitation mercury trends in the eastern USA, 1998-2005: Declines in the Northeast and Midwest, no trend in the Southeast. Atmospheric Environment 42, 1582-1592.

Carpi, A., 1997. Mercury from combustion sources: A review of the chemical species emitted and their transport in the atmosphere. Water, Air, and Soil Pollution 98, 241-254.

Cohen, M.D., Artz, R.S., Draxler, R.R., 2007. Report to Congress: Mercury Contamination in the Great Lakes. NOAA Air Resources Laboratory, Silver Spring, MD.

Draxler, R.R., Hess G.D., 1997. Description of the HYSPLIT_4 Modeling System. NOAA TECHNICAL MEMORANDUM ERL ARL-224.

Draxler, R.R., Hess, G.D., 1998. An overview of the HYSPLIT_4 Modeling System for trajectories, dispersion and deposition. Australian Meteorological Magazine 47, 295-308.

Dye, T.S., Roberst, P.T., Korc, M.E., 1995. Observations of transport processes for ozone and ozone precursors during the 1991 Lake Michigan Ozone Study. Journal of Applied Meteorology 34, 1877-1889.

Environment Canada 2007 National Pollutant Release Inventory (NPRI) (www.ec.gc.ca/inrp-npri/).

Gratz, L.E., Keeler, G.J., Miller, E.K., 2009. Long-term relationships between mercury wet deposition and meteorology. Atmospheric Environment 43, 6218-6229.

Gustin, M.S., Lindberg, S.E., Weisberg, P.J., 2008. An update on the natural sources and sinks of atmospheric mercury. Applied Geochemistry 23, 482-493.

Hynes, A.J., Donohue, D.L., Goodsite, M.E., Hedgecock, I.M.. 2009. Our current understanding of major chemical and physical processes affecting mercury dynamics in the atmosphere and at the air-water/terrestrial interfaces. In *Mercury Fate and Transport in the Global Atmosphere*; Pirrone, N., Mason, R., Eds; Springer Science + Business Media: New York pp 427-457.

Jaffe, D., Prestbo, E., Swartzendruber, P., Weiss-Penzias, P., Kato, S., Takami, A., Hatakeyama, S., Kajii, Y., 2005. Export of atmospheric mercury from Asia. Atmospheric Environment 39, 3029-3028.

Keeler, G.J. and Dvonch, J.T., 2005. Atmospheric Mercury: A Decade of Observations in the Great Lakes. In: *Dynamics of Mercury Pollution on Regional and Global Scales: Atmospheric Processes and Human Exposures around the World.* N. Pirrone and K. Mahaffey Eds. Kluwer Ltd.

Landis, M.S., Keeler, G.J., 2002. Atmospheric mercury deposition to Lake Michigan during the Lake Michigan Mass Balance Study. Environmental Science and Technology 36, 4518-4524.

Landis, M.S., Vette, A.S., Keeler, G.J., 2002. Atmospheric mercury in the Lake Michigan Basin: Influence of the Chicago/Gary urban area. Environmental Science and Technology 36, 4508-4517.

Lin, C.; Pehkonen, S.O., 1997. Aqueous free-radical chemistry of mercury in the presence of iron oxides and ambient aerosol. Atmospheric Environment 31, 4125-4137.

Lin, C., Pehkonen, S.O., 1999. The chemistry of atmospheric mercury. Atmospheric Environment 33, 2067-2079.

Lindberg, S., Bullock, R., Ebinghaus, R., Engstrom, D., Feng, X., Fitzgerald, W., Pirrone, N., Prestbo, E., Seigneur, C., 2007. A synthesis of progress and uncertainties in attributing the sources of mercury in Deposition. Ambio 36 (1), 2007.

Liu, B., Keeler, G.J., Dvonch, J.T., Barres, J.A., Lynam, M.M., Marsik, F.J., Taylor-Morgan, J., 2007. Temporal variability of mercury speciation in urban air. Atmospheric Environment, 41, 1911-1923.

Liu, B., Keeler, G.J., Dvonch, J.T., Barres, J.A., Lynam, M.M., Marsik, F.J., Taylor-Morgan, J., 2010. Urban-rural differences in atmospheric mercury speciation. Atmospheric Environment 44(16), 2013-2023.

Lynam, M.M., Keeler, G.J., 2005. Automated speciated mercury measurements in Michigan. Environmental Science and Technology 39, 9253-9262.

Lyons, W.A., Cole, H.S., 1975. Photochemical oxidant transport: Mesoscale lake breeze and synoptic-scale aspects. Journal of Applied Meteorology 15, 733-743.

Malcolm, E.G., Keeler, G.J., 2002. Measurements of mercury in dew: Atmospheric removal of mercury species to a wetted surface. Environmental Science and Technology 36, 2815-2821.

Marsik, F.J., Keeler, G.J., Landis, M.S., 2007. The dry-deposition of speciated mercury to the Florida Everglades: Measurements and modeling. Atmospheric Environment 41, 136-149.

Mason, R.P., Sullivan, K.A., 1997. Mercury in Lake Michigan. Environmental Science and Technology 31, 942-947.

McCarty, H.B., Miller, K., Brent, RN., Schofield, J., Rossman, R., 2004. Results of the Lake Michigan Mass Balance Study: Mercury Data Report. EPA 905 R-01-012, U.S. EPA Great Lakes National Program Office: Chicago, IL (http://www.epa.gov/greatlakes/lmmb/results/mercury/lmmbhg.pdf).

Munthe, J.; McElroy, W.J., 1992. Some aqueous reactions of potential importance in the atmospheric chemistry of mercury. Atmospheric Environment 26A, 553-557.

Pal, B., Ariya, P.A., 2004. Studies of ozone initiated reactions of gaseous mercury: kinetics, product studies, and atmospheric implications. Physical Chemistry Chemical Physics 6, 572-579.

Poissant, L., Pilote, M., Beauvais, C., Constant, P., Zhang, H.H., 2005. A year of continuous measurements of three atmospheric mercury species (GEM, RGM, and Hg_p) in southern Quebec, Canada. Atmospheric Environment 39, 1275-1287.

Schroeder, W.H., Munthe, J., 1998. Atmospheric mercury - An overview. Atmospheric Environment 32, 809-822.

Seigneur, S; Wrobel, J.; Constantinou, E., 1994. A chemical kinetic mechanism for atmospheric inorganic mercury. Environmental Science and Technology 28, 1589-1597.

Seigneur, C., Lohman, K., Vijayaraghavan, K., Jansen, J., Levin, L., 2006. Modeling atmospheric mercury deposition in the vicinity of power plants. Journal of Air and Waste Management 56, 743-751.

Sillman, S., Samson, P.J., Masters, J.M., 1993. Ozone production in urban plumes transported over water: Photochemical model and case studies in the Northeastern and Midwestern United States. Journal of Geophysical Research 98, 12,687-12,699.

Sillman, S., Marsik, F.J., Al-Wali, K.I., Keeler, G.J., Landis, M.S., 2007. Reactive mercury in the troposphere: Model formation and results for Florida, the northeastern United States, and the Atlantic Ocean. Journal of Geophysical Research 112, D23305.

Tekran, 2001. Tekran Model 1130 mercury speciation unit and Model 1135-P particulate mercury unit User Manual, Toronto, Canada.

U.S. Census Bureau, Metropolitan Statistical Areas (http://www.census.gov/population/www/metroareas/lists/2008/List4.txt).

U.S. Environmental Protection Agency (U.S. EPA), 1994. An Introduction to the Issues and the Ecosystems. EPA-453/B-94/030, Office of Air Quality Planning and Standards: Durham, NC.

U.S. Environmental Protection Agency (U.S. EPA), 1997. Mercury Study Report to Congress. EPA-452/R-97-003; Office of Air Quality Planning and Standards, Office of Research and Development: Washington DC.

U.S. Environmental Protection Agency (U.S.EPA) 2005 National Emissions Inventory (NEI) Data and Documentation (www.epa.gov/ttnchie1/net/2005inventory.html).

Vette, A.S., Landis, M.S., Keeler, G.J., 2002. Deposition and emission of gaseous mercury to and from Lake Michigan during the Lake Michigan Mass Balance Study (July, 1994 – October, 1995). Environmental Science and Technology 36, 4525-4532.

Ward, J.H., 1963. Hierarchical grouping to optimize objective function. Journal of the American Statistical Association 58, 236-244.

Weiss-Penzias, P., Jaffe, D.A., Swartzendruber, P., Dennison, J.B., Chand, D., Hafner, W., Prestbo, E., 2006. Observations of Asian air pollution in the free troposphere at Mount Bachelor Observatory during the spring of 2004. Journal of Geophysical Research 111, D10304.

White, E.M., Keeler, G.J., Landis, M.S., 2009. Spatial variability of mercury wet deposition in Eastern Ohio: Summertime meteorological case study analysis of local source influences. Environmental Science and Technology 43, 4946-4953.

Zhang, L., Brook, J.R., Vet, R., 2003. A revised parameterization for gaseous dry deposition in air-quality models. Atmospheric Chemistry and Physics 3, 2067-2082.
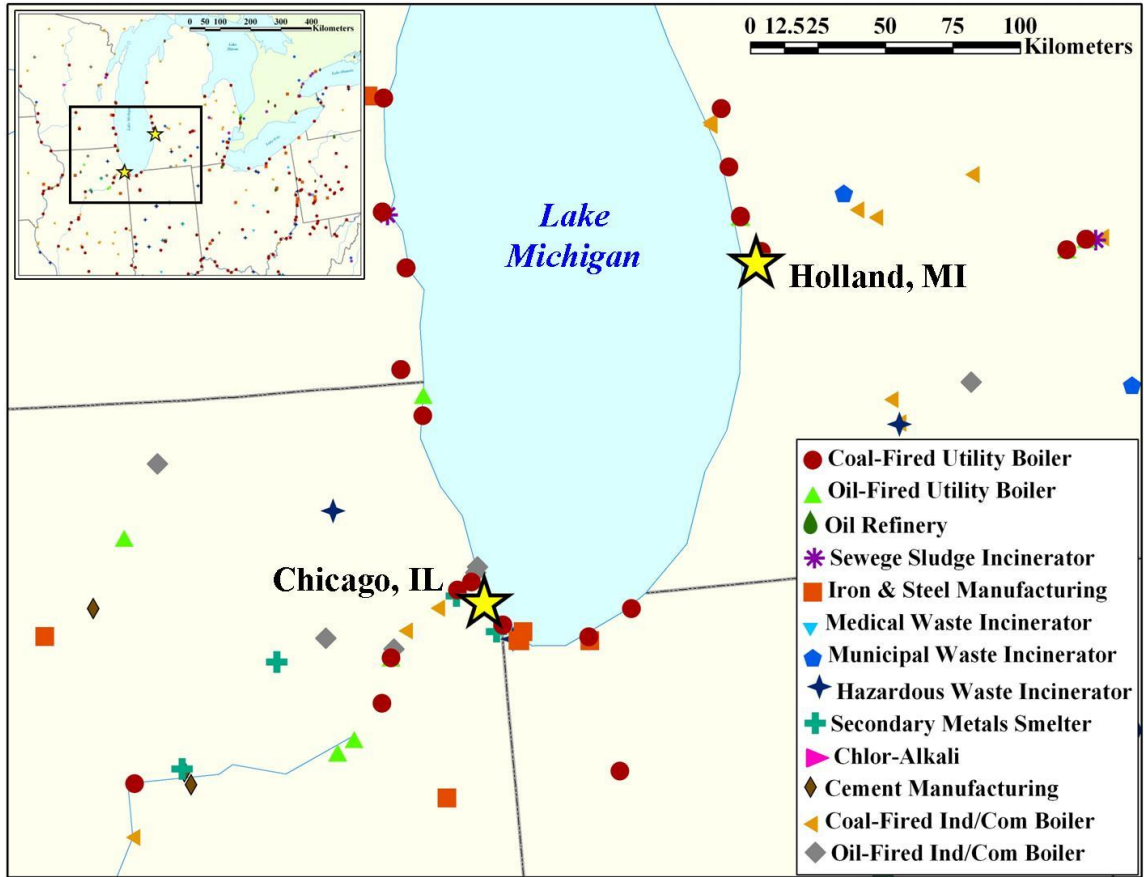
Figure 4.1: Location of Chicago, IL and Holland, MI sites and major Hg point sources emitting ≥ 0.1 kg Hg/yr (U.S. EPA 2005 NEI; Environment Canada 2007 NPRI).
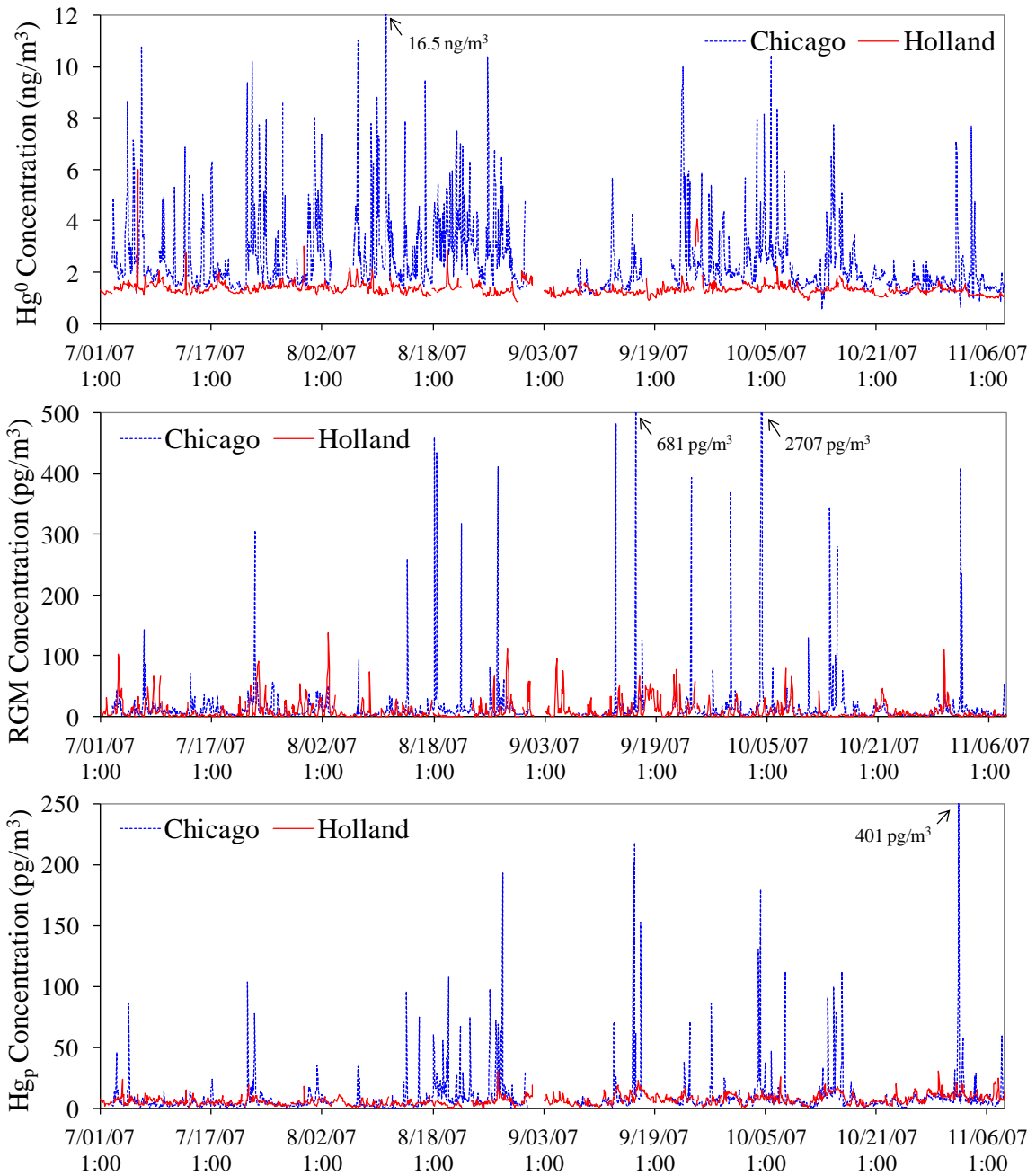
Figure 4.2: Time series of Hg^0, RGM, and Hg_p concentrations at Chicago and Holland from July 1 to November 8, 2007. All times are reported in Eastern Standard Time (EST).

134
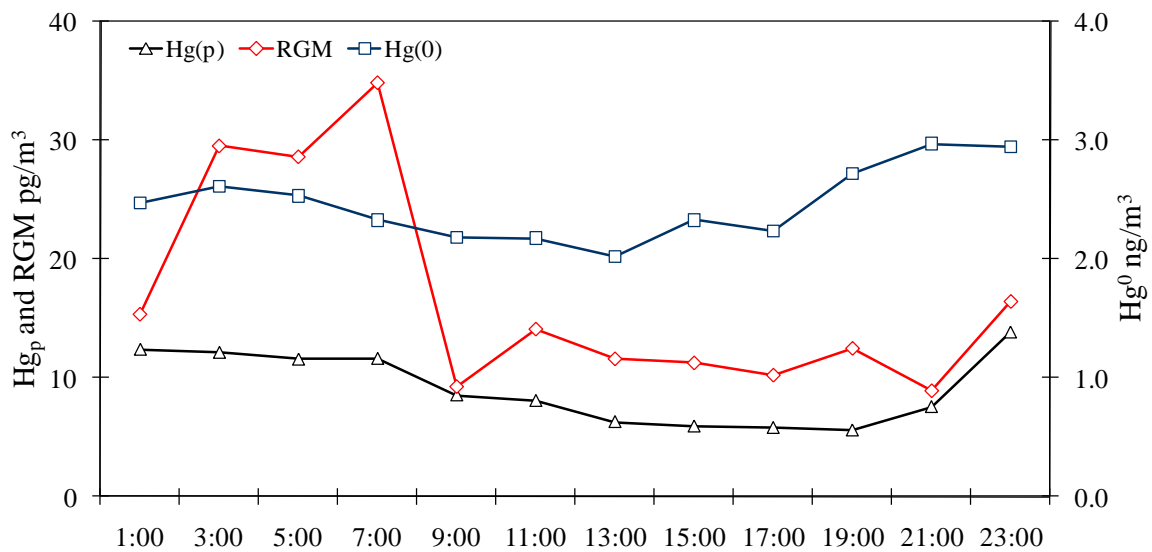
a.
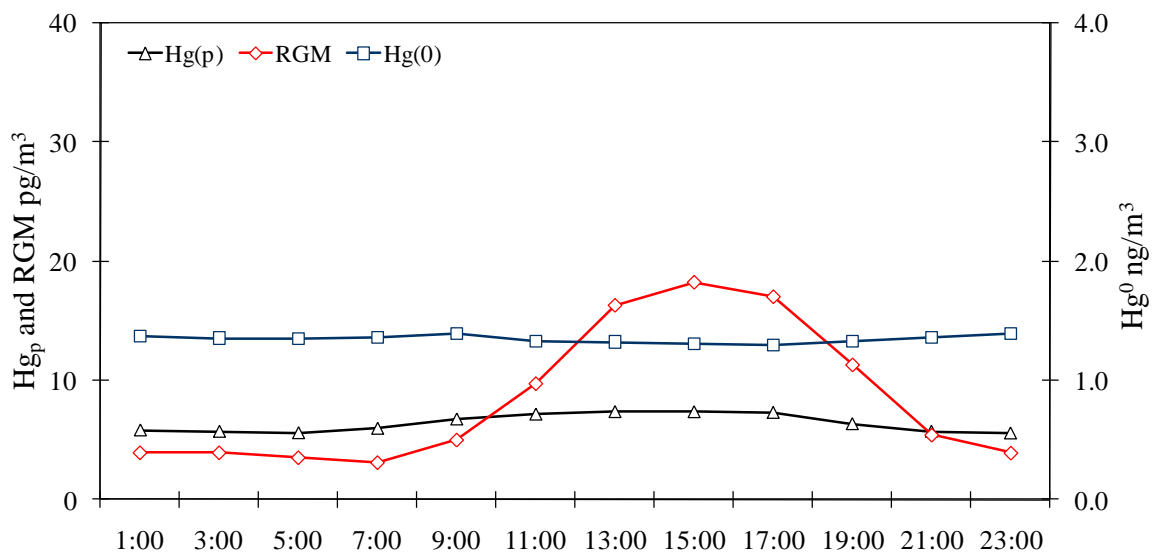
b.

Figure 4.3: Hourly average ambient speciated Hg concentrations at the (a) Chicago and (b) Holland sites. All times are reported in Eastern Standard Time (EST).
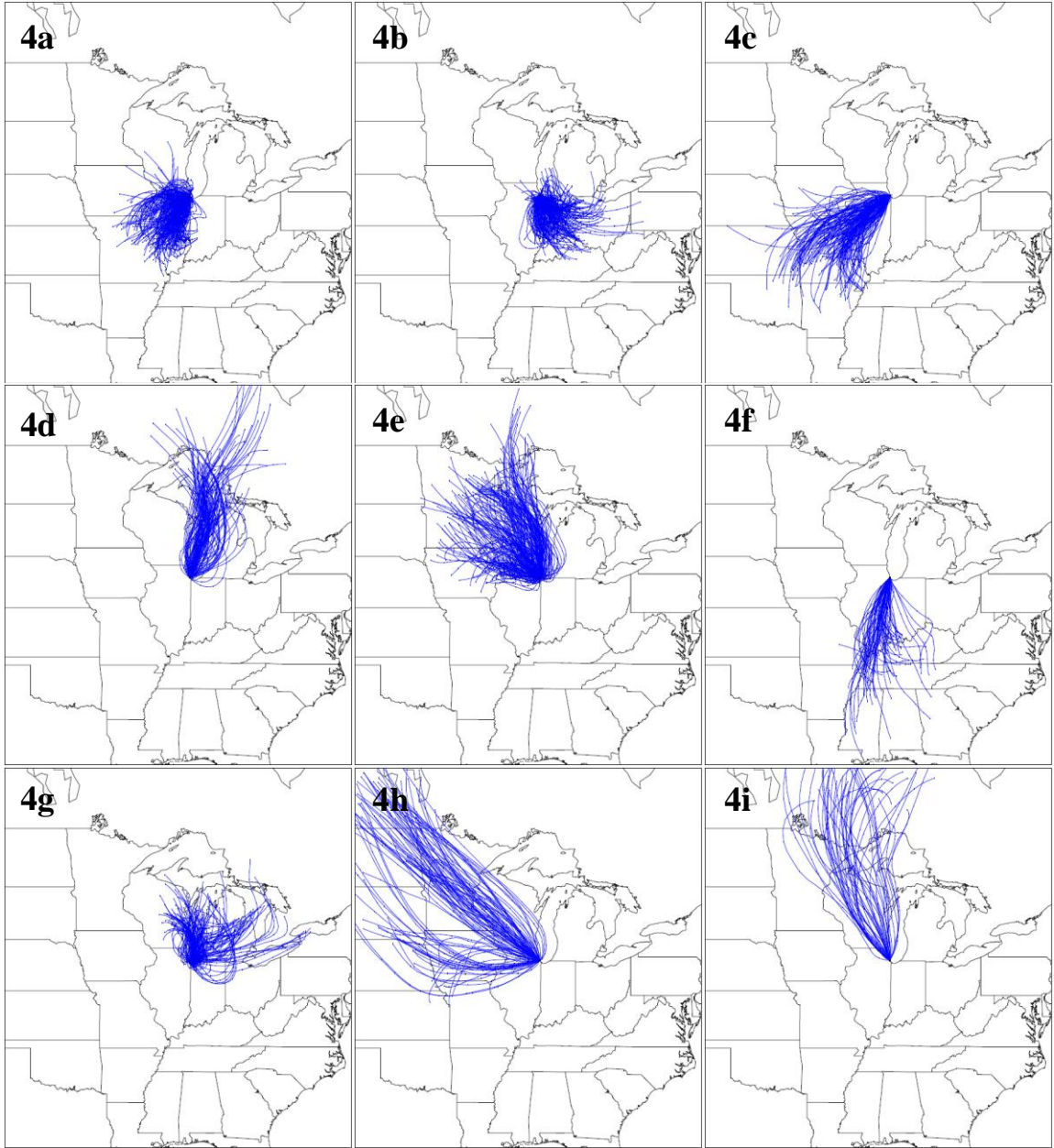
Figure 4.4: 24-hour HYSPLIT back-trajectory clusters for Chicago, IL.
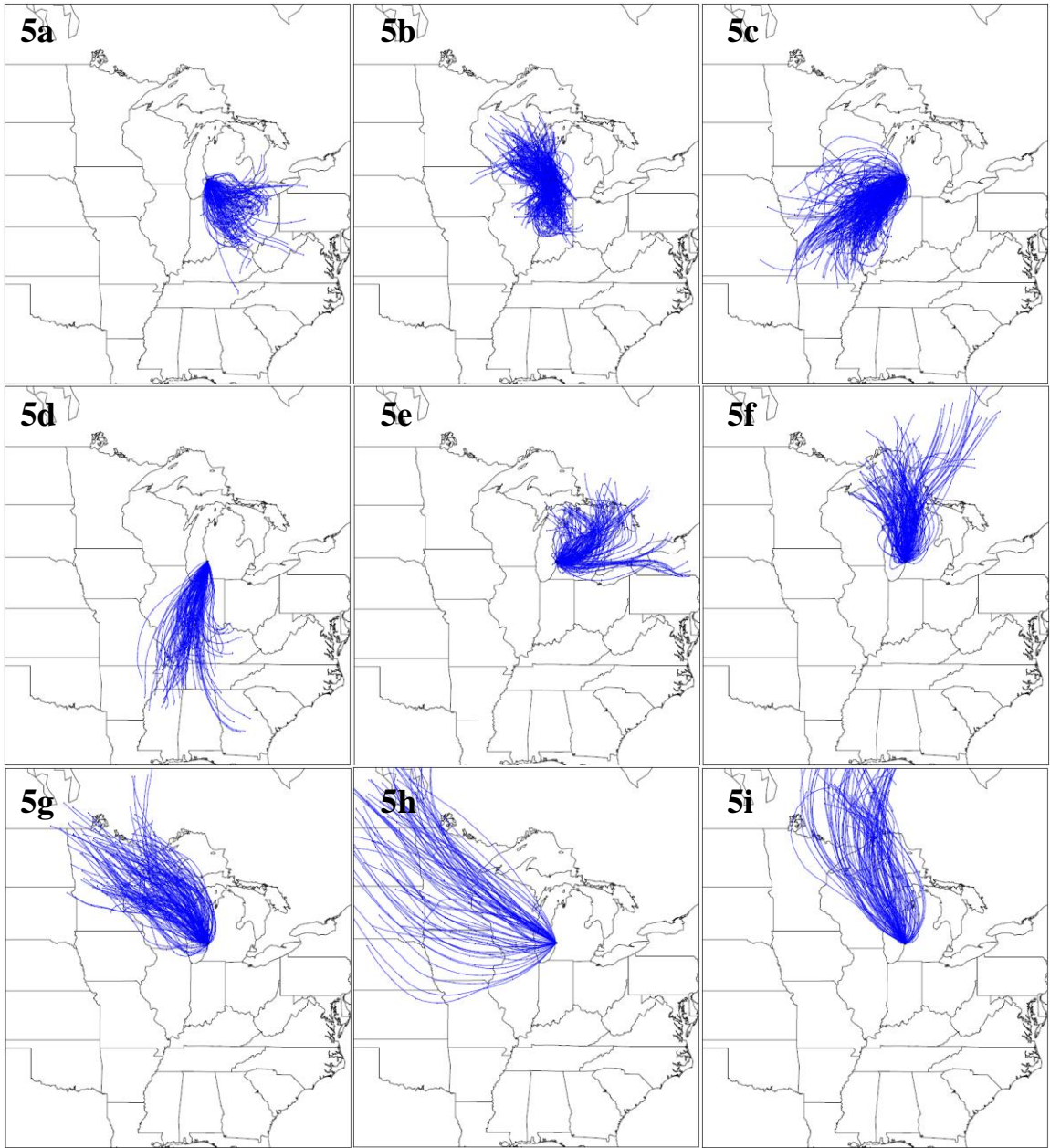
Figure 4.5: 24-hour HYSPLIT back-trajectory clusters for Holland, MI.
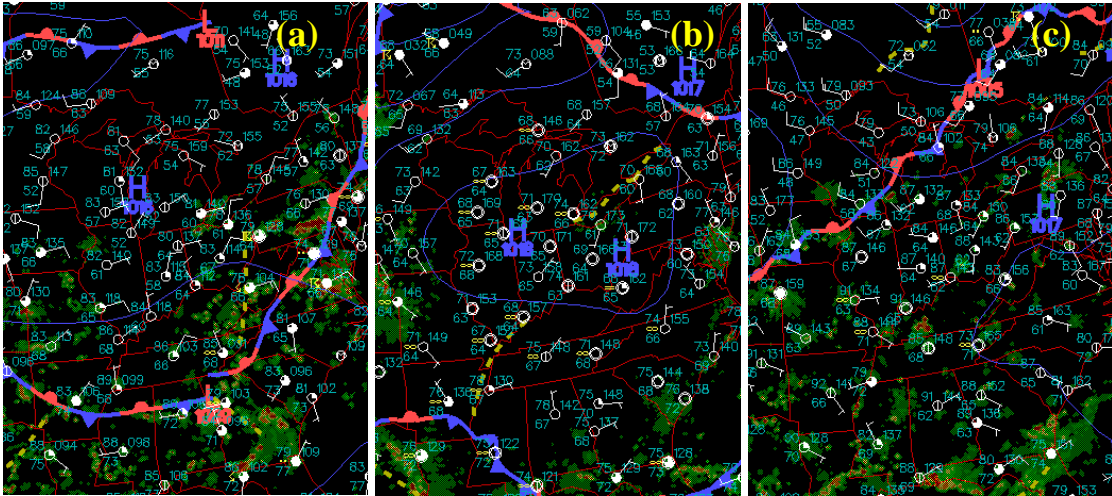
Figure 4.6: Surface maps on (a) July 30 0Z, (b) August 1 12Z, and (c) August 3 0Z, 2007.
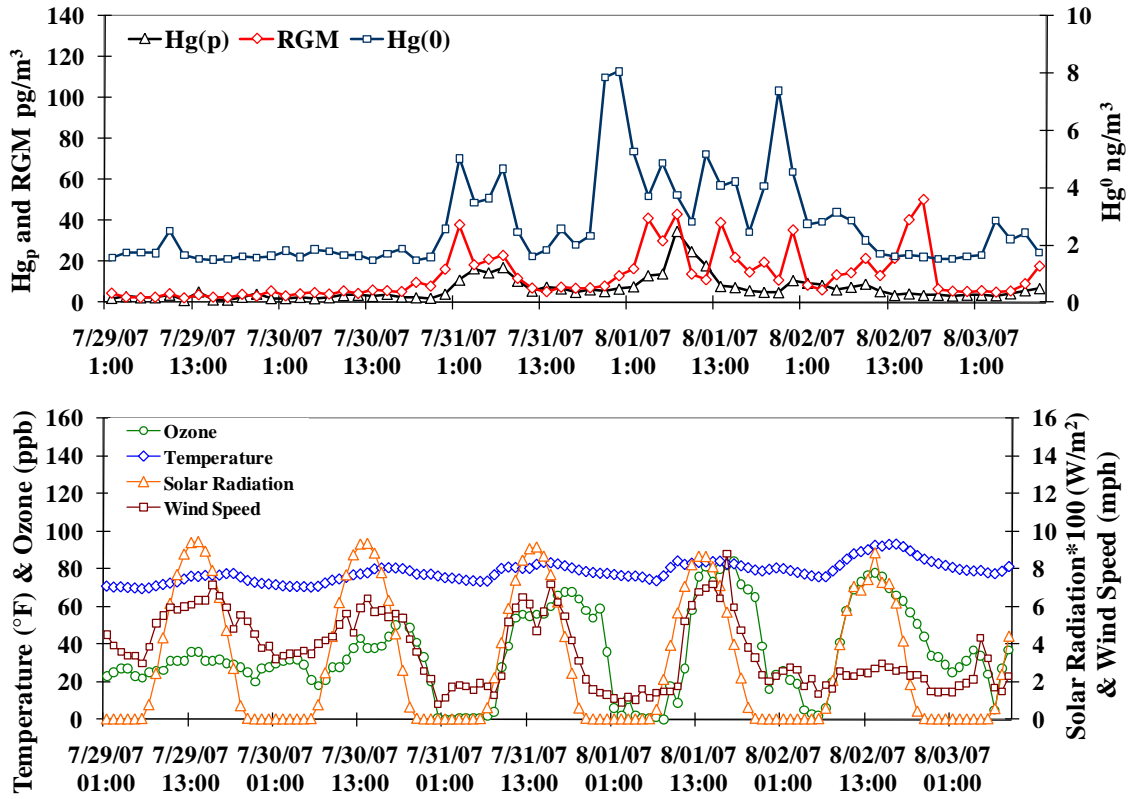
Figure 4.7: Speciated Hg, ozone and meteorological measurements for Chicago, IL on July 29 – August 3, 2007.
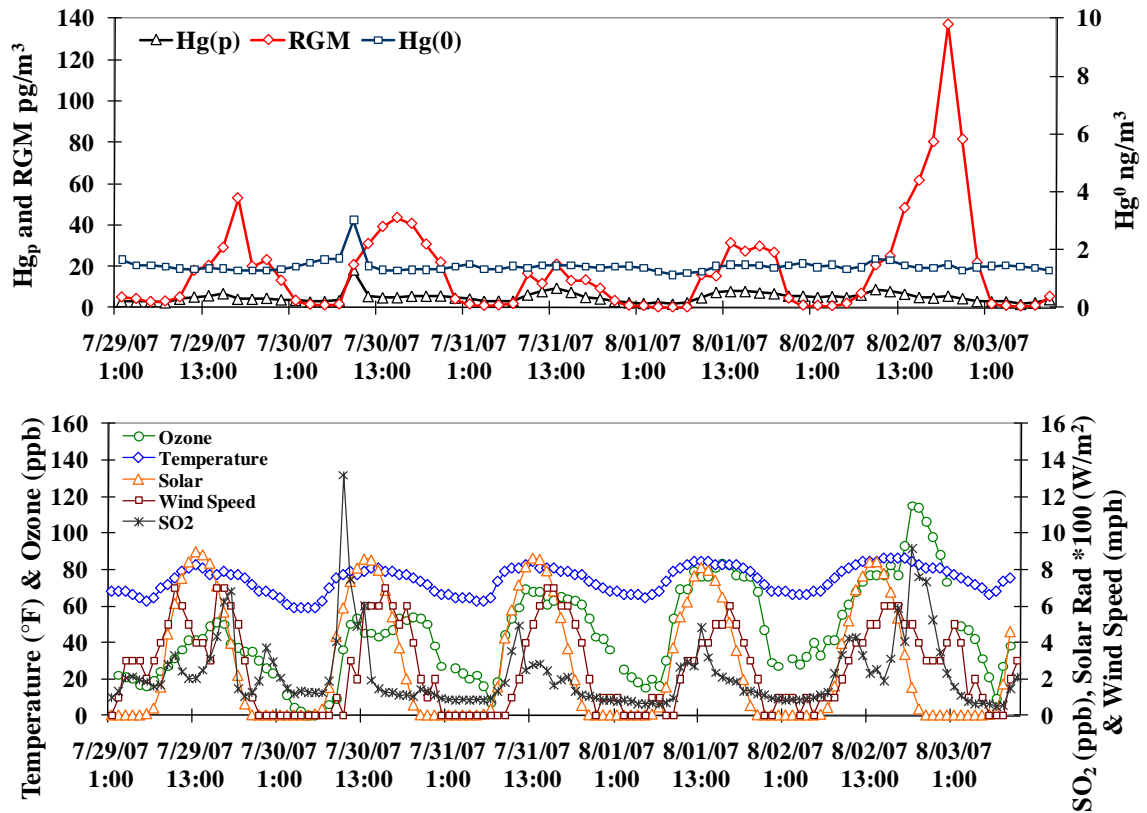
Figure 4.8: Speciated Hg, ozone, SO₂, and meteorological measurements for Holland, MI on July 29 – August 3, 2007.
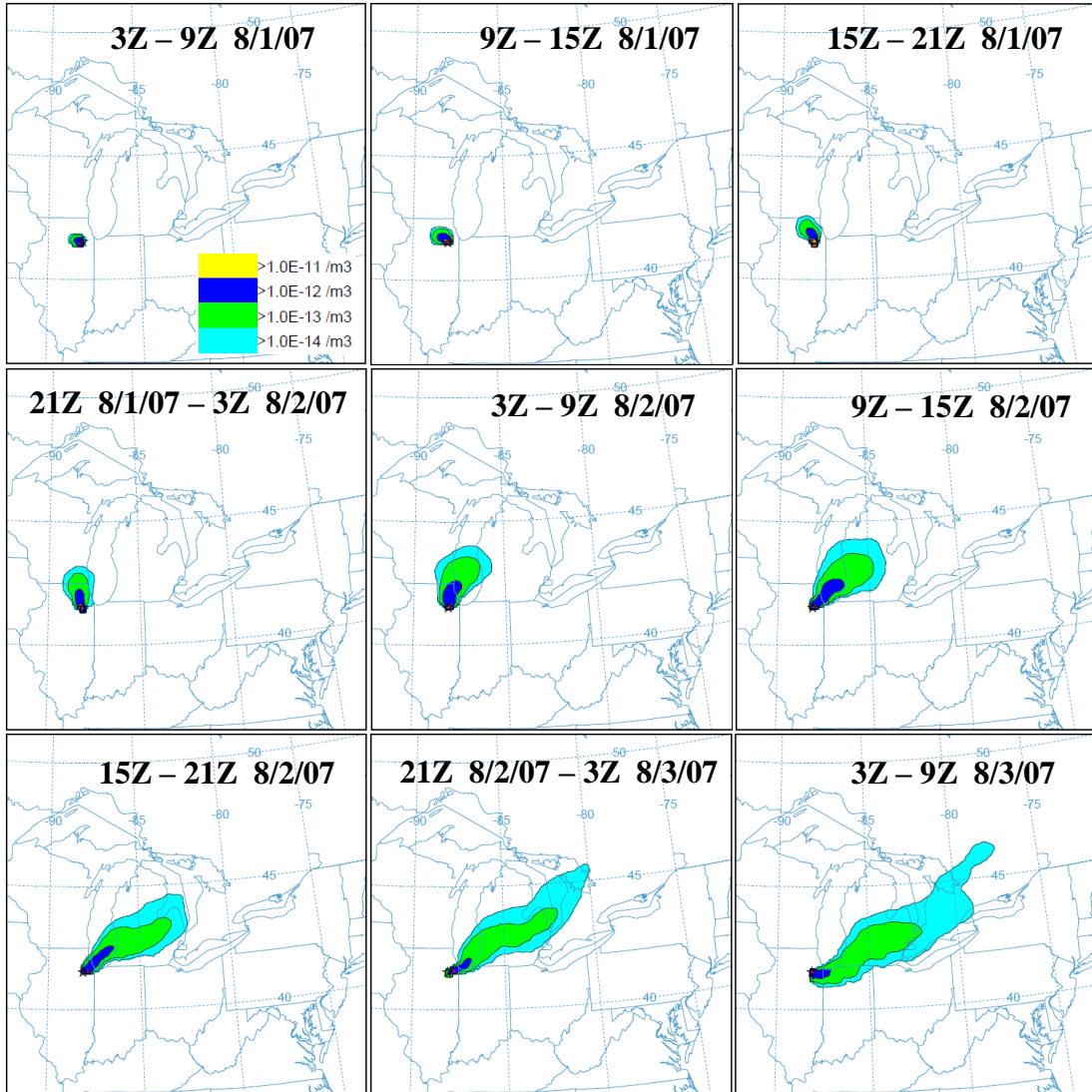
Figure 4.9: HYSPLIT dispersion model output averaged every six hours between 8/1/07 3Z (7/31/07 22:00 EST) and 8/3/07 9Z (4:00 EST) based on continuous emission from 41.495N, 88.125W at 137m AGL. Contours represent the amount of emitted mass per m^3 that was transported from the source location through pure dispersion.
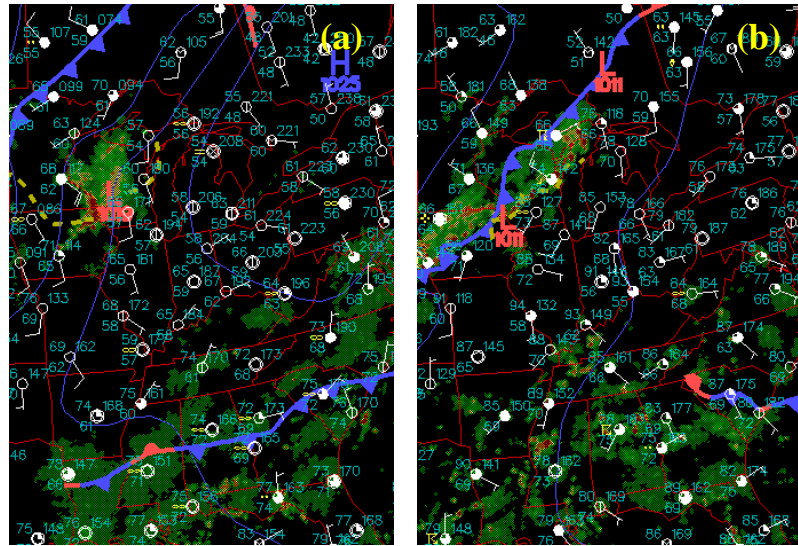
Figure 4.10. Surface maps on (a) August 27 12Z and (b) August 29 0Z, 2007.
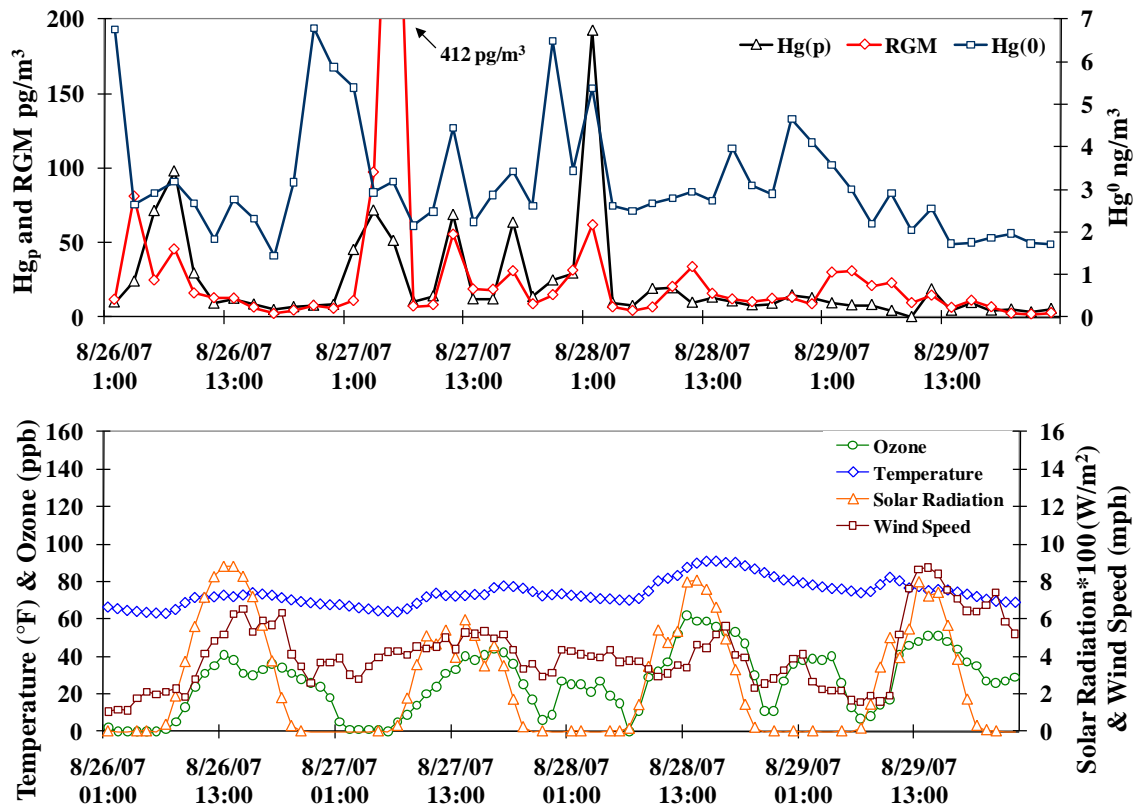
Figure 4.11: Speciated Hg, ozone, and meteorological measurements for Chicago, IL on August 26-29, 2007.
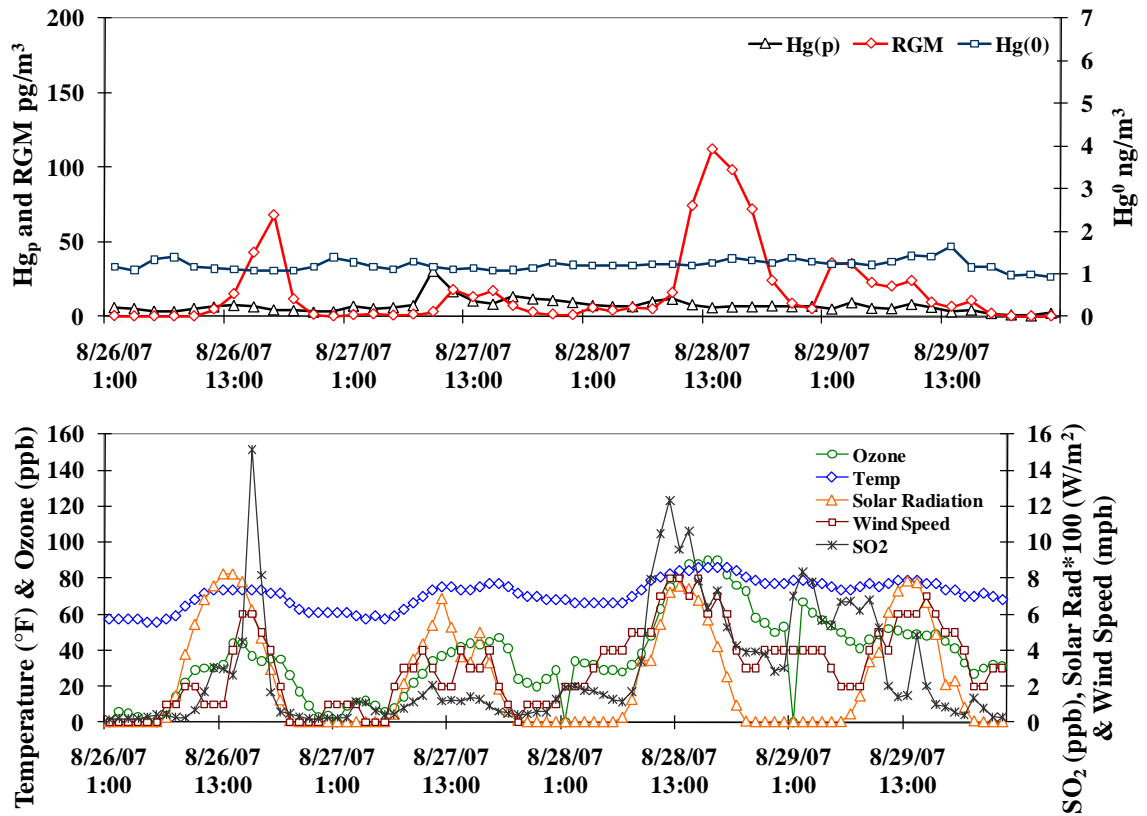
Figure 4.12: Speciated Hg, ozone, SO$_2$, and meteorological measurements for Holland, MI on August 26-29, 2007.
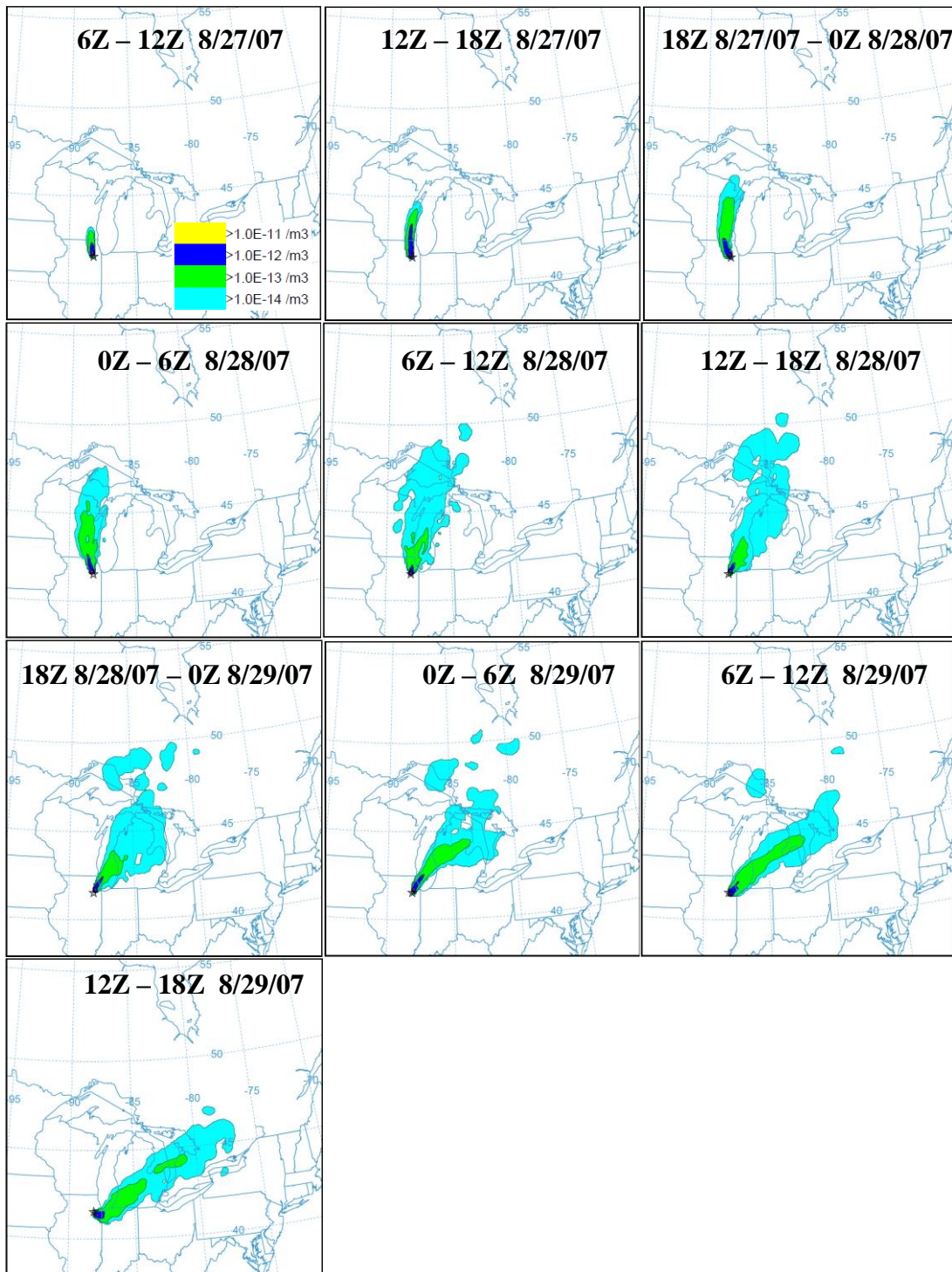
Figure 4.13: HYSPLIT dispersion model output averaged every six hours between 8/27/07 6Z (1:00 EST) and 8/29/07 18Z (13:00 EST) based on continuous emission from 41.495N, 88.125W at 137m AGL. Contours represent the amount of emitted mass per m^3 that was transported from the source location through pure dispersion.

145

Table 4.1: Speciated Hg at Chicago, IL and Holland, MI (Jul 1 – Nov 8, 2007).

	Hg^0 (ng/m^3)		RGM (pg/m^3)		Hg_p (pg/m^3)	
	Chicago	Holland	Chicago	Holland	Chicago	Holland
Mean	2.5	1.3	17	8	9	6
SD	1.5	0.3	87	15	20	4
Median	1.9	1.3	6	2	5	6
25%	1.6	1.2	3	0	3	3
75%	2.8	1.4	13	9	8	8
Max	16.5	6.0	2707	137	401	31
N	1339	1489	1339	1489	1339	1489

Table 4.2: Hg Concentrations in Chicago 24-hour HYSPLIT back-trajectories.

Cluster	Frequency	Hg^0 (ng/m^3)		RGM (pg/m^3)		Hg_p (pg/m^3)	
		Median	Max	Median	Max	Median	Max
4a	19%	2.1	11.1	8	344	6	131
4b	17%	2.7	10.4	14	2707	10	218
4c	11%	2.0	8.7	6	36	4	29
4d	9%	1.6	10.4	3	43	2	29
4e	16%	1.8	9.5	3	409	4	401
4f	5%	1.9	3.4	7	43	5	15
4g	11%	2.2	16.5	6	460	4	202
4h	7%	1.5	7.1	4	28	5	31
4i	3%	1.4	5.3	3	130	3	11

Table 4.3: Hg Concentrations in Holland 24-hour HYSPLIT back-trajectories.

Cluster	Frequency	Hg^0 (ng/m^3)		RGM (pg/m^3)		Hg_p (pg/m^3)	
		Median	Max	Median	Max	Median	Max
5a	8%	1.4	2.9	2	90	8	30
5b	25%	1.4	3.0	1	103	5	23
5c	20%	1.4	4.1	6	137	6	31
5d	7%	1.3	4.1	14	112	6	15
5e	9%	1.3	1.9	2	53	4	19
5f	10%	1.2	6.0	1	68	4	24
5g	9%	1.3	2.8	2	43	5	18
5h	5%	1.3	1.6	1	54	7	21
5i	6%	1.2	1.5	1	72	4	22

CHAPTER 5

Isotopic Composition and Fractionation of Mercury in Great Lakes Precipitation and Ambient Air

Abstract

Atmospheric deposition is a primary pathway by which mercury (Hg) enters terrestrial and aquatic ecosystems; however, the chemical and meteorological processes that Hg undergoes from emission to deposition are not well understood. Hg stable isotope geochemistry is a steadily growing field used to better understand Hg biogeochemical cycling that may offer a new perspective on atmospheric processes. To conduct an initial examination of atmospheric Hg isotopic composition in the Great Lakes, precipitation and ambient vapor phase Hg samples were collected in Chicago, IL, Holland, MI, and Dexter, MI, USA between April 2007 and September 2009. Precipitation samples were characterized by predominantly negative δ^{202}Hg while most ambient samples displayed positive δ^{202}Hg. Positive Δ^{199}Hg up to 0.61‰ (±0.09‰, 2SD) was observed in precipitation; however, Δ^{199}Hg was insignificant in most ambient vapor phase samples. Significant positive Δ^{200}Hg up to 0.22‰ (±0.03‰, 2SD) was also observed in precipitation. These results are in contrast to recent predictions of the isotopic composition of atmospheric Hg, suggesting that in addition to aqueous photoreduction of Hg, other atmospheric redox reactions and source related processes may contribute to

isotopic fractionation of atmospheric Hg and should be considered in future research endeavors.

5.1 Introduction

Mercury (Hg) is a hazardous air pollutant and a toxic metal of significant environmental concern. Once Hg enters terrestrial and aquatic ecosystems it may be converted to its organic form, methylmercury, which bioaccumulates within aquatic food webs ultimately threatening human health through consumption of contaminated fish (U.S. EPA, 1997). It is critical to identify and understand the sources and transport mechanisms of Hg in the atmosphere in order to effectively regulate emissions and reduce the threat of Hg to sensitive ecosystems and human health.

Hg behaves uniquely in the atmosphere due to its complex speciation. Hg exists in the atmosphere in three main forms: gaseous elemental Hg (Hg^0), divalent reactive gaseous Hg (RGM), and fine particulate bound Hg (Hg_p) (Schroeder and Munthe, 1998). Hg^0 comprises more than 90% of the Hg in ambient air (Slemr et al., 1985; Lin and Pehkonen, 1999). It has low solubility in water and consequently can be transported long distances in the atmosphere (Schroeder and Munthe, 1998; Lin and Pehkonen, 1999). In contrast, RGM and Hg_p are much more reactive and deposit readily, either close to sources (White et al., 2009) or upon oxidation of Hg^0 during atmospheric transport (Schroeder and Munthe, 1998; Lin and Pehkonen, 1999). Because Hg is a local, regional, and global pollutant, identification of the transport pathways, chemical transformations, and deposition mechanisms that Hg undergoes in the atmosphere can be challenging.

Hg isotope analysis is a relatively new tool for examining Hg biogeochemical cycling. Hg has considerable potential for isotopic fractionation because it has seven stable isotopes (196, 198, 199, 200, 201, 202, and 204 amu), active redox chemistry, and an ability to form covalent bonds as well as exist in the solid, aqueous, and gas phases. Mass-dependent fractionation (MDF) results from differences in zero-point vibrational energies between the isotopes due to their differing masses. MDF of Hg isotopes has been observed experimentally during microbial reduction (Kritee et al., 2007; Kritee et al., 2008) and dark abiotic aqueous reduction (Bergquist and Blum, 2007). MDF is also observed in natural settings, including hydrothermal systems (Hintelmann and Lu, 2003; Smith et al., 2009; Sherman et al., 2009) and terrestrial and marine sediments (Foucher and Hintelmann, 2006; Gehrke et al., 2009).

Recent studies have also demonstrated that mass-independent fractionation (MIF) of Hg isotopes can occur in natural systems. MIF of Hg is predicted to occur either due to variations in the nuclear charge radius of different isotopes caused by variability in the packing of protons and neutrons in the nucleus (nuclear volume effect) (Schauble, 2007) or due to the influence of nuclear spin in the odd-mass isotopes on radical pair reaction rates (magnetic isotope effect) (Turro, 1983; Buchachenko, 2001; Buchachenko et al., 2007). The nuclear volume theory describes MIF of Hg during equilibrium reactions (Schauble, 2007), whereas the magnetic isotope effect influences kinetic reactions (Turro, 1983; Buchachenko, 2001; Buchachenko et al., 2007). The nuclear volume theory predicts that MIF will be greatest for ^{199}Hg and ^{204}Hg, but also predicts MIF for ^{201}Hg and to a lesser degree for ^{200}Hg (Schauble, 2007). In contrast, MIF due to the magnetic isotope effect can only occur in the odd-mass isotopes of Hg (^{199}Hg and ^{201}Hg)

(Buchachenko et al., 2007). MIF and MDF have been observed during photoreduction of Hg^{2+} and methylmercury (Bergquist and Blum, 2007), as well as in peats (Biswas et al., 2008; Ghosh et al., 2008), sediments (Gehrke et al., 2009), hydrothermal waters (Sherman et al., 2009), coal deposits (Biswas et al., 2008), fish tissue (Jackson et al., 2008, Bergquist and Blum, 2007), lichens (Carignan et al., 2009), and Arctic snow (Sherman et al., 2010).

Analyses to date suggest that quantification of Hg isotope fractionation may offer information on the sources of Hg to the environment (Biswas et al., 2008) as well as the processes affecting Hg in terrestrial and aquatic ecosystems (Bergquist and Blum, 2007; Carignan et al., 2009; Sherman et al., 2010). Atmospheric deposition is the dominant pathway for Hg to enter aquatic ecosystems (Landis and Keeler, 2002; Hammerschmidt and Fitzgerald, 2006) and is thus a key component of the Hg biogeochemical cycle. However, Hg isotopes have only recently been directly measured in atmospheric reservoirs (Sherman et al., 2010).

The Great Lakes region was chosen for atmospheric Hg isotope measurements because atmospheric sources of Hg in this region are well-identified (Hoyer et al., 1995; Great Lakes Commission, 1999; Landis et al., 2002; Keeler et al., 2006; Cohen et al., 2007) and elevated levels of Hg deposition to the Great Lakes have been observed in recent decades (U.S. EPA, 1994). Previous studies demonstrated the influence of major Hg sources in the Chicago/Gary urban area on Hg concentrations in Lake Michigan as well as in ambient air and precipitation in the surrounding region (Landis and Keeler, 2002; Landis et al., 2002; Vette et al., 2002). However, there is still much to be understood regarding Hg sources in the Great Lakes region and Hg biogeochemical

152

cycling. The analysis of atmospheric samples for Hg isotopes may offer additional information on the transport mechanisms and chemical processes that Hg undergoes in the atmosphere.

5.2 Experimental Section

5.2.1 Site Descriptions

Precipitation samples were collected in Chicago, IL and Holland, MI from July 2007 to November 2007 and in Dexter, MI from April 2007 to November 2008 (Figure 5.SI-1). Ambient vapor phase Hg samples were also collected periodically in Dexter from August 2007 to September 2009. An additional vapor phase Hg sample was collected in Chicago in September 2009.

The Chicago, IL site (UOC) was ~2 km west of Lake Michigan on the University of Chicago campus. This site was in close proximity to atmospheric Hg sources southwest of Chicago and along southern Lake Michigan in the Chicago/Gary industrial region, including coal-fired utility boilers, metal smelters, and iron and steel manufacturing facilities. The Holland, MI site (HOL) was located on the eastern shore of Lake Michigan ~162 km northeast of Chicago at the Michigan Department of Environmental Quality (MDEQ) monitoring station, ~5 km east of Lake Michigan. This site was considered semi-rural because although there are local sources, they are far fewer in number than those surrounding the industrial Chicago site. Additionally, because the Holland site was south and west of these local point sources, they would minimally impact samples collected in Holland during southwest transport from Chicago/Gary. The Dexter, MI site (DXT) was located approximately 60 km west of Detroit, MI. It is a remote location with no major local Hg point sources, so the air

masses sampled at this site primarily represent background ambient air (Lynam and Keeler, 2005; Liu et al., 2010).

5.2.2 Sample Collection

Precipitation samples were collected using a modified wet-only University of Michigan MIC-B (MIC, Thornhill, Ontario) automated precipitation collector. The sampling train was modeled after the design described by Landis and Keeler (1997) for daily-event wet-only precipitation collection. However, because substantially more Hg is needed for high precision isotopic analysis than for Hg concentration analysis, precipitation was collected into 2-L fluorinated polyethylene bottles, rather than the 1-L bottles typically used in daily-event collection (Landis and Keeler, 1997). All supplies and samples were handled and prepared using clean techniques in a Class-100 clean room. Two borosilicate glass funnels (collection area 191 ± 9 cm^2), each equipped with a glass vapor lock inside a Teflon adapter to prevent Hg loss, were deployed in the MIC-B (Landis and Keeler, 1997). The vapor locks were fitted with 23 cm long silicone tubes (0.48 cm i.d.) attached to a polypropylene bottle cap through a Y-shaped adapter. Funnels and vapor locks were prepared using a rigorous acid cleaning procedure (Landis and Keeler, 1997). The fluorinated bottles were cleaned using a two-day soak in 2% BrCl followed by a thorough rinse in ultra-purified Milli-Q water. Lab and field blanks of the fluorinated bottles yielded < 2 pg of Hg/bottle. Silicone tubing was rinsed extensively with 2L of ultra-pure Milli-Q water before deployment in the field and individual lengths of tubing were not used for more than one sample. Sample bottles were typically deployed for 1-2 weeks to allow for sufficient volume collection.

Consequently, samples collected during this study represent composite samples rather than true event samples.

Ambient vapor phase Hg samples were collected onto eight gold coated bead traps deployed in parallel on a PVC manifold. Air was pulled through all eight traps by a single pump at a constant flow rate of ~1.8 lpm per trap. The total volume of air sampled was recorded using a calibrated dry test meter (DTM) and the total flow rate was verified using a calibrated rotameter. Quartz filters were placed on the upstream end of the traps to remove particulate Hg from the air stream. The traps were wrapped in heat tape and kept at ~60°C to prevent condensation. Samples were collected in the field for 2-3 days at a time.

5.2.3 Sample Processing and Analysis

Following collection, precipitation samples were oxidized with 1% (v/v) BrCl and stored in a dark cold room for at least 24-hours. Precipitation samples were analyzed for total Hg concentration using cold vapor atomic fluorescence spectrometry (CVAFS) on a Tekran® Series 2600. Of the 56 samples collected at Dexter, Holland, and Chicago, 20 contained sufficient Hg for isotopic analysis (> 8 ng).

Prior to isotopic analysis, the Hg from each sample was isolated and concentrated into a 2% $KMnO_4$ (w/w) liquid trap. Each precipitation sample was first transferred to a clean 2-L pyrex bottle. The reducing agents, consisting of 10% SnCl (w/v), 50% H_2SO_4 (w/v) and 1% NH_2OH (w/v), were mixed in a separate 2-L pyrex bottle. The sample and reagents were then introduced simultaneously onto a frosted-tip gas-liquid separator at a flow rate of 0.8 ml/min. The reduced $Hg^0_{(g)}$ was transferred to 25 g of 2% $KMnO_4$ (w/w) solution by a counter-flow of Ar gas (0.9 L/min). Procedural standards (NIST SRM 3133

in 1-L of 1% BrCl (v/v)) and blank solutions (1-L of 1% BrCl (v/v)) were pre-concentrated in the same manner.

Ambient vapor phase samples were also pre-concentrated into 25 g of 2% $KMnO_4$ (w/w). The gold coated bead traps were thermally desorbed by slowly heating each trap to 500°C over 3-hours, following the heating profile described in Sherman et al. (2010) while an Ar gas stream (50 ml/min) transferred the released $Hg^0_{(g)}$ into the 2% $KMnO_4$ solution.

The 25 g 2% $KMnO_4$ (w/w) solutions were subsequently concentrated into 8 g of 2% $KMnO_4$ (w/w) to sufficiently concentrate Hg in the samples to $\geq$ 1 ng/g for isotopic analysis. Each 25 g solution was first partially reduced with NH_2OH, then divided into 5 ml sub-samples which were individually reduced with 20 µl of 30% NH_2OH, 250 µl of 20% $SnCl_2$ and 250 µl of 50% H_2SO_4 and bubbled into 8 g of 2% $KMnO_4$ (w/w). The 8 g solutions were then partially reduced with NH_2OH prior to isotopic analysis.

The isotopic compositions of samples and procedural standards were determined using a multi-collector inductively coupled plasma mass spectrometer (MC-ICP-MS; Nu instruments) following previously reported methods (Bergquist and Blum, 2007; Blum and Bergquist, 2007). MDF for a given sample is reported in delta notation with respect to the average of the NIST 3133 bracketing standards (Blum and Bergquist, 2007), following equation (1):

(1) $\delta^{xxx}Hg$ (‰) = ([($^{xxx}Hg/^{198}Hg)_{sample}/(^{xxx}Hg/^{198}Hg)_{NIST\ SRM\ 133}] - 1) * 1000$

MIF is reported using capital delta notation (Blum and Bergquist, 2007) as the deviation from predicted kinetic MDF according to equations (2), (3), and (4) where the constants

represent the theoretically predicted MDF for ^{199}Hg, ^{200}Hg, and ^{201}Hg based on the measured ^{202}Hg/^{198}Hg ratio (Blum and Bergquist, 2007).

(2) Δ^{199}Hg (‰) = δ^{199}Hg – (δ^{202}Hg * 0.252)

(3) Δ^{200}Hg (‰) = δ^{200}Hg – (δ^{202}Hg * 0.502)

(4) Δ^{201}Hg (‰) = δ^{201}Hg – (δ^{202}Hg * 0.752)

To assess the analytical uncertainty of the isotopic analyses, the UM-Almadén standard solution (Blum and Bergquist, 2007) was analyzed during each mass spectrometry analytical session at the same concentration as sample solutions. Procedural standard analyses (NIST SRM 3133) emulating the preparation, concentration and analysis of precipitation and vapor phase samples were also performed throughout the study. In the following discussion, analytical uncertainties are reported as the larger value of either 2SD of the long-term reproducibility of the UM-Almadén standard or 2SD of the reproducibility of procedural standards.

5.3 Results

These data represent the first reported Hg isotope analyses conducted on atmospheric samples collected in the Great Lakes region. Figure 5.1 summarizes the isotopic composition of Hg in Great Lakes atmospheric samples (Δ^{199}Hg versus δ^{202}Hg). Precipitation samples were primarily characterized by negative δ^{202}Hg (δ^{202}Hg = -0.79‰ to 0.21‰ ± 0.17‰, 2SD), whereas δ^{202}Hg of ambient samples was predominantly positive with the exception of two samples (δ^{202}Hg = -0.59‰ to 0.48‰ ± 0.12‰, 2SD). Significant positive MIF of the odd-mass isotopes (^{199}Hg and ^{201}Hg) was measured in precipitation samples (Δ^{199}Hg = 0.07‰ to 0.61‰ ± 0.09‰, 2SD; Δ^{201}Hg = 0.05‰ to 0.55‰ ± 0.08‰, 2SD) (Figure 5.2). In contrast, Δ^{199}Hg and Δ^{201}Hg values were

indistinguishable from zero in most ambient vapor phase Hg samples (Δ^{199}Hg = -0.17‰ to 0.06‰ ± 0.07‰, 2SD; Δ^{201}Hg = -0.12‰ to 0.03‰ ± 0.08‰, 2SD). A linear regression of Δ^{199}Hg versus Δ^{201}Hg for all atmospheric samples (precipitation and ambient vapor phase Hg) yielded a slope of 0.82 ± 0.26 (r^2 = 0.58) (Figure 5.2).

Significant MIF of ^{200}Hg has never been reported in previous studies. However, Δ^{200}Hg was significantly different from zero in several precipitation samples with values up to 0.22‰ (± 0.03‰, 2SD) observed. In contrast, Δ^{200}Hg of ambient vapor phase samples was slightly negative (Δ^{200}Hg = -0.12‰ to 0.02‰ ± 0.04‰, 2SD). A linear regression of Δ^{199}Hg versus Δ^{200}Hg in all atmospheric samples yielded a slope of 1.69 ± 0.43 (r^2 = 0.79) (Figure 5.3). A summary of the precipitation and ambient vapor phase isotopic compositions can be found in the Supporting Information (Tables 5.SI-1, 5.SI-2).

5.4 Discussion

5.4.1 Ambient Sample Characterization

The range in Hg isotopic composition of ambient vapor phase samples suggests that Hg isotope measurements may potentially be used to distinguish background Hg^0 from Hg emitted from industrial sources. Five of the six Dexter vapor phase samples (DXT-VP-1; DXT-VP-3 through 6) had comparable δ^{202}Hg values within the reported 2SD analytical uncertainty and generally showed insignificant MIF (Figure 5.1). Because the Dexter site was at a more rural location, these samples may represent the regional background isotopic composition of ambient vapor phase Hg, which is predominantly Hg^0 (Slemr et al., 1985; Lin and Pehkonen, 1999; Lynam and Keeler, 2005). In contrast, one vapor phase sample from Dexter (DXT-VP-2) displayed negative δ^{202}Hg (-0.39‰ ± 0.12‰, 2SD) and significant negative Δ^{199}Hg (-0.17‰ ± 0.07‰,

2SD). DXT-VP-2 was the only vapor phase sample collected at Dexter during south-southeasterly flow, whereas all other Dexter vapor phase samples, with the exception of DXT-VP-5, captured northerly flow. It is possible that the south-southeasterly flow transported Hg from major point sources in southeast Michigan or the Ohio River Valley where coal combustion is the dominant contributor to atmospheric Hg (Keeler et al., 2006) (Figure 5.SI-1). The negative δ^{202}Hg and Δ^{199}Hg in DXT-VP-2 are similar in magnitude to those observed in some western USA coal deposits (Biswas et al., 2008), which are burned in the Great Lakes region (Hower et al., 1999; Freme, 2008). Interestingly, DXT-VP-5 (δ^{202}Hg = 0.27‰ ± 0.12‰, 2SD; Δ^{199}Hg = 0.0‰ ± 0.07‰, 2SD) was collected under south-southwesterly flow conditions but is not isotopically similar to DXT-VP-2. Although speculative, the differences between these samples may be explained by the meteorological conditions under which they were collected. During the sampling period for DXT-VP-2 (2/23/09 – 2/25/09) the average boundary layer height at Dexter was 236 m above ground level (AGL) with a range of 10 – 700 m AGL, as determined from HYSPLIT V4.8 modeled mixed layer depths every six hours at the sampling location (Draxler and Hess, 1998), and the average hourly ambient temperature in Dexter was -5°C (CASTNET). These conditions suggest that there was limited vertical mixing due to the low boundary layer and cold temperatures. During the collection of DXT-VP-2 under southeasterly flow the sky was 60-100% obscured by clouds (NCDC) and the average hourly solar insolation was 142 W/m^2 with a maximum of 668 W/m^2 (CASTNET), suggesting a potential reduction in photochemical activity due to reflection of incoming radiation. In contrast, during the collection of DXT-VP-5 (5/20/09-5/22/09), the average hourly temperature in Dexter was 20°C, the average

hourly solar insolation was 342 W/m^2 with a maximum value of 979 W/m^2 recorded (CASTNET), the sky was clear with few scattered clouds (NCDC), and the average boundary layer depth was ~450 m AGL with daytime heights above 1000 m AGL. This may suggest greater potential for vertical mixing of point source emissions and photochemical activity during collection of DXT-VP-5 as compared to DXT-VP-2. It is therefore possible that DXT-VP-2 more strongly retained the isotopic signature imparted by regional coal combustion. Additional sampling of the emissions from different source types and finer time resolution sampling of ambient Hg under different flow regimes is needed to better evaluate this hypothesis.

The Chicago vapor phase sample (UOC-VP-1) displayed similar negative $\delta^{202}Hg$ (-0.59‰ ± 0.12‰, 2SD) to DXT-VP-2. The difference in $\delta^{202}Hg$ between the Chicago vapor phase sample and the other Dexter samples may be related to the proximity of the Chicago site to many large industrial sources (e.g., coal combustion and iron-steel manufacturing) (Figure 5.SI-1) that strongly influence the concentration and possibly the isotopic composition of atmospheric Hg. Additional samples are needed at the urban Chicago site to draw clear distinctions from the remote Dexter site.

5.4.2 Precipitation Sample Characterization

It is difficult to characterize the meteorological history of the precipitation samples collected during this study because each sample was a composite of up to six discrete events. Each event may have had different synoptic conditions leading to the formation of precipitation as well as different sources emitting Hg into the associated air mass. Previous studies have clearly demonstrated that event-based sampling is essential to distinctly characterize air mass transport and deposition using meteorological data,

modeled air mass back-trajectories, and trace element concentrations in precipitation (White et al., 2009; Dvonch et al., 1998; Dvonch et al., 1999; Gratz et al., 2009). When multiple events are combined into a single sample, it is very difficult and perhaps no longer possible to separate the signatures of specific source emissions. Despite the inability to identify specific source contributions using only Hg isotopes in composite precipitation samples, the data presented here do offer new insights into atmospheric processes and highlight important reaction mechanisms that need further examination.

5.4.3 Mass-Independent Fractionation Mechanisms

The precise mechanism(s) causing MIF of Hg isotopes are not fully understood, but previous work suggests that significant MIF can occur due to the magnetic isotope effect (Bergquist and Blum, 2007; Ghosh et al., 2008; Carignan et al., 2009; Sherman et al., 2010). This effect occurs during photochemical reactions in which long-lived radical pairs are formed. In such reactions, differences in magnetic moments and nuclear spin between the even- and odd-mass isotopes can cause varying radical pair recombination rates among the isotopes, leading to variability in the reaction products (Bergquist and Blum, 2007; Buchachenko, 2001; Buchachenko et al., 2007). In contrast, the nuclear volume effect can occur during both dark and light reactions but the extent of fractionation caused by this effect is much smaller (Zheng and Hintelmann, 2009). Given that there are several Hg redox reactions that occur in the atmosphere, it is possible that both the magnetic isotope effect and nuclear volume effects could affect the isotopic composition of atmospheric Hg depending on the dominant reaction. It is also possible that there are other mechanisms contributing to Hg isotope fractionation in the atmosphere that have not yet been identified.

Previous studies of MIF in natural systems suggest that the magnetic isotope effect may produce a $\Delta^{199}Hg/\Delta^{201}Hg$ ratio of ~1:1 (Bergquist and Blum, 2007; Ghosh et al., 2008; Carignan et al., 2009; Sherman et al., 2010), whereas the nuclear volume effect is theoretically predicted to produce a $\Delta^{199}Hg/\Delta^{201}Hg$ ratio of ~2.5:1 (Schauble, 2007; Ghosh et al., 2008; Estrade et al., 2009). The $\Delta^{199}Hg/\Delta^{201}Hg$ ratio observed in precipitation and vapor phase Hg samples (Figure 5.2) is similar to the ratio suggested for the magnetic isotope effect and is indistinguishable from 1:1. However, the substantial variability in the $\Delta^{199}Hg/\Delta^{201}Hg$ ratios for individual samples may suggest that more than one reaction and/or more than one mechanism are causing the observed MIF.

5.4.4 Comparison of Results to Previous Studies

The observed positive MIF of ^{199}Hg and ^{201}Hg in precipitation and insignificant MIF of ^{199}Hg and ^{201}Hg in ambient vapor phase samples are in contrast to previous studies which suggested that atmospheric Hg should display negative MIF (Carignan et al., 2009). During aqueous photoreduction experiments by Bergquist and Blum (2007) in which $Hg^0_{(g)}$ was volatilized from solutions containing dissolved organic carbon (DOC), the Hg^{2+} remaining in solution displayed increasingly positive MIF of ^{199}Hg and ^{201}Hg. It was therefore hypothesized that Hg^0 released to the atmosphere through aqueous photoreduction should display negative MIF (Bergquist and Blum, 2007). Additionally, recent studies reported negative MIF in lichens from Switzerland, northeast France, and northern Quebec, Canada with $\Delta^{199}Hg$ ranging from -1.0‰ to -0.3‰ (± 0.15‰, 2SD) (Carignan et al., 2009). Because lichens take up Hg through wet and dry deposition (including direct absorption of Hg^0 from the atmosphere), it was proposed that the Hg isotopic composition of lichens might be representative of isotopic values of atmospheric

Hg (Carignan et al., 2009). It was further suggested that the atmosphere and aquatic environment may be complementary reservoirs with respect to the photoreduction of Hg and that aqueous photoreduction may be the dominant process contributing to atmospheric Hg (Carignan et al., 2009). However, the results of the present study suggest that aqueous photoreduction in the presence of DOC is not the only process contributing to atmospheric Hg isotope fractionation.

The sources and processes relevant to atmospheric Hg cycling vary on local and regional scales due to the relative density of sources, which emit varying amounts of Hg as well as varying fractions of the elemental and reactive forms of Hg, and the availability of other atmospheric constituents. Therefore, the dominant processes influencing Hg isotopic fractionation should be examined carefully for each location of interest. The isotopic composition of $Hg^0_{(g)}$ released during aqueous photoreduction does not represent the isotopic composition of $Hg^0_{(g)}$ released from anthropogenic sources or produced via other reaction mechanisms. Although aqueous photoreduction is a potential source of atmospheric $Hg^0_{(g)}$ in the Lake Michigan Basin, the density of industrial sources in the region likely also contributes to the isotopic composition of Hg in atmospheric samples.

In addition to source impacts, there are a wide range of gas phase, aqueous phase, and heterogeneous reactions that Hg can undergo between emission and deposition. For example, Hg^0 can be oxidized in the gas and aqueous phases by hydroxyl radicals, ozone, and halogen compounds (Munthe, 1992; Lin and Pehkonen, 1997; Hynes et al., 2009). Reduction of Hg^{2+} can occur in the aqueous phase by sulfite, halogen species, or hydroperoxyl radicals (Lin and Pehkonen, 1999; Hynes et al., 2009; Munthe et al., 1991).

Photoreduction has been suggested to occur in the atmosphere through heterogeneous chemistry in cloud droplets (Lin and Pehkonen, 1997; Seigneur et al., 1994) and within power plant plumes (Lohman et al., 2006).

The importance of heterogeneous chemistry in Hg isotopic fractionation was recently demonstrated in Arctic snow samples. Following photochemical reduction of Hg^{2+} in surface snow through reactions likely involving Hg-halogen radical pair intermediates, $\Delta^{199}Hg$ in the surface snow decreased significantly (to $< -4‰$) while the emitted $Hg^0_{(g)}$ displayed less negative $\Delta^{199}Hg$ values than the original surface snow (Sherman et al., 2010). These findings highlight the importance of photochemistry to Hg isotopic fractionation and suggest that Hg fractionation in the atmosphere may occur during similar processes. Halogen reactions are typically important in Arctic environments (Lindberg et al., 2002; Tackett et al., 2007) and the marine boundary layer (Hedgecock and Pirrone, 2001; Lin et al., 2006), whereas in the industrial Great Lakes region ozone is more readily available (Dye et al., 1995) and therefore may dominate Hg^0 oxidation (Munthe and McElroy, 1992). However, there may also be important industrial halogen sources in the Great Lakes region, such as municipal solid waste incinerators (Carpi, 1997), which could contribute to Hg^0 oxidation.

Photoreduction in cloud droplets may also facilitate the release of some Hg^0 back to the interstitial air. Cloud droplets contain some DOC (Kesselmeier and Staudt, 1999; Willey et al., 2000), and if the experiments conducted by Bergquist and Blum (2007) are relevant to this system, then the odd-mass isotopes of Hg would be preferentially retained as Hg^{2+} in the cloud droplet. As a result, the cloud droplets could become increasingly positive with respect to $\Delta^{199}Hg$. Oxidation reactions in the atmosphere may also cause

164

MIF of Hg isotopes; however, because oxidation by ozone or halogen radicals is not a direct photochemical process and thus does not produce long-lived radical pairs it is unlikely that this process will produce significant MIF of Hg isotopes (Buchachenko, 2001; Zheng and Hintelmann, 2009). The possible mechanisms and full range of reactions responsible for MIF of Hg in the atmosphere need to be examined more closely and under carefully controlled experimental conditions.

5.4.5 Mass-Independent Fractionation of ^{200}Hg

Significant MIF of ^{200}Hg was observed in precipitation and ambient vapor phase Hg samples. Such MIF of an even-mass isotope of Hg has not been previously reported in natural samples. Although the observed values for Δ^{200}Hg in atmospheric samples are relatively small, many are significant and show a consistent pattern relative to Δ^{199}Hg (Figure 5.3). There is no indication that this MIF is the result of instrumental artifacts and none of the blank or standard solutions included in the analytical sessions displayed significant Δ^{200}Hg. Because the even-mass Hg isotopes do not have nuclear magnetic moments or nuclear spin, MIF of ^{200}Hg cannot be caused by the magnetic isotope effect (Turro, 1983; Buchachenko et al., 2007). It is possible that the nuclear volume effect might cause slight MIF of the even isotopes of Hg, but this effect should not be large enough to be detected (Schauble, 2007). However it is possible that a combination of nuclear volume and magnetic isotope effects could produce the small Δ^{200}Hg anomaly. It is important to note that because capital delta notation is calculated with respect to δ^{202}Hg, by definition MIF of ^{198}Hg would not be detected. Therefore the MIF observed here for ^{200}Hg could involve ^{198}Hg, ^{200}Hg, or ^{202}Hg.

5.4.6 Implications

The results of this study demonstrate that the isotopic composition of Hg can be measured with high precision in atmospheric samples. Analysis indicates that MIF of atmospheric Hg may be caused by a combination of emission source differences as well as complex reactions in the atmosphere. Although the specific processes and source emissions contributing to the MDF and MIF in samples collected during this study could not be explicitly identified, the data suggests the potential for identifying sources and atmospheric processes using Hg isotopes. It will be critical to collect large volume event-based precipitation samples in the future for isotope analysis so that the source identification techniques currently applied to event precipitation samples can be applied to Hg isotope samples. In contrast to the suggestions of previous studies, ambient vapor phase samples collected during this study did not display negative MIF. While aqueous photoreduction is a potential source of atmospheric Hg^0 in the Great Lakes, the density of industrial point sources elevates Hg levels in the region and likely contributes to fractionation observed in atmospheric samples. Additionally, there are a range of atmospheric redox reactions that may influence the observed Hg isotopic compositions. Therefore, conclusions obtained based upon application of the limited Hg isotope fractionation data to regional or global Hg budgets or mass balance studies should be viewed with great caution until the processes that result in atmospheric Hg fractionation are better understood.

References

Bergquist, B.A., Blum, J.D., 2007. Mass-dependent and mass-independent fractionation of Hg isotopes by photoreduction in aquatic systems. Science 318, 417-420.

Biswas, A., Blum, J.D., Bergquist, B.A., Keeler, G.J., Zhouqing, X., 2008. Natural mercury isotope variation in coal deposits and organic soils. Environmental Science & Technology 42, 8303-8309.

Blum, J.D., Bergquist, B.A., 2007. Reporting the variations in the natural isotopic composition of mercury. Analytical and Bioanalytical Chemistry 388, 353-359.

Buchachenko, A.L., 2001. The magnetic isotope effect: Nuclear spin control of chemical reactions. Journal of Physical Chemistry 105(44), 9995-10011.

Buchachenko, A.L., Ivanov, V.L., Roznyatovskii, V.A., Artamina, G.A., Vorob'ev, A.Kh., Ustynyuk, Yu.A., 2007. Magnetic isotope effect for mercury nuclei in photolysis of bis(p-trifluoromethylbenzyl)mercury. Doklady Physical Chemistry 413, 39-41.

Carignan, J., Estrade, N., Sonke, J.E., Donard, O.F.X., 2009. Odd isotope deficits in atmospheric Hg measured in lichens. Environmental Science & Technology 43, 5660-5664.

Carpi, A., 1997. Mercury from combustion sources: A review of the chemical species emitted and their transport in the atmosphere. Water, Air and Soil Pollution 98, 241-254.

Clean Air Status and Trends Network (CASTNET) (http://www.epa.gov/castnet/).

Cohen, M.D., Artz, R.S., Draxler, R.R., 2007. *Report to Congress: Mercury Contamination in the Great Lakes;* NOAA Air Resources Laboratory, Silver Spring, MD (http://www.arl.noaa.gov/documents/reports/cohen/NOAA_GL_Hg.pdf).

Draxler, R.R., Hess G.D., 1998. An overview of the HYSPLIT_4 modelling system for trajectories, dispersion and deposition. Australian Meteorological Magazine 47, 295-308.

Dvonch, J.T., Graney, J.R., Marsik, F.J., Keeler, G.J., Stevens, R.K., 1998. An investigation of source-receptor relationships for mercury in south Florida using event precipitation data. Science of the Total Environment 213, 95-108.

Dvonch, J.T., Graney, J.R., Keeler, G.J., Stevens, R.K., 1999. Use of Elemental Tracers to Source Apportion Mercury in South Florida Precipitation. Environmental Science & Technology 33, 4522-4527.

Dye, T.S., Roberts, P.T., Korc, M.E., 1995. Observations of transport processes for ozone and ozone precursors during the 1991 Lake Michigan Ozone Study. Journal of Applied Meteorology 34, 1877-1889.

Estrade, N., Carignan, J., Sonke, J.E., Donard, O.F.X., 2009. Mercury isotope fractionation during liquid-vapor evaporation experiments. Geochimica et Cosmochimica Acta 73, 2693-2711.

Foucher, D., Hintelmann, H., 2006. High-precision measurement of mercury isotope ratios in sediments using cold-vapor generation multi-collector inductively coupled plasma mass spectrometry. Analytical and Bioanalytical Chemistry 384, 1470-1478.

Freme, F., 2008. *U.S. Coal Supply and Demand: 2008 Review*; U.S. Department of Energy, Energy Information Administration (http://www.eia.doe.gov/cneaf/coal/page/special/article_dc.pdf).

Gehrke, G.E., Blum J.D., Meyers, P.A., 2009. The geochemical behavior and isotopic composition of Hg in a mid-Pleistocene western Mediterranean sapropel. Geochimica et Cosmochimica Acta 73, 1651-1665.

Ghosh, S., Xu, Y., Humayun, M., Odom, L., 2008. Mass-independent fractionation of mercury isotopes in the environment. Geochemistry Geophysics Geosystems 9(3), Q03004.

Gratz, L.E., Keeler, G.J., Miller, E.K., 2009. Long-term relationships between mercury wet deposition and meteorology. Atmospheric Environment 43, 6218-6229.

Great Lakes Commission, 1999. *1999 Inventory of Toxic Air Emissions: Point, Area, and Mobile Sources*. Ann Arbor, MI (http://www.glc.org/air/inventory/1999/).

Hammerschmidt, C.R., Fitzgerald, W.F., 2006. Methylmercury in freshwater fish linked to atmospheric mercury deposition. Environmental Science & Technology 40, 7764-7770.

Hedgecock, I.M., Pirrone, N., 2001. Mercury and photochemistry in the marine boundary layer-modeling studies suggest the in situ production of reactive gas phase mercury. Atmospheric Environment 35, 3055-3062.

Hintelmann, H., Lu, S., 2003. High precision isotope ratio measurements of mercury isotopes in cinnabar ores using multi-collector inductively coupled plasma mass spectrometry. Analyst 128, 635-639.

Hower, J.C., Thomas, G.A., Palmer, J., 1999. Impact of the conversion to low-NOx combustion on ash characteristics in a utility boiler burning Western US coal. Fuel Processing Technology 61, 175-195.

Hoyer, M., Burke, J., Keeler, G.J., 1995. Atmospheric Sources, Transport and Deposition of Mercury in Michigan – 2 Years of Event Precipitation. Water, Air, and Soil Pollution 80, 199-208.

Hynes, A.J., Donohue, D.L., Goodsite, M.E., Hedgecock, I.M., 2009. Our current understanding of major chemical and physical processes affecting mercury dynamics in the atmosphere and at the air-water/terrestrial interfaces. In *Mercury Fate and Transport in the Global Atmosphere*; Pirrone, N., Mason, R., Eds; Springer Science + Business Media: New York pp 427-457.

Jackson, T.A., Whittle, D.M., Evans, M.S., Muir, D.C.G., 2008. Evidence for mass-independent and mass-dependent fractionation of the stable isotopes of mercury by natural processes in aquatic ecosystems. Applied Geochemistry 23, 547-571.

Keeler, G.J., Landis, M.S., Norris, G.A., Christianson, E.M., Dvonch, J.T., 2006. Sources of Mercury Wet Deposition in Eastern Ohio, USA. Environmental Science & Technology 40, 5874-5881.

Kesselmeier, J., Staudt, M., 1999. Biogenic volatile organic compounds (VOC): An overview on emission, physiology and ecology. Journal of Atmospheric Chemistry 33, 23-88.

Kritee, K., Blum, J.D., Johnson, M.W., Bergquist, B.A., Barkay, T., 2007. Mercury stable isotope fractionation during reduction of Hg(II) to Hg(0) by mercury resistant microorganisms. Environment Science Technology 41, 1889-1895.

Kritee, K., Blum, J.D., Barkay, T., 2008. Mercury stable isotope fractionation during reduction of Hg(II) by different microbial pathways. Environmental Science & Technology 42, 9171-9177.

Landis, M.S., Keeler, G.J., 1997. Critical Evaluation of a Modified Automatic Wet-Only Precipitation Collector for Mercury and Trace Element Determinations. Environmental Science & Technology 31, 2610-2615.

Landis, M.S., Keeler, G.J, 2002. Atmospheric mercury deposition to Lake Michigan during the Lake Michigan Mass Balance Study. Environmental Science & Technology 36, 4518-4524.

Landis, M.S., Vette, A.S., Keeler, G.J., 2002. Atmospheric Mercury in the Lake Michigan Basin: Influence of the Chicago/Gary Urban Area. Environmental Science & Technology 36, 4508-4517.

Lin, C., Pehkonen, S.O., 1997. Aqueous free-radical chemistry of mercury in the presence of iron oxides and ambient aerosol. Atmospheric Environment 31, 4125-4137.

Lin, C., Pehkonen, S.O., 1999. The chemistry of atmospheric mercury. Atmospheric Environment 33, 2067-2079.

Lin, C., Pongprueska, P., Lindberg, S.E., Pehkonen, S.O., Byun, D., Jang, C., 2006. Scientific uncertainties in atmospheric mercury models I: Model science evaluation. Atmospheric Environment 40, 2911-2928.

Lindberg, S.E., Brooks, S., Lin, C.-J., Scott, K.J., Landis, M.S., Stevens, R.K., Goodsite, M., Richter, A., 2002. Dynamic oxidation of gaseous mercury in the arctic troposphere at polar sunrise. Environmental Science & Technology 36, 1245-1256.

Liu, B., Keeler, G.J., Dvonch, J.T., Barres, J.A., Lynam, M.M., Marsik, F.J., Taylor-Morgan, J., 2010. Urban-rural differences in atmospheric mercury speciation. Atmospheric Environment 44(16), 2013-2023.

Lohman, K., Seigneur, C., Edgerton, E., Jansen, J., 2006. Modeling mercury in power plant plumes. Environmental Science & Technology 40, 3848-3854.

Lynam, M.M., Keeler, G.J., 2005. Automated speciated mercury measurements in Michigan. Environmental Science & Technology 39(23), 9253-9262.

Munthe, J., Xiao, Z.F., Lindqvist, O., 1991. The aqueous reduction of divalent mercury by sulfite. Water, Air and Soil Pollution 56, 621-630.

Munthe, J., 1992. The aqueous oxidation of elemental mercury by ozone. Atmospheric Environment 26A, 1461-1468.

Munthe, J., McElroy, W.J., 1992. Some aqueous reactions of potential importance in the atmospheric chemistry of mercury. Atmospheric Environment 26A, 553-557.

National Climatic Data Center, Local Climatological Data Publication (http://www7.ncdc.noaa.gov/IPS/lcd/lcd.html).

Schauble, E.A., 2007. Role of nuclear volume in driving equilibrium stable isotope fractionation of mercury, thallium, and other very heavy metals. Geochimica et Cosmochimica Acta 71, 2170-2189.

Schroeder, W.H., Munthe, J., 1998. Atmospheric mercury - An overview. Atmospheric Environment 32, 809-822.

Seigneur, S., Wrobel, J., Constantinou, E., 1994. A chemical kinetic mechanism for atmospheric inorganic mercury. Environmental Science & Technology 28, 1589-1597.

Sherman, L.S., Blum, J.D., Nordstrom, D.K., McClesky, R.B., Barkay, T., Vetriani, C., 2009. Mercury isotopic composition of hydrothermal systems in the Yellowstone

Plateau volcanic field and Guayamas Basin sea-floor rift. Earth and Planetary Science Letters 279, 86-96.

Sherman, L.S., Blum, J.D., Johnson, K.P., Keeler, G.J., Barres, J.A., Douglas, T.A., 2010. Mass-independent fractionation of mercury isotopes in Arctic snow driven by sunlight. Nature Geoscience 3, 173-177.

Slemr, F., Schuster, G., Seiler, W., 1985. Distribution, speciation, and budget of atmospheric mercury. Journal of Atmospheric Chemistry 3, 407-434.

Smith, C.N., Kesler, S.E., Klaue, B., Blum, J.D., 2009. Mercury isotope fractionation in fossil hydrothermal systems. Geology 33(10), 825-828.

Tackett, P.J., Cavender, A.E., Keil, A.D., Shepson, P.B., Bottenheim, J.W., Morin, S., Deary, J., Steffen, A., Doerge, C., 2007. A study of the vertical scale of halogen chemistry in the Arctic troposphere during Polar Sunrise at Barrow, Alaska. Journal of Geophysical Research 112, D07306.

Turro, N.J., 1983. Influence of nuclear spin on chemical reactions: Magnetic isotope and magnetic field effects (A review). Proceedings of the National Academy of Sciences 80, 609-621.

U.S. Environmental Protection Agency (U.S. EPA), 1994. *An Introduction to the Issues and the Ecosystems.* EPA-453/B-94/030; Office of Air Quality Planning and Standards: Durham, NC (http://www.epa.gov/air/oaqps/gr8water/xbrochure/index.html).

U.S. Environmental Protection Agency (U.S. EPA), 1997. *Mercury Study Report to Congress, Volume 2.* EPA-452/R-97-003; U.S. Environmental Protection Agency (U.S. EPA) Office of Air Quality Planning and Standards, Office of Research and Development: Washington DC (http://www.epa.gov/mercury/report.htm).

Vette, A.S., Landis, M.S., Keeler, G.J., 2002. Deposition and emission of gaseous mercury to and from Lake Michigan during the Lake Michigan Mass Balance Study (July, 1994 – October, 1995). Environmental Science & Technology 36, 4525-4532.

White, E.M., Keeler, G.J., Landis, M.S., 2009. Spatial variability of mercury wet deposition in Eastern Ohio: Summertime meteorological case study analysis of local source influences. Environmental & Science Technology 43, 4946-4953.

Willey, J.D., Kieber, R.J., Eyman, M.S., Avery, G.B., 2000. Rainwater dissolved organic carbon: Concentrations and global flux. Global Biogeochemical Cycles 14(1), 139-148.

Zheng, W, Hintelmann, H., 2009. Mercury isotope fractionation during photoreduction in natural water is controlled by its Hg/DOC ratio. Geochimica et Cosmochimica Acta 73, 6704-6715.
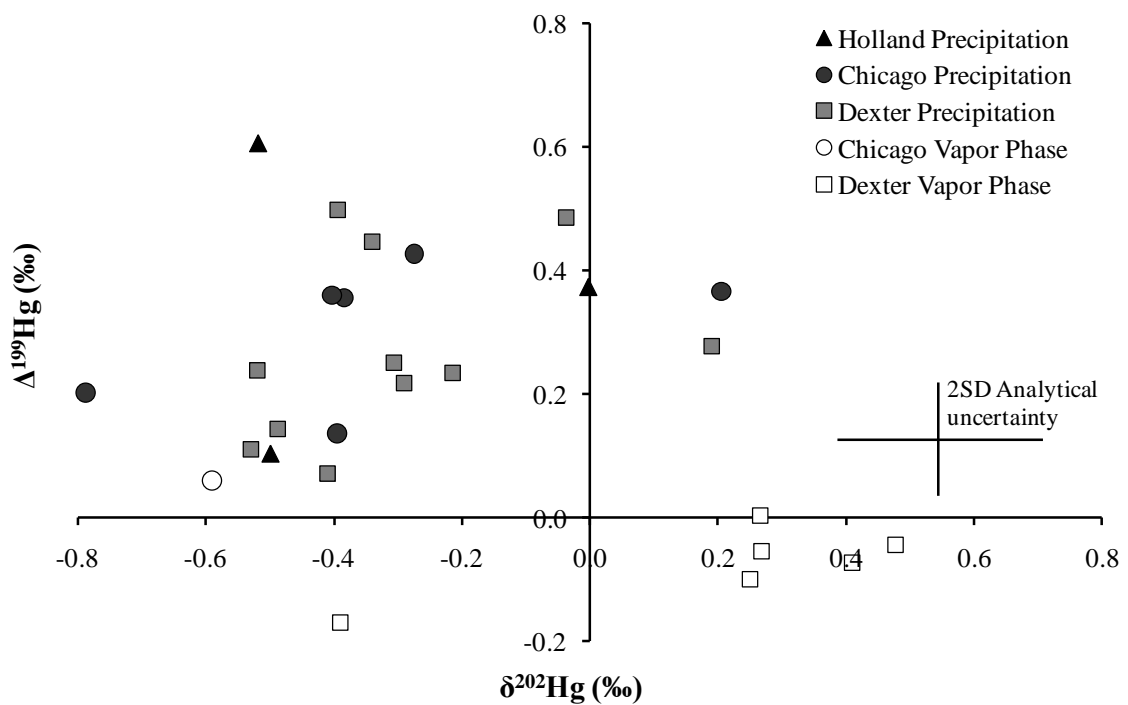
Figure 5.1: Δ^{199}Hg (‰) vs. δ^{202}Hg (‰) for precipitation and ambient vapor phase samples. Representative 2SD analytical uncertainty is determined by the reproducibility of the UM-Almadén standard and other procedural standards.

Figure 5.2: Δ^{199}Hg (‰) vs. Δ^{201}Hg (‰) for Great Lakes precipitation and ambient vapor phase samples. Representative 2SD analytical uncertainty is determined by the reproducibility of the UM-Almadén standard and other procedural standards.

Figure 5.3: Δ^{199}Hg (‰) vs. Δ^{200}Hg (‰) for precipitation and ambient vapor phase samples. Representative 2SD analytical uncertainty is determined by the reproducibility of the UM-Almadén standard and other procedural standards.
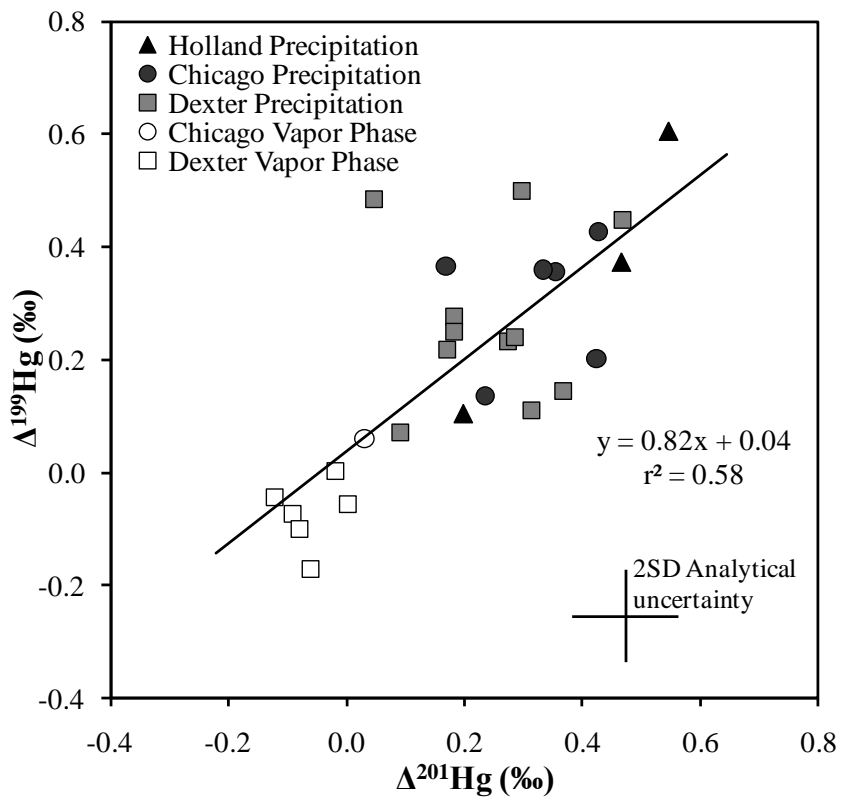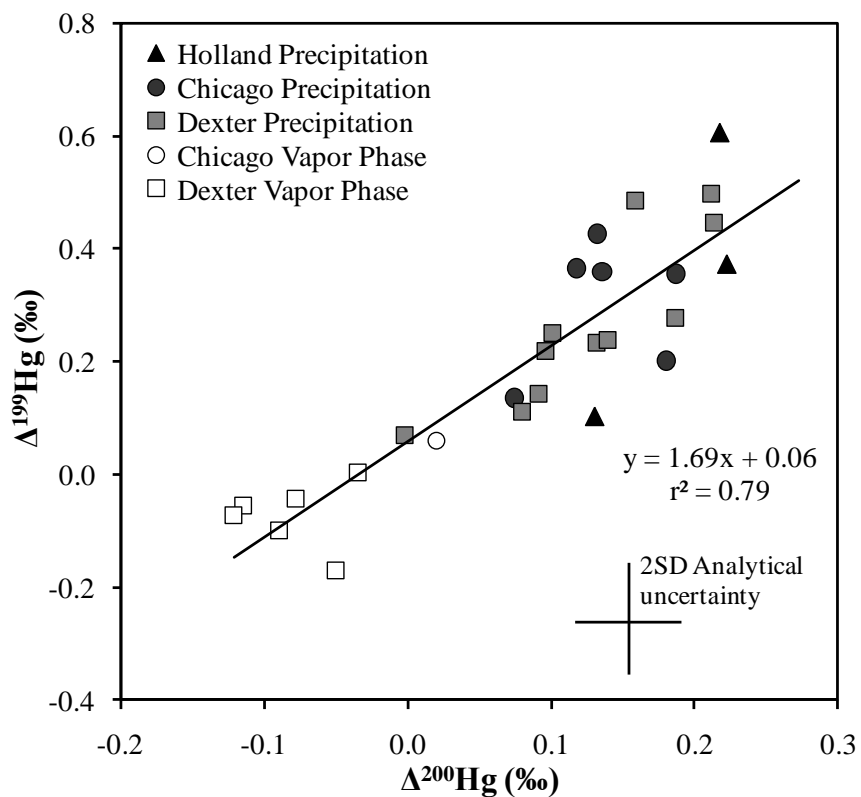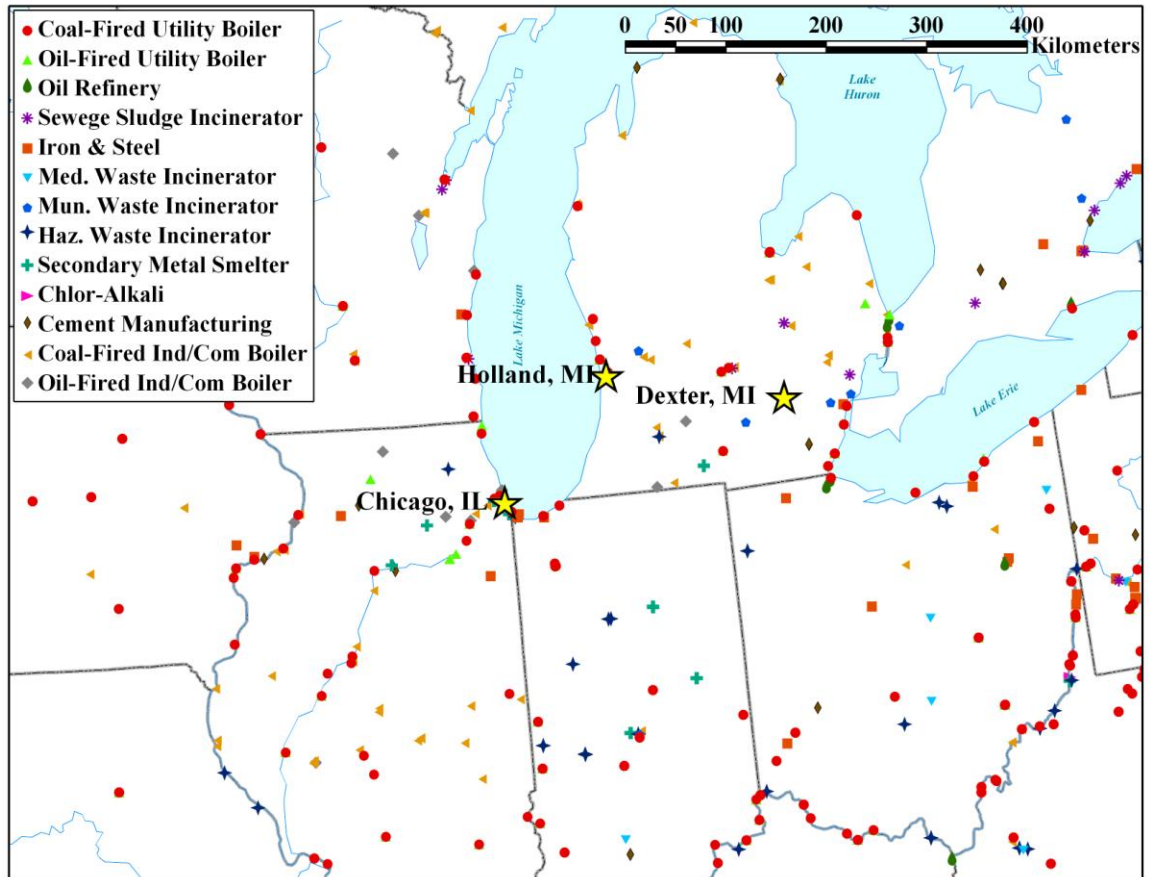
Figure 5.SI-1: Location of Chicago, IL, Holland, MI, and Dexter, MI monitoring locations relative to major Hg point sources emitting ≥ 0.1 kg Hg/year (2005 U.S. EPA NEI; 2007 Environment Canada NPRI).

Table 5.SI-1: Summary of precipitation samples collected and analyzed for Hg isotopic composition at Dexter, MI, Holland, MI and Chicago, IL. Hg isotopic compositions (δ^{202}Hg, Δ^{199}Hg, Δ^{200}Hg, and Δ^{201}Hg) are reported in delta and capital delta notation.

Location	Sample ID	Sampling Period	# Events Collected	Volume (mL)	Sample Hg Concentration (ng/L)	% Recovery	δ^{202}Hg (‰)	Δ^{199}Hg (‰)	Δ^{200}Hg (‰)	Δ^{201}Hg (‰)
Dexter	DXT-1	4/22/07 - 4/27/07	1	1444	9.5	82	-0.39	0.50	0.21	0.30
Dexter	DXT-2	4/27/07 - 5/2/07	3	1057	29.3	82	-0.34	0.45	0.21	0.47
Dexter	DXT-3A	5/2/07 - 5/17/07	2	2072	6.9	91	-0.04	0.48	0.16	0.05
Dexter	DXT-5	5/28/07 - 6/4/07	3	2090	9.0	85	-0.29	0.22	0.10	0.17
Dexter	DXT-7	6/17/07 - 6/29/07	2	1555	10.4	80	-0.53	0.11	0.08	0.31
Dexter	DXT-11	8/8/07 - 8/20/07	2	2092	9.7	93	-0.49	0.14	0.09	0.37
Dexter	DXT-13	8/21/07 - 9/5/07	4	1619	19.2	91	-0.21	0.23	0.13	0.27
Dexter	DXT-26	3/6/08 - 3/31/08	3	1650	11.6	85	-0.41	0.07	0.00	0.09
Dexter	DXT-27	3/31/08 - 4/17/08	5	1423	15.4	86	0.19	0.28	0.19	0.18
Dexter	DXT-28	4/17/08 - 5/15/08	5	1367	12.9	81	-0.31	0.25	0.10	0.18
Dexter	DXT-29	5/15/08 - 6/8/08	6	2122	11.6	72	-0.52	0.24	0.14	0.28
Holland	HOL-2	8/18/07 - 8/23/07	5	2116	20.6	85	-0.52	0.61	0.22	0.55
Holland	HOL-5	9/24/07 - 10/8/07	5	812	10.7	89	0.00	0.37	0.22	0.47
Holland	HOL-7	10/15/07 - 10/22/07	4	1335	17.6	95	-0.50	0.10	0.13	0.20
Chicago	UOC-1	8/10/07 - 8/17/07	3	1708	15.4	86	-0.27	0.43	0.13	0.43
Chicago	UOC-2A	8/17/07 - 8/23/07	6	2141	18.3	86	-0.38	0.36	0.19	0.35
Chicago	UOC-2B	8/23/07 - 8/24/07	1	1782	13.8	98	-0.40	0.36	0.14	0.33
Chicago	UOC-5	9/24/07 - 10/8/07	4	712	12.4	85	-0.79	0.20	0.18	0.42
Chicago	UOC-7	10/8/07 - 10/22/07	6	1895	17.8	90	-0.40	0.14	0.07	0.23
Chicago	UOC-8	10/22/07 - 11/13/07	3	631	14.8	97	0.21	0.37	0.12	0.17

Table 5.SI-2: Summary of vapor phase samples collected and analyzed for Hg isotopic composition at Dexter, MI, Holland, MI and Chicago, IL. Hg isotopic compositions (δ^{202}Hg, Δ^{199}Hg, Δ^{200}Hg, and Δ^{201}Hg) are reported in delta and capital delta notation. Samples were concentrated into 8 g 2% $KMnO_4$ solutions.

Location	Sample ID	Sampling Period	Hg in Sample (ng)	δ^{202}Hg (‰)	Δ^{199}Hg (‰)	Δ^{200}Hg (‰)	Δ^{201}Hg (‰)
Dexter	DXT-VP-1	8/12/08 - 8/26/08	23.6	0.48	-0.04	-0.08	-0.12
Dexter	DXT-VP-2	2/23/09 - 2/25/09	17.8	-0.39	-0.17	-0.05	-0.06
Dexter	DXT-VP-3	2/27/09 - 3/2/09	49.2	0.27	-0.06	-0.11	0.00
Dexter	DXT-VP-4	5/10/09 - 5/12/09	31.7	0.41	-0.07	-0.12	-0.09
Dexter	DXT-VP-5	5/20/09 - 5/22/09	15.9	0.27	0.00	-0.04	-0.02
Dexter	DXT-VP-6	9/6/09 - 9/8/09	17.9	0.25	-0.10	-0.09	-0.08
Chicago	UOC-VP-1	9/14/09 - 9/16/09	18.1	-0.59	0.06	0.02	0.03

CHAPTER 6

Conclusion

Atmospheric deposition is a dominant pathway for mercury (Hg) to enter terrestrial and aquatic ecosystems. In order to effectively reduce the levels of Hg in the environment, the sources and processes which make Hg available for atmospheric removal need to be quantified. Our understanding of Hg sources and atmospheric cycling has progressed substantially in the past two decades with the advancement of wet-only precipitation collectors, innovative techniques for measuring Hg dry deposition, the ability to semi-continuously measure speciated ambient Hg, and new techniques for quantifying the Hg isotopic composition in various environmental reservoirs.

Regulatory actions and pollution prevention efforts have drastically reduced Hg air emissions from waste incineration, previously one of the largest anthropogenic Hg source categories in the U.S. However, Hg deposition to sensitive ecosystems remains a persistent problem, demonstrating that there is still much to learn with respect to the relative importance of local, regional, and global source emissions and the processes that Hg undergoes between emission and deposition. While many questions still remain, the research presented here adds to the current understanding of atmospheric Hg sources, transport, and deposition.

6.1 Summary of Key Findings

Analysis of 12-years of daily-event precipitation samples collected at Underhill, VT from 1995 to 2006 demonstrated that annual Hg wet deposition at this remote New England location has not declined over time despite significant Hg emission reductions in the region. Although the volume-weighted mean (VWM) Hg concentration did decline significantly from 2001 to 2006, this decline was more likely due to local scale meteorological and climatological variability than to a reduction in anthropogenic Hg emissions to the atmosphere. The annual precipitation depth measured in Underhill, VT increased significantly over time, a change which was strongly related to changes in the amount and type of precipitation that fell seasonally. The coincident increase in precipitation amount and decline in VWM concentration suggests that a relatively constant amount of Hg was available for scavenging from the atmosphere, resulting in declining annual concentrations but unchanging levels of total Hg wet deposition.

Analysis of calculated air mass back-trajectories and measured on-site meteorological parameters suggested that annual Hg wet deposition at Underhill did not change significantly because transport of emissions from sources in the industrialized Midwest and along the East Coast of the United States consistently contributed to the largest observed Hg wet deposition events over the 12-year period. Furthermore, it appears that the transport of Hg emissions from municipal and medical waste incinerators in the New England region was not a strong enough pathway to the northern Vermont site for the reduction in Hg emissions from this source category during the late 1990s to result in lower measured Hg wet deposition.

This analysis of Hg wet deposition and meteorological data illuminated the transport pathways and meteorological conditions which were most conducive to elevated Hg wet deposition and suggested that regional sources were the dominant contributors to Hg wet deposition at Underhill. However, given that Underhill is a relatively remote location lacking clear local anthropogenic source inputs, the range of regional or global sources that could contribute to Hg deposition at this site should be considered. An independent and complimentary technique was therefore needed in order to corroborate the importance of regional Hg sources and identify the specific source types contributing to Hg wet deposition.

To this end, multivariate and hybrid-receptor models were applied to the Hg and trace element wet deposition measurements from Underhill. Source apportionment analysis using the multivariate receptor model EPA PMF 3.0 suggested that emissions from coal-fired utility boilers (CFUBs) contributed ~60% of Hg wet deposition at Underhill from 1995 to 2006 and the dominance of this source type impacting Underhill did not change significantly over time. The other source types identified in the PMF model output were mixed metal smelting and incineration, a phosphorus source hypothesized to represent wood-burning and fertilizer application, oil combustion, and iron-steel manufacturing. In addition to coal combustion, only the smelting/incineration and phosphorus sources contributed significantly to Hg deposition in the PMF model, accounting for ~13% and ~27% of Hg deposition, respectively, from 1995 to 2006. The model accounted for 78% of the total measured Hg wet deposition at Underhill over this 12-year period. The remaining 22% not accounted for by the model may include a contribution from those

sources not well-characterized by the suite of trace elements measured in the wet deposition as well as a contribution from the global atmospheric Hg pool. The strong relationships observed between Hg and other specific trace elements in precipitation supports the conclusion that the dominant contribution to Hg wet deposition was from regional anthropogenic sources.

Although waste incineration was previously a major source of Hg emissions in the U.S. and especially in the Northeast States, a distinct signature and substantial contribution to Hg deposition from this source type was not apparent in the source apportionment analysis. Past aerosol source apportionment studies at Underhill have suggested that it may be difficult to isolate a separate incineration signature in atmospheric aerosol samples at this location due to the fact that several tracer elements for incineration, e.g. Zn and Pb, are also emitted from nonferrous metal smelters in the region. Additionally, because municipal or medical waste incinerators are not located within 100 km of the Underhill site and the emissions of Hg species from the relatively short waste incinerator stacks are predominantly divalent reactive gaseous mercury (RGM), the highly reactive form of Hg that is readily removed from the atmosphere, Hg emissions are unlikely to be transported to the remote Underhill site and be evident in precipitation samples collected there. For this reason, despite persistent efforts by the Northeast States and Canadian Provinces to drastically reduce Hg impacts from waste incineration in the region, it appears that Hg wet deposition has not significantly declined at the northern Vermont site at Underhill because regional CFUB emissions have consistently been the dominant source of Hg to Underhill.

The coal combustion signature was further examined using quantitative transport bias analysis (QTBA), a trajectory-based hybrid-receptor model. QTBA consistently calculated that the likely source region for emissions of Hg, S, and Se was the Midwestern U.S. where it is known that the density of CFUBs is largest. With knowledge of emission source locations in the region and the species that are released from each source type, it was possible to reconcile the model output for the major trace elements and confirm that QTBA successfully identified their respective source locations. These results further lent credence that QTBA would also effectively resolve the likely Hg source locations. The combined results of meteorological analysis and receptor modeling are consistent and compelling, strongly predicting that the emissions from regional CFUBs were the largest contributor to Hg deposition at Underhill over the 12-years and this source impact has not changed significantly over time.

The dry deposition of Hg is thought to be equally as important as wet deposition as an input to ecosystems, especially in urban/industrial source areas. However, our current understanding of the transport and deposition of atmospheric Hg species, specifically RGM, is somewhat limited. Distinguishing the relative importance of direct RGM transport from RGM formed in the atmosphere via Hg^{0} oxidation is critical for understanding atmospheric Hg cycling as well as the spatial impact of Hg emissions. The relative importance of direct transport and oxidation on RGM concentrations at a given location should vary with distance from sources as well as the availability of atmospheric oxidants. For example, the Hg wet deposition measurements at Underhill suggested that Hg emitted as RGM from waste

incinerators > 100 km away was not likely transported over this large distance due to the propensity for near-field RGM removal. It is critical to more closely investigate the behavior of Hg once it is emitted to the atmosphere and explore the potential chemical activity and removal processes that may occur.

To this end, speciated Hg measurements were made in the Lake Michigan basin during the summer of 2007 to elucidate the influence of speciated Hg emissions from anthropogenic sources and the spatial scale of Hg transport from an urban/industrial area. Large lakes, such as Lake Michigan, promote a stable atmosphere in which air pollutants are not likely to mix vertically and can easily be transported from sources to distant receptors located along the shoreline. The stable layers that form over the lake are also conducive to daytime photochemical reactions during transport which could enhance the potential for Hg^0 oxidation. To explore the fate of industrial emissions within this lake system, speciated Hg measurements were made in downtown Chicago, IL where major emission point sources were located within 10 km of the site. A second site was positioned in Holland, MI, northeast of Chicago on the eastern shore of Lake Michigan, in order to measure local source emissions under northerly transport but also intercept across-lake emissions under southwesterly transport.

Urban-rural differences were apparent in the speciated Hg measurements from the two monitoring sites, as the mean Hg_p concentration was ~1.5 times higher in Chicago than Holland, while Hg^0 and RGM concentrations were ~2 times higher in Chicago. Significantly elevated concentrations occurred in all three Hg species in Chicago, typically in sharp peaks overnight when local source emissions were

contained within the nocturnal boundary layer. Elevated Hg^0 concentrations in Holland also occurred primarily during the night and early morning hours under northerly or easterly flow with ozone concentrations < 40 ppb, suggesting the influence of local source emissions. Peak Hg_p concentrations at Holland occurred more often toward the end of the study, when hourly on-site temperatures declined to less than 20°C (68°F), due to the preference for Hg(II) to partition to the condensed phase and bind to particles under cooler temperatures. In contrast, elevated RGM concentrations at Holland were dominantly observed during the daytime, occurring in broad peaks under southwesterly flow. These RGM peaks were often accompanied by elevated ozone concentrations, suggesting the potential importance of daytime RGM production through Hg^0 oxidation.

Cluster analysis of 24-hour air mass back-trajectories associated with the speciated Hg measurements suggested that Chicago/Gary sources were the dominant contributor to summertime ambient Hg concentrations at the Holland site. Under south-southwesterly flow, the median RGM concentration was nearly five times greater than the median concentration observed under all other flow regimes.

Two short-duration case studies were selected from the summer study to explore variability in Hg concentrations at the two sites under changing meteorological conditions and flow patterns. Local source impacts could be observed at the Holland site with northerly flow, but substantially larger RGM concentrations were measured under southwesterly transport. Application of the HYSPLIT dispersion model to the case study periods suggested that as much as 52% of the RGM in Holland under southwesterly flow could be attributed to direct transport of

185

primary Hg emissions from Chicago/Gary sources, with the remaining fraction due to Hg^0 oxidation during transport over the lake surface. These findings were supported by a significant positive correlation ($R^2 = 0.62 – 0.64$) between ozone, one of many known oxidants of Hg^0 that is likely important in the Lake Michigan basin, and RGM during the modeled periods. The combined role of transport and chemical production of RGM is reasonable considering that RGM is expected to be removed near sources through wet and dry deposition, but in the absence of precipitation could be transported further downwind under specific conditions. These findings suggest the need to further explore the chemical activity that Hg may undergo during transport over this and other lake systems.

Finally, the application of Hg isotope measurements to ambient vapor phase and wet deposited Hg suggests that this relatively new analytical tool may be used to further our understanding of Hg cycling in the environment. Hg has been shown to undergo two types of isotopic fractionation in the environment: mass-dependent fractionation (MDF) and mass-independent fractionation (MIF). MDF occurs due to differences in zero-point vibrational energies between the isotopes due to their differing masses. MIF likely occurs either due to variations in the nuclear charge radii of different isotopes (nuclear volume effect) or due to the influence of nuclear spin in the odd-mass isotopes on radical pair reaction rates (magnetic isotope effect). The nuclear volume theory, which describes MIF of Hg during equilibrium reactions, could occur during both light and dark reactions whereas the magnetic isotope effect influences kinetic reactions and occurs during photochemical processes in which long-lived radical pairs are formed. The extent of fractionation caused by the nuclear

volume effect is expected to be much smaller than that caused by the magnetic isotope effect. The observation of MIF of Hg, as well as the magnitude and sign of the fractionation, may be used to suggest the reactions and processes that Hg undergoes in the environment.

At this time, relatively little is known about the impact of source emissions and atmospheric cycling on Hg isotopic fractionation, but recent findings offer insight on chemical mechanisms of potential importance. For example, laboratory experiments recently demonstrated that during aqueous photoreduction in the presence of dissolved organic carbon (DOC) when Hg^0 was volatilized from solution, the Hg^{2+} remaining in solution displayed positive MIF of ^{199}Hg and ^{201}Hg. This demonstrated that the odd isotopes of Hg were preferentially retained in solution during this photochemical reaction. Furthermore, these findings suggested that the Hg^0 released to the atmosphere through aqueous photoreduction in the presence of DOC should display negative MIF of ^{199}Hg and ^{201}Hg. Another recent study published the isotopic composition of Hg in lichens, which are composite organisms of fungi and algae typically found on trees, rocks, and other exposed surfaces. Lichens take up atmospheric Hg through wet and dry deposition and gaseous absorption, and thus were thought to be a reasonable approximation for the isotopic composition of atmospheric Hg. Based on observations of negative MIF of ^{199}Hg and ^{201}Hg in lichens which was similar in magnitude to the MIF observed in solution during aqueous photoreduction experiments, it was suggested that aqueous photoreduction of Hg^{2+} may be a dominant source of Hg^0 to the atmosphere.

Ambient vapor phase Hg collected in Dexter, MI and Chicago, IL for the purpose of defining the ambient isotopic composition of Hg displayed predominantly insignificant MIF of ^{199}Hg and ^{201}Hg. In contrast, precipitation samples from Chicago, Holland, and Dexter were dominantly categorized by positive MIF of ^{199}Hg and ^{201}Hg. These findings are dissimilar to the predictions based on measurements of Hg isotopes in lichens that atmospheric Hg might display negative MIF of Hg. It should be noted that Hg is known to undergo a range of oxidation and reduction reactions in the environment, of which aqueous photoreduction is only one example. The measurements of Hg isotopic composition and fractionation in Great Lakes atmospheric samples suggest that aqueous photoreduction is not the only process contributing to isotopic variations in atmospheric Hg in this region. The potential influence of source emissions and atmospheric redox reactions on atmospheric Hg fractionation needs to be further studied before isotopic measurements can be conclusively applied to atmospheric Hg cycling.

6.2 Recommendations for Future Work

The analysis of 12-years of precipitation at Underhill, VT demonstrates the value of long-term monitoring. With this dataset, it was possible to quantify trends in Hg concentration and deposition over time. It was also possible to identify the major sources contributing to Hg in precipitation and determine whether their contributions have declined as emission regulations have been implemented. Furthermore, it was possible to examine the impact of changing meteorological conditions over time on Hg deposition collected on an event basis. Acknowledging that 12-years is a relatively short dataset in which to draw conclusions on climatological changes, the

results presented here suggest that meteorological variability had a measureable influence on Hg deposition patterns at the Underhill site. Additional datasets of this nature are needed, but are unlikely to be collected due to cost and personnel constraints, so different approaches for identifying deposition patterns and source impacts over time will need to be considered. One possibility would be a long-term modeling study which includes climatological variability as well as atmospheric Hg chemistry and source emissions to determine how changes in precipitation amount and type over time, as well as varying emission scenarios, might affect Hg deposition.

It is also critical to examine long-term trends in both Hg concentration and deposition. At a remote location such as Underhill where there are no large local sources, the concentration in precipitation samples is highly influenced by precipitation amount as much of the Hg is removed in the onset of precipitation and additional precipitation can act to dilute the concentration within the sample. Thus trends in concentration alone cannot be used to conclusively evaluate trends in atmospheric Hg over time without acknowledging the coinciding variability in precipitation amount and type. Analysis of the Underhill precipitation data demonstrates that it is possible to extrapolate these various meteorological influences and determine whether the introduction of Hg to the ecosystem through precipitation has in fact changed over time.

Additionally, the analysis of precipitation samples using back-trajectories and receptor models would not have been possible without the collection of daily-event precipitation samples. While weekly precipitation collection may be more cost and time effective, it causes individual events to be combined into a single sample,

effectively eliminating any ability to isolate source influences or specific transport pathways contributing to deposition. It is for this reason that specific source influences or atmospheric processes could not be identified in the precipitation samples analyzed for Hg isotopes. For future precipitation sample collection, it is strongly recommended that event-based sampling be employed for Hg, trace element, and Hg isotope analysis so that distinct source influences and atmospheric processes can be better characterized. Event-based sampling techniques have already been developed and implemented for Hg and trace element analysis, as evidenced by the Underhill monitoring study. In the case of Hg isotopes where larger samples are needed in order to collect sufficient Hg for analysis, event-based sampling could be accomplishes by deploying multiple bottle/funnel apparatuses in the field during a single event, or by attaching a larger funnel to the sample bottles.

Longer duration speciated monitoring would also be a valuable contribution to the current understanding of atmospheric Hg speciation and chemistry. Monitoring campaigns of this nature in Detroit, MI and Dexter, MI have demonstrated seasonal variability in speciated Hg concentrations and the influence of atmospheric transport and chemistry at different times of year. The measurements in Chicago and Holland were conducted primarily in summer months, which was optimal for capturing southwest transport episodes and quantifying the impact of Chicago/Gary emissions on southwest Michigan. Changes in the relative amounts of RGM and Hg_p measured at the Holland site in the latter portion of the study (October-November) strongly suggest that the seasonal variability in speciated Hg should be monitored at this location. Given that northerly flow is typically more common in winter months it

seems likely that local sources may be more evident at Holland at that time of year. However, during winter months RGM concentrations are expected to be much lower than during the summer due to reduced temperatures and photochemical activity, while Hg_p concentrations should be slightly elevated as Hg(II) preferentially binds to particles under cooler temperatures. Therefore speciated measurements Chicago and Holland for a year or more would provide a more complete picture of the overall influence of Chicago/Gary sources on southwest Michigan.

Additionally, it is recommended that the Lake Michigan transport case studies be further analyzed using more comprehensive models that include speciated Hg emissions and atmospheric Hg chemistry. This will provide further verification of the dispersion estimates presented as well as emulate the chemical processes that Hg may undergo during transport.

Finally, in addition to collecting event-based precipitation samples for Hg isotope analysis, it is recommended that shorter duration ambient vapor phase Hg samples be collected for similar reasons. The samples presented here were collected over the span of several days, during which transport direction can vary substantially. The collection of samples on the order of hours rather than days, and in both remote and urban/industrial locations, will provide more information on source influences and atmospheric processes contributing to the observed Hg fractionation in atmospheric samples.

The presented Hg isotope analysis also suggests that processes other than aqueous photoreduction are responsible for the observed Hg isotopic composition of atmospheric samples. Other potentially important atmospheric mechanisms, such as

Hg^0 oxidation, could potentially be studied in controlled laboratory settings to estimate their impact on Hg isotopic fractionation. Additional measurements of Hg isotopic fractionation in the atmosphere could also be compared against atmospheric chemistry models to determine the relative importance of atmospheric reactions and their effect on Hg isotopic fractionation. Exercises of this nature are necessary before the measurements of Hg fractionation in environmental reservoirs can be used to confidently explain Hg biogeochemical cycling.